Multibody Dynamics Modeling of Flexible Aircraft Flight Dynamics

Load Prediction in the Preliminary Design Phase

R.L.C. Kalthof

Master of Science Thesis

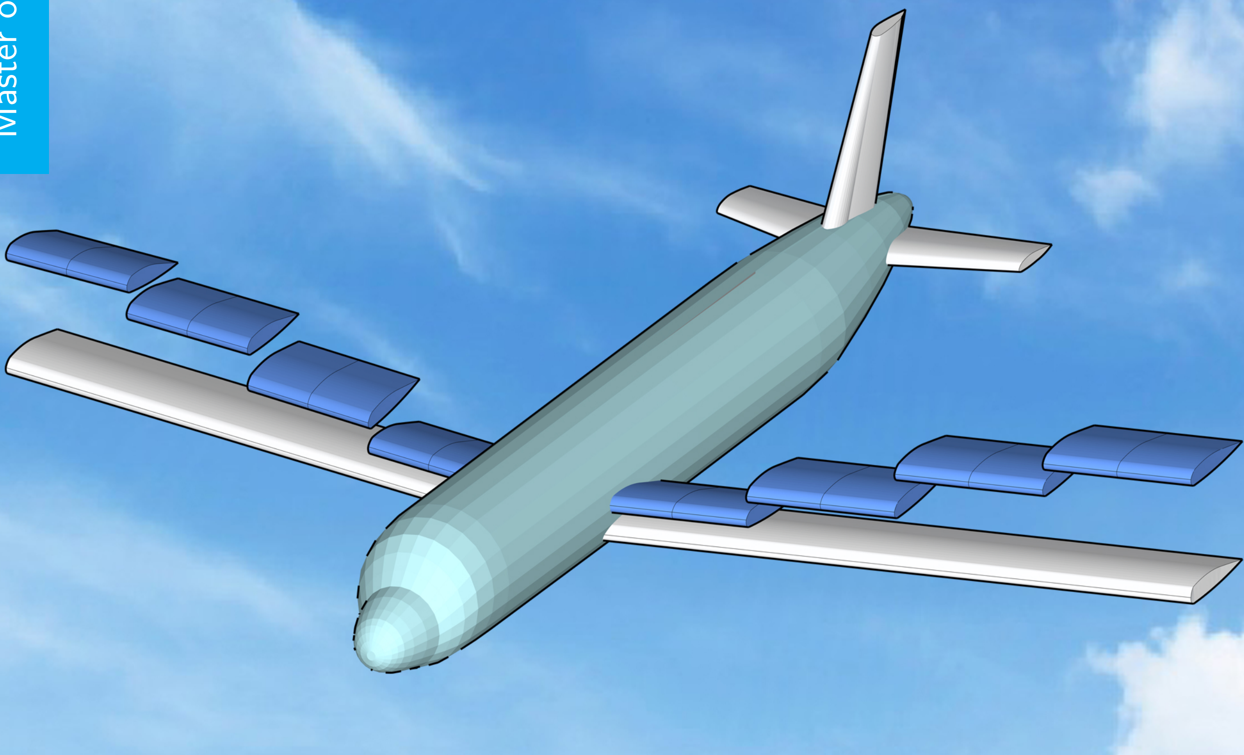

Delft University of Technology

Multibody Dynamics Modeling of Flexible Aircraft Flight Dynamics

Load Prediction in the Preliminary Design Phase

Master of Science Thesis

For obtaining the degree of Master of Science in Aerospace Engineering at Delft University of Technology

R.L.C. Kalthof

June 12, 2014

007#14#MT#FPP
Faculty of Aerospace Engineering · Delft University of Technology

Delft University of Technology
Department of
Flight Performance and Propulsion

The undersigned hereby certify that they have read and recommend to the Faculty of Aerospace Engineering for acceptance a thesis entitled

Multibody Dynamics Modeling of Flexible Aircraft Flight Dynamics

by

R.L.C. Kalthof

in partial fulfillment of the requirements for the degree of

Master of Science Aerospace Engineering

Dated: June 12, 2014

Head of department: ______________________
Prof. dr. ir. L.L.M. Veldhuis

Supervisor: ______________________
Dr. ir. M. Voskuijl

Readers: ______________________
Dr. ir. R. De Breuker

____
Dr. ir. R. Vos

Acknowledgements

This thesis report is written as a part of the Master Program in Flight Performance and Propulsion at the Faculty of Aerospace Engineering of Delft University of Technology. It forms the final step in completing this study and thereby also the end of my time as a student in Delft.

Looking back at performing seven months of research, reading roughly 200 articles and writing some 10 000 lines of code, I would like to thank a number of people for their help. First of all, I would like to express my gratitude towards my supervisor, dr. ir. Mark Voskuijl, for his excellent guidance during the project, from beginning to end, and for his invaluable advice, especially on the subject of flight mechanics. Furthermore, I would like to thank dr. ir. Roeland De Breuker, for sharing with me his knowledge about aeroelasticity. I would also like to thank prof. dr. ir. Leo Veldhuis and dr. ir. Roelof Vos, for completing my graduation committee.

Many thanks to all the people that helped make my time as a student absolutely terrific. Although there are too many to mention here, I would like to extend a special thanks to the people that helped me during this thesis research: the students of *Kamertje 1*, for the many laughs, discussions and other pleasant distractions, and Almira, Bob, Diego, Max and Niels for reading through part of this report and providing me with valuable comments. I would also like to thank my parents, who have supported me in everything I did and whose positive attitude reflected on me. Finally, I would like to address a special person, my girlfriend Nanda, for her continuing support, involvement and encouragements.

Roelant Kalthof

Delft, June 2014

Abstract

Because of the focus on weight minimization, aircraft are becoming more and more flexible. Therefore, the frequency separation between flight mechanics motion and structural vibration decreases. This calls for a flight mechanics model that includes aeroelasticity. The development of such a model was the subject of the current research. This model can be used for gust and maneuver load prediction in the preliminary design phase. With accurate load prediction, structural integrity can be ensured and unstable flight conditions can be avoided. Moreover, the model may be used to design active load alleviation systems to increase passenger comfort, reduce fatigue, and decrease loads on the wing structure.

Table 1 shows the approaches that were used for the disciplines involved in the aeroelastic flight mechanics model. The upper part represents the aeroelastic wing model, which was extensively verified. The qualitative, steady-state and transient behavior were assessed and a comparison was made with an existing lumped-parameter model. The lower part represents the flight mechanics model, which was verified as well. For an A320-like aircraft, the qualitative behavior was investigated and the stability characteristics and trim conditions were compared with information from literature. Validation has not been performed, because of the absence of complete validation data for aeroelastic flight mechanics models.

Table 1: The approaches taken for the various disciplines.

Discipline	**Approach**
Structures	Modal approach in a linear time-invariant state-space system
Aerodynamics	Look-up tables using the quasi-steady α_{eff}
Control surfaces	Only aerodynamic contribution considered
Load prediction	Summation of forces (with multibody system dynamics)
Fluid-structure interaction	Conventional serial staggered partitioned approach
Flight Dynamics	Multibody system dynamics
Trimming	Combined implicit and explicit Jacobian approach
Linearization	Jacobian linearization

The complete multibody system dynamics model can be constructed automatically, based on

user input. In this manner, it can be included in a design optimization framework and many different analyses can be easily performed.

An A320-like aircraft was analyzed in the current research. The effect of aeroelasticity on flight mechanics was investigated. Inclusion of flexibility substantially affected the trim control variables, but had an almost negligible effect on the flight mechanics modes and stability derivatives. When flexibility increases, these parameters are affected. Aeroelasticity has a non-negligible effect on the (peak) wing loads after maneuvers or disturbances. Especially for maneuvers or disturbances that increase lift, and therefore wing deformation, the peak loads are affected. Moreover, wing loads are particularly affected by disturbances that have a direct effect on the wing, such as aileron deflection.

The objective of the current research was to improve on an existing aeroelastic flight mechanics model, based on the lumped-parameter approach. The modal model created in the current research proved to have a computational effort that is several times lower than the lumped-parameter model. In addition, the accuracy of the modal model can be increased beyond that of the lumped-parameter model at only a small additional computational cost. Because of the reduced computational cost, and the potentially increased accuracy, the modal model performs better than the lumped-parameter model.

Due to the qualitative nature of these conclusions, it is probable that they can be extended to other conventional, low aspect-ratio aircraft in the subsonic flight regime. Definitive, quantitative conclusions could not be formulated, because of the absence of complete validation data.

Table of Contents

Glossary

List of Acronyms

2D	Two-dimensional
3D	Three-dimensional
a.c.	aerodynamic center
a.p.	application point
AFM	Aeroelastic Flight Mechanics
CFD	Computational Fluid Dynamics
c.g.	center of gravity
CPACS	Common Parametric Aircraft Configuration Scheme
DLM	Doublet-Lattice Method
DR	Dutch Roll
e.a.	elastic axis
FEA	Finite Element Analysis
FSI	Fluid-Structure Interaction
LPM	Lumped-Parameter Method
MD	Mode-Displacement
mlb	massless body
MSD	Multibody System Dynamics
ODEs	Ordinary Differential Equations
POM	Position, Orientation and Motion

RS	Roll Subsidence	
SOF	Summation of Forces	
SP	Short-Period	
WRBM	Wing Root Bending Moment	

List of Symbols

α	Angle of attack	$[rad]$
α_{eff}	Effective angle of attack	$[rad]$
$\alpha_{fw,eff}$	Effective flexible wing angle of attack	$[rad]$
α_{rw}	Rigid wing angle of attack	$[rad]$
β	Sideslip angle	$[rad]$
χ	Flight track angle	$[rad]$
δ	Control surface deflection angle	$[rad]$
δ_a	Aileron right wing down deflection angle	$[rad]$
δ_e	Elevator downward deflection angle	$[rad]$
δ_f	Flap deflection angle	$[rad]$
δ_r	Rudder rightward deflection angle	$[rad]$
δ_{ij}	Kronecker delta	$[-]$
ϵ	Finite difference	N/A
η	Dimensionless semispan	$[-]$
Γ	Modal damping matrix	$[rad\, s^{-1}]$
γ	Flight path angle	$[rad]$
γ	Torsional constant	$[m^4]$
Λ	Spectral matrix	$[rad^2 s^{-2}]$
λ	Wave number	$[m^{-1}]$
$\ddot{\theta}_{\mathbf{b}}$	Vector of bending rotations	$[rad]$
$\ddot{\theta}_{\mathbf{t}}$	Vector of torsion rotations	$[rad]$
ϕ	Mode shape or eigenvector	$[m, rad]$
ω	Natural frequency	$[rad\, s^{-1}]$
Φ	Matrix holding relevant mode shapes	$[m, rad]$
ϕ	Aircraft roll angle	$[rad]$
ψ	Aircraft yaw angle	$[rad]$
ρ	Air density	$[kg\, m^{-3}]$
τ	Rigid wing pitch rotation	$[rad]$
θ	Aircraft pitch angle	$[rad]$
ξ	Aeroelastic twist deflection	$[rad]$

ζ	Modal damping ratio	$[-]$
$\bar{w}_g$	Maximum gust vertical velocity	$[m\,s^{-1}]$
$\dot{h}_{\dot{\alpha},0.75c}$	Plunge speed due to pitching velocity at three-quarter-chord point	$[m\,s^{-1}]$
$\mathbf{c}$	Control vector	$[rad, N]$
$\mathbf{F}$	External force vector	$[N]$
$\mathbf{o}$	Objective vector	$[ms^{-2}, rads^{-2}, rad]$
$\mathbf{P}$	Vector of net loads	$[N]$
$\mathbf{q}$	Vector of generalized coordinates	$[-]$
$\mathbf{s}$	Vector of response coordinates	$[m, rad]$
$\mathbf{u}$	Input vector	N/A
$\mathbf{v}$	Input vector deviation from equilibrium position	N/A
$\mathbf{w}$	Output vector deviation from equilibrium position	N/A
$\mathbf{x}$	State vector	N/A
$\mathbf{y}$	Output vector	N/A
$\mathbf{z}$	State vector deviation from equilibrium position	N/A
$\mathbf{q}_e$	Vector of generalized elastic coordinates	$[-]$
$\mathbf{q}_r$	Vector of generalized rigid body coordinates	$[-]$
$\mathbf{C}(k)$	Theodorsen's function	$[-]$
$\tilde{K}$	Mass-normalized stiffness matrix	$[s^{-2}]$
A	Cross-sectional area	$[m^2]$
A	State matrix	N/A
a	Distance between midchord and elastic axis in semichords	$[m]$
B	Input matrix	N/A
b	Semichord	$[m]$
C	Damping matrix	$[Nm^{-1}s, Nm\,s]$
C	Output matrix	N/A
C_D	Drag coefficient	$[-]$
c_i	Section midchord	$[m]$
C_L	Lift coefficient	$[-]$
C_M	Pitching moment coefficient	$[-]$
$c_{\dot{\xi}}$	Pitch velocity effect on effective angle of attack	$[rad]$
C_{aero}	Aerodynamic damping matrix	$[Ns, Nm^{-1}s, Nm\,s]$
C_{ee}	Damping matrix of elastic deformation modes	$[-]$
$C_{H\alpha}$	Effect of angle of attack on horizontal force	$[N]$
$C_{H\ddot{\alpha}}$	Effect of angular acceleration on horizontal force	$[Ns^2]$
$C_{H\ddot{h}}$	Effect of plunge acceleration on horizontal force	$[Nm^{-1}s^2]$
$C_{H\dot{\alpha}}$	Effect of angular velocity on horizontal force	$[Ns]$
$C_{H\dot{h}}$	Effect of plunge speed on horizontal force	$[Nm^{-1}s]$
C_{l0}	Lift coefficient at zero angle of attack	$[-]$
$C_{l\alpha}$	Lift curve gradient	$[-]$

$C_{L_V}(V)$	Effect of speed on lift	$[N]$
$C_{l_{\delta_a}}$	Stability derivative of L due to a change in δ_a	$[-]$
$C_{M\alpha}$	Effect of angle of attack on moment	$[Nm]$
$C_{M\ddot{\alpha}}$	Effect of angular acceleration on moment	$[Nm\,s^2]$
$C_{M\ddot{h}}$	Effect of plunge acceleration on moment	$[Ns^2]$
$C_{M\dot{\alpha}}$	Effect of angular velocity on moment	$[Nm\,s]$
$C_{M\dot{h}}$	Effect of plunge speed on moment	$[Ns]$
C_{n_p}	Stability derivative of n due to a change in p	$[-]$
C_{n_q}	Stability derivative of N due to a change in q	$[-]$
$C_{n_{\delta_a}}$	Stability derivative of n due to a change in δ_a	$[-]$
$C_{V\alpha}$	Effect of angle of attack on vertical force	$[N]$
$C_{V\ddot{\alpha}}$	Effect of angular acceleration on vertical force	$[Ns^2]$
$C_{V\ddot{h}}$	Effect of plunge acceleration on vertical force	$[Nm^{-1}s^2]$
$C_{V\dot{\alpha}}$	Effect of angular velocity on vertical force	$[Ns]$
$C_{V\dot{h}}$	Effect of plunge speed on vertical force	$[Nm^{-1}s]$
C_{X_β}	Stability derivative of X due to a change in β	$[-]$
C_{X_q}	Stability derivative of X due to a change in q	$[-]$
$C_{X_{\delta_e}}$	Stability derivative of X due to a change in δ_e	$[-]$
$C_{Y_{\delta_a}}$	Stability derivative of Y due to a change in δ_a	$[-]$
C_{Z_u}	Stability derivative of Z due to a change in u	$[-]$
D	Drag force	$[N]$
D	Feedthrough matrix	N/A
d_i	Distance between root and wing section	$[m]$
$d_{ea,0.75c}$	Distance between elastic axis and three-quarter-chord point	$[m]$
E	Elastic modulus	$[Pa]$
F_a	Aerodynamic reference frame	N/A
F_b	Body-fixed reference frame	N/A
F_c	Idealized control force	$[N]$
F_c^*	Idealized control coefficient	$[m^2]$
F_E	Vehicle-carried normal Earth reference frame	N/A
$F_{fw,eff}$	Effective flexible-wing reference frame	N/A
F_{fw}	Flexible-wing reference frame	N/A
F_{rw}	Rigid-wing reference frame	N/A
G	Shear modulus	$[Pa]$
g	Forward deflection	$[m]$
H	Force parallel to rigid-wing plane	$[N]$
h	Downward (plunge) deflection	$[m]$
$h_{\alpha,0.75c}$	Plunge translation due to pitch angle at three-quarter-chord point	$[m]$
I	Area moment of inertia	$[m^4]$
I	Identity matrix	$[-]$

J	Mass moment of inertia	$[kg\,m^2]$
J_i	Jacobian matrix	$[ms^{-2}, ms^{-2}N^{-1}, s^{-2}, s^{-2}N^{-1}]$
J_p	Polar moment of area	$[m^4]$
J_{bi}	Bending mass moment of inertia	$[kg\,m^2]$
J_{ti}	Torsion mass moment of inertia	$[kg\,m^2]$
K	Stiffness matrix	$[Nm^{-1}, Nm]$
k	Reduced frequency	$[-]$
k_2	Torsion constant	$[m^4]$
K_b	Bending stiffness matrix	$[Nm]$
K_t	Torsion stiffness matrix	$[Nm]$
K_{aero}	Aerodynamic stiffness matrix	$[N, Nm]$
k_{bi}	Bending stiffness coefficient	$[Nm]$
K_{ee}	Stiffness matrix of elastic deformation modes	$[-]$
k_{ti}	Torsional stiffness coefficient	$[Nm]$
L	Aerodynamic moment about the X_b-axis	$[Nm]$
L	Lift force	$[N]$
L_g	Gust length	$[s]$
M	Mass matrix	$[kg, kg\,m^2]$
M	Pitch-up moment	$[Nm]$
m	Number of modes included	$[-]$
m	Wing section mass	$[kg]$
M_b	Bending mass matrix	$[kg\,m^2]$
M_R	Reaction moment at root	$[Nm]$
M_t	Torsion mass matrix	$[kg\,m^2]$
M_{aero}	Aerodynamic mass matrix	$[Ns^2, Nm^{-1}s^2, Nm\,s^2]$
M_{ee}	Mass matrix of elastic deformation modes	$[-]$
M_{er}	Coupling mass matrix of rigid body to elastic deformation modes	$[-]$
M_{re}	Coupling mass matrix of elastic deformation to rigid body modes	$[-]$
M_{rr}	Mass matrix of rigid body modes	$[-]$
N	Aerodynamic moment about the Z_b-axis	$[Nm]$
n	Number of spanwise sections	$[-]$
$N_{control,flex}$	Number of control variables	$[-]$
N_{impl}	Number of implicit iterations	$[-]$
P	Matrix of eigenvectors	$[rad]$
p	Aircraft angular velocity about the X_b-axis	$[rad\,s^{-1}]$
q	Aircraft angular velocity about the Y_b-axis	$[rad\,s^{-1}]$
q	Dynamic pressure	$[kg\,m^{-1}s^{-2}]$
Q_e	Vector of generalized forces on elastic deformation modes	$[-]$
Q_r	Vector of generalized forces on rigid body modes	$[-]$
r	Aircraft angular velocity about the Z_b-axis	$[rad\,s^{-1}]$

r	Mode shape index	$[-]$
S	Non-normalized mode shape vector	$[rad]$
S	Side-force	$[N]$
S_i	Section surface area	$[m^2]$
T	Thrust force	$[N]$
T_{int}	Internal torsion moment	$[Nm]$
tol_{obj}	Objective tolerance	$[-]$
u	Aircraft velocity in X_b direction	$[m\,s^{-1}]$
u_E	Aircraft northward velocity	$[m\,s^{-1}]$
u_{rw}	Forward velocity in rigid-wing reference frame	$[m\,s^{-1}]$
V	Airspeed	$[m\ s^{-1}]$
V	Force orthogonal to rigid-wing plane	$[N]$
v_E	Aircraft eastward velocity	$[m\,s^{-1}]$
V_R	Vertical reaction force at root	$[N]$
W	Weight	$[N]$
w	Aircraft velocity in Z_b direction	$[m\,s^{-1}]$
w	Distributed load	$[Nm^{-1}]$
w_E	Aircraft downward velocity	$[m\,s^{-1}]$
w_g	Gust vertical velocity	$[m\,s^{-1}]$
w_{rw}	Downward velocity in rigid-wing reference frame	$[m\,s^{-1}]$
X	Aerodynamic force in X_b direction	$[N]$
x_E	Aircraft northward position	$[m]$
Y	Aerodynamic force in Y_b direction	$[N]$
y_E	Aircraft eastward position	$[m]$
Z	Aerodynamic force in Z_b direction	$[N]$
z_E	Aircraft downward position	$[m]$

Chapter 1

Introduction

1-1 Background

Flight mechanics and aeroelasticity are often treated as independent disciplines and simulations are performed using separate models. This is a valid assumption when coupling of the two is negligible, i.e. when structural vibration frequencies are considerably higher than the frequencies associated with flight mechanics. However, the current focus on weight minimization of aircraft leads to more and more flexible designs [1]. Therefore, the structure vibrates at a lower frequency [2], resulting in a decrease of the frequency separation between flight mechanics motion and structural vibrations [3].

Because of that, accurate load prediction requires a flight mechanics model that takes aeroelastic deformation into account. With accurate load prediction, structural integrity can be ensured and unstable flight conditions can be avoided. Furthermore, a better understanding of the coupled aeroelastic and flight mechanics response is crucial for the design of effective control systems. These systems may be used for active load alleviation, which can lead to increased passenger comfort, reduced fatigue and decreased loads on the wing structure [4]. Thus, the focus of aeroelastic research shifts from prevention of undesirable effects to exploitation of beneficial effects. A notable fact is that this is also the origin of aeroelastic research: the Wright brothers investigated aeroelasticity for their wing-warp method for roll control [5].

1-1-1 Aeroelasticity

A thorough understanding of aeroelasticity is essential in order to model flexible aircraft flight mechanics. In the following chapters, aeroelasticity is treated in detail, but a concise overview of the subject is presented here.

At the core of aeroelasticity is the interaction between elastic, inertial and aerodynamic forces, as is nicely shown in Collar's aeroelasticity triangle in figure 1-1 [6]. When the structure deforms, the aerodynamic forces change. This change in aerodynamic forces in turn causes

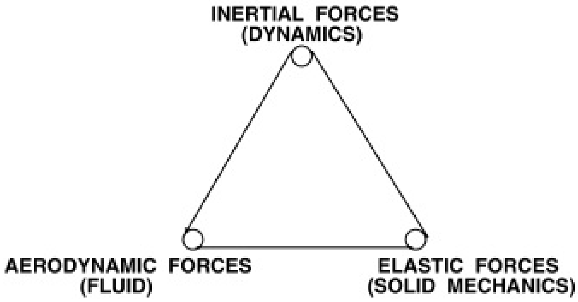

Figure 1-1: Collar's aeroelasticity triangle [7].

a structural deformation. This interference requires simultaneous simulation of the complete fluid-structure interaction system.

More recently, Friedmann extended Collar's triangle to include controls and thermal effects, as is shown in Figure 1-2 [8]. The upper half of the hexahedron represents aeroservoelasticity, which is the subject of this thesis. It includes the analysis of the aircraft response due to control input and the investigation of control algorithms for e.g. trim or load alleviation. This research field is evermore relevant, because of the rise of electronics, the improvement in sensors and the improving theories about automatic control [9].

The lower half of the hexahedron represents aerothermoelasticity, in which thermal effects are added to the classical aeroelastic model. Aerothermoelasticity is important in the hypersonic flight regime [10]. Since this is not the subject of the current research, it will not be treated.

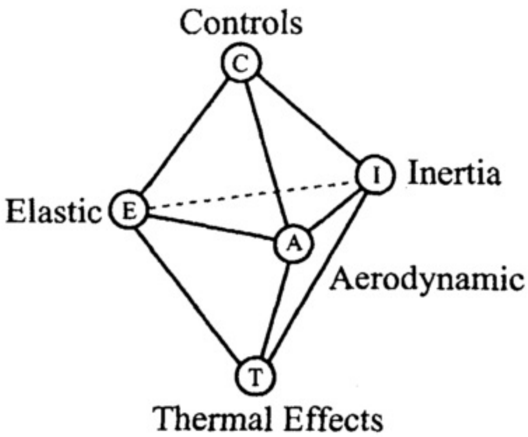

Figure 1-2: Friedmann's aeroelasticity hexahedron [8].

The aero(servo)elastic problem can be approached in several ways. One can look at the static (i.e. steady-state) response or one can also include transient effects and thus look at the dynamic response. In addition, one has to choose between searching for only aeroelastic instability limits or modeling the whole response. Aeroelastic instability can be of the form of divergence or flutter. Instability analysis simplifies the analysis by effectively ignoring most parts of the response and only looking for negatively damped motion. Since the goal of the current research is load prediction in the entire flight regime, the whole dynamic response of the structure must be modeled. This is the most demanding aeroelastic analysis that can be performed.

1-1-2 Current Status of Aeroelastic Flight Mechanics

Aeroelasticity of stationary wings is considered a mature research field and most conclusions therein are believed to remain valid and timeless [8]. However, aeroelasticity in general is still a field in development. Examples of subjects where major advancement is still taking place are aeroelasticity in the transonic flight regime [11], load alleviation using adaptive structures [12], and inclusion of aeroelasticity in flight mechanics [3]. This last challenge is the subject of the current research, which thence is positioned in a research field in progress.

Several attempts have already been made to create an effective Aeroelastic Flight Mechanics (AFM) model, but no consensus of modeling techniques has been reached. Indeed, computer simulation of the flight of flexible aircraft is no trivial matter [13]. Most models try to capture both disciplines in a unified model. For instance, Etkin [14], McLean [15] and Pedro [16] have augmented the traditional flight mechanics equations with elastic degrees of freedom. The aerodynamic effect was simply included as the product of the amplitudes of normal vibration modes and constant aerodynamic coefficients. Others, such as Waszak and Schmidt [17] and Reschke [18], derived a unified AFM model from first principles, using Lagrange's equations. All the above models assume decoupled flight mechanics and structural deformation (often by using the mean axes assumption), which is, unfortunately, too limiting [3]. A more inclusive, but more complex, approach to create a unified model was created by Meirovitch and Tuczu [13]. That approach includes coupling effects between flight mechanics and structural deformation using a multi-step approach assisted by perturbation methods. The interested reader is referred to the original paper where the model was derived [13].

Instead of a unified approach, a model can also use dedicated tools for the different disciplines associated with AFM. For instance, the models created by Schutte [19] or Snyder [20] couple three high-fidelity methods: Computational Fluid Dynamics (CFD), Finite Element Analysis (FEA) and a dedicated flight mechanics tool. This yields very accurate results, but unfortunately with a very high computational time, which is in the order of days for a four-second maneuver [21]. Often, a multibody dynamics system serves as the platform that couples the different disciplines. Various researchers [3, 22, 23] have combined a multibody systems approach (for structural deformation and for flight mechanics) with a CFD solver. The exact modeling techniques are the subject of chapters 2 and 5. By using the inherent strengths of the multibody dynamics approach, these researchers decreased computational time, whilst largely retaining model accuracy.

Models that are used in the preliminary design phase require a further reduction in computational time. This is usually achieved by using simpler aerodynamic models, such as a quasi-steady model or an unsteady panel method (see section 2-2). For instance, Zhao [24] has combined such an aerodynamic model with a lumped mass approach in the multibody environment. A model based on these assumptions also exists at the TU Delft and was created by Mark Voskuijl. Furthermore, Spieck [23] has conceptually described a model that uses simple aerodynamic models together with modal superposition in the multibody environment (see section 2-1). Further simplification is used for models that are used in the conceptual design phase. An example is NeoCass [25], in which the structural model is represented by simple beam elements.

1-2 Objectives, Scope and Structure

In the previous paragraphs, the general field of AFM was discussed. Now the specific context of this thesis will be treated.

1-2-1 Thesis Objective

The main goal of this thesis research is the creation of an Aeroelastic Flight Mechanics (AFM) model for gust and maneuver load prediction. This is highly relevant because it allows safer designs and paves the way for load alleviation efforts. The literature study, which was performed by the author prior to this work, concluded with the objective statement for the current research. The investigations leading to this statement will be concisely treated in chapters 2 and 5. The research objective is as follows:

To create an accurate and fast model for load prediction of subsonic, flexible aircraft by using structural modal superposition and quasi-steady aerodynamics fitted into a multibody system environment.

The model that will be created, consists of two levels. The first level is a model for the dynamic aeroservoelastic response of a single moving wing. This model captures the aerodynamics, the structural deformation and the effect of control input on wing deformation and root loads. The second level is the flight mechanics model, which combines several moving lifting surfaces using multibody system dynamics. These lifting surfaces are based on the model of the first level. The research sub-objectives are based on these two levels. They are:

a. To create an efficient model for the dynamic aeroservoelastic response of a single moving wing by combining quasi-steady aerodynamics and modal deformation in a partitioned manner.

b. To create a flight mechanics model for flexible aircraft by combining the models of several flexible lifting surfaces in a multibody system framework.

The research objective and sub-objectives require some context. The created model will be used to enhance the preliminary design capabilities at the TU Delft. As was stated in section 1-1-2, models for preliminary design require some simplifying assumptions, in order to reduce the computational time. The model that already exists at the TU Delft (created by Mark Voskuijl) is based on the structural lumped-parameter approach within a multibody dynamics framework. The novelty of the current research rests in the fact that the existing model will be improved by using structural modal superposition. Both approaches are treated in section 2-1.

It is expected that this improves both accuracy and computational cost, which constitutes the increased efficiency. Although this seems conflicting, literature suggests that this is possible. Accuracy is improved for two reasons. Firstly, because the lumped-parameter approach is not suited for load prediction and requires additional assumptions, in contrast to modal superposition [26]. And secondly, because the modal superposition approach can model more complex structures than the lumped-parameter approach, as long as they behave linearly [27].

This is the case for aircraft wings that are modeled in the current research (see section 2-1-2). The computational cost can be reduced for the following two reasons. Firstly, because modal superposition reduces the model size by several orders of magnitude [28]. And secondly, because modal superposition allows the use of a state-space representation, which can be solved very fast [29]. The improved model will enhance the preliminary aircraft design capabilities at the TU Delft.

The created model will be compared to the existing lumped-parameter model. It will also be compared to a rigid flight mechanics model, in order to investigate the effect of aeroelasticity on flight mechanics. The accuracy comparisons will be done for similar flight maneuvers. Although the structural model will be improved, inaccuracies will still exist because of the low-fidelity aerodynamic model. The study on accuracy improvement will thus focus on the improvement due to a change of the structural model. The computational effort for the different structural models can easily be compared, since all other parameters (i.e. aerodynamic and flight condition) remain unchanged. All this leads to the following research questions.

a. Can a lumped-parameter model for load prediction of subsonic, flexible aircraft be improved in terms of accuracy and computational cost by using structural modal superposition and quasi-steady aerodynamics in a multibody system environment?

b. What is the effect of elasticity of lifting surfaces on aircraft flight mechanics?

1-2-2 Thesis Scope

The thesis research has to be performed in a limited time span of seven months. Therefore, the research scope was defined at the beginning of the research.

The AFM model will be used for preliminary aircraft design at the TU Delft. To that end, multiple analysis tools are combined in the so-called Design and Engineering Engine, of which the paradigm is shown in figure 1-3. This figure basically shows that a design solution is determined by iteratively evaluating aircraft designs, starting from an initial design, which is based on top-level requirements. The current research creates a model that fits in the "Analysis tools". It receives input, e.g. structural or aerodynamic data, from the product model and from other analysis tools. After evaluation, it creates output which can be used by other tools. Since the created model is just one piece of the Design and Engineering Engine, the research will not focus on the creation of structural and aerodynamic input data, nor on aircraft design optimization. In addition, the model must be compatible with other tools that are used for preliminary aircraft design at the TU Delft and with the existing flight mechanics environment. This requires that the model is created in a MATLAB environment, or more specifically with the SimMechanics toolbox. SimMechanics is a part of Simulink and provides a multibody simulation environment.

All in all, the current research focuses on the creation of a model that is capable of simulating the flexible aircraft response and the associated loads on the structure. This must be possible for a variety of flight mechanics applications, such as control input and gust encounters. The creation of a control system or load alleviation algorithm is not part of the scope, but may be the subject of further research after the current work.

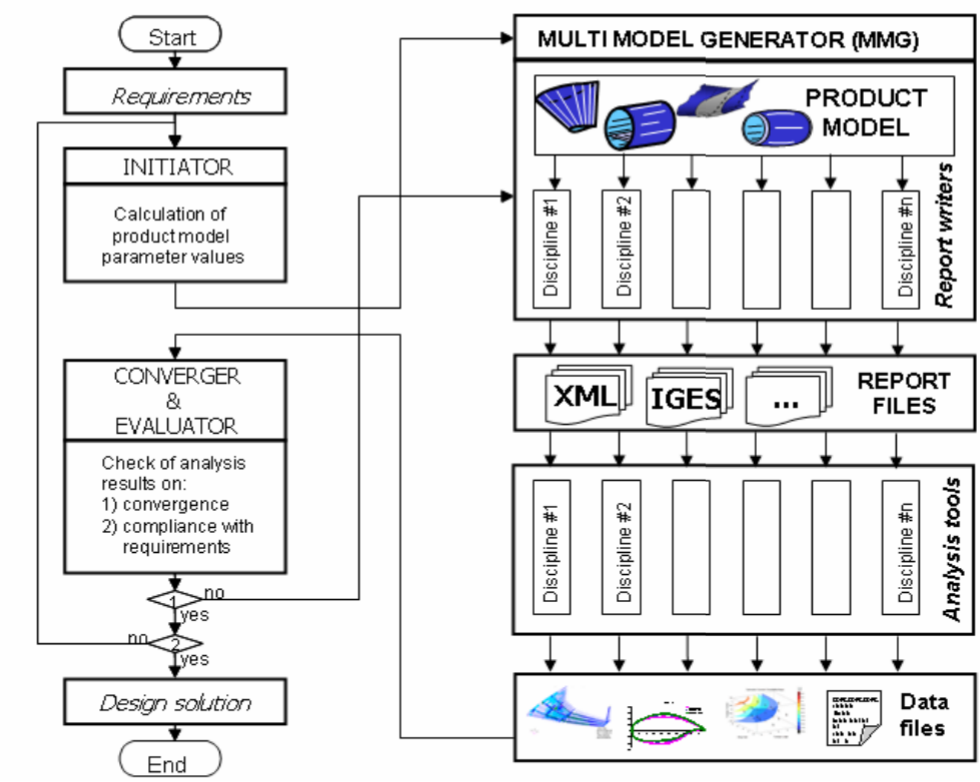

Figure 1-3: Paradigm of the Design and Engineering Engine [30].

1-2-3 Thesis Structure

This report consists of two main parts, reflecting the two levels of the model. Part I treats the aeroelastic wing model and consists of three chapters. First, chapter 2 treats the theoretical background for the structural model, the aerodynamics, the fluid-structure interaction and the effect of control surfaces on aerodynamics. Second, the subject of chapter 3 is the methodology, i.e. how this theory was used to create an aeroelastic wing model. And last, the verification of the aeroelastic wing model is discussed in chapter 4. This gives credibility to the aeroelastic wing model, which is at the core of the AFM model and forms the novelty of the current research.

Part II treats the AFM model, which encapsulates the aeroelastic wing model. Chapter 5 treats the theoretical background of the multibody systems environment, flight mechanics, trimming and linearization. Then, the methodology is the subject of chapter 6. In this chapter, the implementation of the AFM is discussed. Thereafter, verification is treated in chapter 7. Analyses and results are presented and discussed in chapter 8. There is some overlap in these last two chapters, since the verification studies already present interesting results of the AFM model. The results presented in chapter 8 focus more on the capabilities of the model and the effect elasticity has on flight mechanics. Lastly, the conclusions and recommendations are treated in chapters 9 and 10, respectively.

Part I

The Wing Model

Chapter 2

Aeroelastic Wing Theory

This chapter treats the theory behind the aeroelastic wing model. Section 2-1 discusses the structural model and section 2-2 treats the aerodynamic model. The combination of these two models, i.e. fluid-structure interaction, is the subject of section 2-3. Section 2-4 presents a short discussion about the influence of control surfaces on aerodynamics and wing deformation. Section 2-5 concludes the chapter with a short summary.

2-1 Structures

In this section, the structural model is discussed. This model captures both the deformation and the dynamics of a wing. In chapter 1 it was already stated that the modal approach will be used for the model, with the goal of improving the current aeroelastic model based on the Lumped-Parameter Method (LPM) approach. Note that the flight mechanics model is not treated here, but in chapter 6.

In section 2-1-1 this modal approach is explained, after which section 2-1-2 discusses the motivation behind using this approach. Then, the LPM approach is shortly treated in section 2-1-3, to gain an understanding of the model that is to be improved. Lastly, load prediction, being an important part of the model, is discussed in section 2-1-4.

2-1-1 The Modal Approach

The central assumption of the modal approach is the concept of modal superpositioning. This concept will be treated first, after which the application to an aeroelastic problem is discussed.

Modal Superpositioning

With modal superpositioning, it is assumed that the deflections of the structure can be represented as a linear combination of a limited set of vibration modes [31]. The amplitudes of these modes form the so-called generalized coordinates. The use of generalized coordinates makes the structural model compact: the system state is not defined by the deflections of every single node, but instead by only the amplitudes of the mode shapes. This reduces the structural model size by several orders of magnitude compared to an approach where all nodes are modeled individually, e.g. a finite element approach [28].

Figure 2-1 shows examples of mode shapes of a wing. In this figure, mode shape 2 (top-left), which has a low natural frequency, is the first bending mode. Mode shape 11 (bottom-right), with a higher natural frequency, is a higher torsional mode. The other modes are in between these two. The lower modes have lower frequencies and often higher amplitudes; thus the lower modes are more dominant than the higher modes. For this reason, higher modes are usually neglected in the modal approach.

Note that for simple, isotropic structures, made of e.g. metals, bending and torsion generally occur in distinct modes. For anisotropic structures, made of e.g. composites, or for more complex wings, coupling between torsion and bending often occurs within mode shapes [32]. Although these coupled mode shapes may be slightly more difficult to determine, they can be used to accurately represent the structure [32].

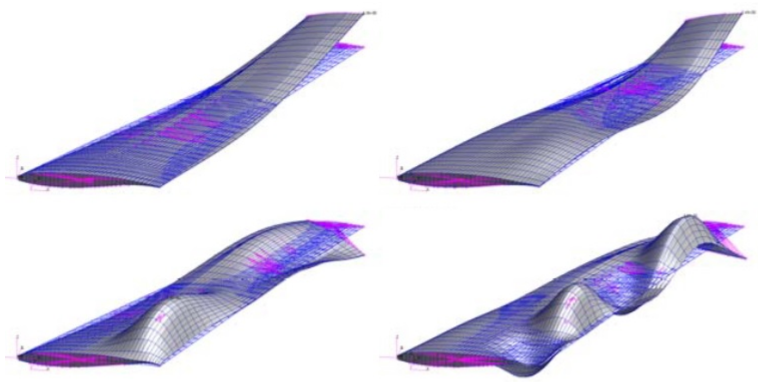

Figure 2-1: Mode shapes 2, 5, 6 and 11, determined with a finite element model [4].

Equation (2-1) is the governing equation of the modal approach. In this equation, Φ is the matrix that holds the relevant (i.e. lower) mode shapes as its columns. These mode shapes are orthogonal and can be normalized [33]. A column of Φ contains the values of the different degrees of freedom (rotations and translations of all nodes of interest) relative to one another for the particular mode shape. The columns of Φ are normalized, which determines the actual values of the column entries. Furthermore, $\mathbf{s}$ is the vector of response coordinates, which are the values of the degrees of freedom, and $\mathbf{q}$ is the vector of generalized coordinates, which are the amplitudes of the mode shapes. In essence, equation (2-1) represents a coordinate transformation from the physical coordinates $\mathbf{s}$ to the modal coordinates $\mathbf{q}$. This coordinate transformation causes the reduction of the structural problem size.

$$\mathbf{s}(t) = \Phi\mathbf{q}(t) \tag{2-1}$$

Application to Aeroelasticity

The coordinate transformation is often used for aeroelastic problems, which is the subject of this section. First, consider equation (2-2), which shows the general equation of vibration. In this equation, M is the mass matrix, C is the damping matrix, and K is the stiffness matrix. Furthermore, $\mathbf{s}$ is the vector of response coordinates. It is of the form shown in equation (2-3), where h is the downward deflection, or plunge, g is the forward deflection, or sweep, and ξ is the pitch-up deflection, or twist. The subscripts refer to the spanwise section, ranging from 1 to the number of spanwise sections, n. Lastly, $\mathbf{F}$ represents the external force vector. It is of the form shown in equation (2-4), where V is the downward force, H is the forward force and M is the pitch-up moment.

$$M\ddot{\mathbf{s}} + C\dot{\mathbf{s}} + K\mathbf{s} = \mathbf{F} \tag{2-2}$$

$$\mathbf{s} = \begin{bmatrix} h_1 & g_1 & \xi_1 & \cdots & h_n & g_n & \xi_n \end{bmatrix}^T \tag{2-3}$$

$$\mathbf{F} = \begin{bmatrix} V_1 & H_1 & M_1 & \cdots & V_n & H_n & M_n \end{bmatrix}^T \tag{2-4}$$

Since mode shapes are often determined in an environment without damping and external forces, equation (2-5) shows the absence of damping and external forces. This equation will be solved in the following. Structural damping and external forces will be added later in this section.

$$M\ddot{\mathbf{s}} + K\mathbf{s} = \mathbf{0} \tag{2-5}$$

A solution to differential equation (2-5) of the form $\mathbf{s}(t) = \phi e^{i\omega t}$ is proposed. Substituting this solution in (2-5), one obtains equation (2-6). This equation represents a typical eigenvalue problem. There are a number of eigenvectors ϕ that solve the eigenvalue problem for corresponding eigenvalues ω^2. Note that these eigenvectors represent the mode shapes of the structure and ω represents a natural frequency related to a mode shape.

$$K\phi = \omega^2 M\phi \tag{2-6}$$

The mode shapes are orthogonal with respect to the mass and stiffness matrices [33]. If the mode shapes are normalized with respect to the mass matrix and thus become "M-orthonormal", equation (2-7) holds. In this equation δ_{ij} is the Kronecker delta, which is zero for every combination of i and j, except when $i = j$, in which case it is 1. M-orthonormality can also be written using the mode shape matrix, as is shown in equation (2-8). In this equation, I is the identity matrix.

$$\phi_i^T M \phi_j = \delta_{ij} \tag{2-7}$$

$$\Phi^T M \Phi = I \tag{2-8}$$

If the coordinate transformation to modal coordinates of equation (2-1) is applied to equation (2-2) and if all terms are pre-multiplied with Φ^T and equation (2-8) is substituted, this yields equation (2-9) [26]. In this equation, Λ is the spectral matrix with the eigenvalues (the natural frequencies squared) on the diagonal, as is shown in equation (2-10). This is a property of the eigenvalue problem [2]. Γ is the modal damping matrix, which will be treated subsequently.

$$I\ddot{\mathbf{q}} + 2\Gamma\dot{\mathbf{q}} + \Lambda\mathbf{q} = \Phi^T\mathbf{F} \tag{2-9}$$

$$\Lambda = \Phi^T K \Phi = \begin{bmatrix} \omega_1^2 & & \\ & \ddots & \\ & & \omega_m^2 \end{bmatrix} \tag{2-10}$$

Note that without Γ and $\mathbf{F}$, the system of vibration equations in (2-9) could be uncoupled because matrices I and Λ are diagonal. Generally, the modal damping matrix Γ is not diagonal, because the mode shapes are not orthogonal with respect to the damping matrix. However, an assumption that is often used is that the damping occurs in the form of "Rayleigh Damping" [34]. A definition of Rayleigh Damping is given in equation (2-11), which shows that the damping matrix C is a linear combination of mass matrix M and stiffness matrix K (c_1 and c_2 are constant scalars). Since M and K are diagonal, the damping matrix becomes diagonal as well. If Rayleigh Damping is assumed, the modal damping matrix Γ in equation (2-9) will be of the form shown in equation (2-12). This type of damping is also called "proportional damping", since every mode is individually damped, because of its diagonal form [26]. In this equation ζ represents the modal damping ratio. Proportional damping might look like a restrictive assumption. However, as damping is difficult to determine for complex structures (such as a wing), the extra error in assuming proportional damping is of the order of the error in the original damping matrix itself [35]. Because proportional damping does not introduce large inaccuracies, this assumption is made in the current research.

$$C = c_1 M + c_2 K \tag{2-11}$$

$$2\Gamma = \Phi^T C \Phi = \begin{bmatrix} 2\zeta_1\omega_1 & & \\ & \ddots & \\ & & 2\zeta_m\omega_m \end{bmatrix} \tag{2-12}$$

At this point, a structural state-space system can be created which allows fast computation of the structural deformation in the SimMechanics environment, in which the model is made (see chapter 1) [26]. A state-space system has the form of equation (2-13). Here $\mathbf{x}$ is the vector containing the state variables that represent the entire state of the system, $\mathbf{y}$ is the vector containing the output variables, $\mathbf{u}$ is the vector containing the input variables, A is the state matrix, B is the input matrix, C is the output matrix and D is the feedthrough matrix.

$$\begin{aligned} \dot{\mathbf{x}} &= A\mathbf{x} + B\mathbf{u} \\ \mathbf{y} &= C\mathbf{x} + D\mathbf{u} \end{aligned} \tag{2-13}$$

One can now define the state vector $\mathbf{x}$ as in equation (2-14), which will prove to be sufficient to define the system. The output vector $\mathbf{y}$ is defined in equation (2-15) and contains the vector of response coordinates, the vector of modal coordinates and their first and second derivatives. Input $\mathbf{u}$ is simply the external force vector $\mathbf{F}$ from equation (2-2). Now the state equation can be created from equation (2-9), yielding equation (2-16). The output equation is shown in equation (2-17).

$$\mathbf{x} = \begin{bmatrix} \mathbf{q} \\ \dot{\mathbf{q}} \end{bmatrix} \tag{2-14}$$

$$\mathbf{y} = \begin{bmatrix} \mathbf{s} \\ \dot{\mathbf{s}} \\ \ddot{\mathbf{s}} \\ \mathbf{q} \\ \dot{\mathbf{q}} \\ \ddot{\mathbf{q}} \end{bmatrix} = \begin{bmatrix} \Phi\mathbf{q} \\ \Phi\dot{\mathbf{q}} \\ \Phi\ddot{\mathbf{q}} \\ \mathbf{q} \\ \dot{\mathbf{q}} \\ \ddot{\mathbf{q}} \end{bmatrix} \tag{2-15}$$

$$\begin{bmatrix} \dot{\mathbf{q}} \\ \ddot{\mathbf{q}} \end{bmatrix} = \begin{bmatrix} 0 & I \\ -\Lambda & -2\Gamma \end{bmatrix} \begin{bmatrix} \mathbf{q} \\ \dot{\mathbf{q}} \end{bmatrix} + \begin{bmatrix} 0 \\ \Phi^T \end{bmatrix} \mathbf{F} \tag{2-16}$$

$$\begin{bmatrix} \Phi\mathbf{q} \\ \Phi\dot{\mathbf{q}} \\ \Phi\ddot{\mathbf{q}} \\ \mathbf{q} \\ \dot{\mathbf{q}} \\ \ddot{\mathbf{q}} \end{bmatrix} = \begin{bmatrix} \Phi & 0 \\ 0 & \Phi \\ -\Phi\Lambda & -2\Phi\Gamma \\ I & 0 \\ 0 & I \\ -\Lambda & -2\Gamma \end{bmatrix} \begin{bmatrix} \mathbf{q} \\ \dot{\mathbf{q}} \end{bmatrix} + \begin{bmatrix} 0 \\ 0 \\ \Phi\Phi^T \\ 0 \\ 0 \\ \Phi^T \end{bmatrix} \mathbf{F} \tag{2-17}$$

Besides the above mathematical derivation of the modal state-space system, the mode shapes themselves are also of interest. The number of modes required to achieve accurate results for a wing depends on the suitability of the modes. In theory any set of modes could be used to model the structural deformation and vibration, but many different modes would be required to attain a desirable accuracy. In practice, a set of free-free vibration modes is mostly used for aeroelastic applications [27, 36]. Here "free-free" means that no forces and moments are applied at both ends. This is appropriate because the aircraft is in the free-flight condition [37]. Literature suggests that the number of modes m that should be included for an accurate Aeroelastic Flight Mechanics (AFM) analysis should be between 15 [33] and 25 [28].

The mode shapes must be defined with respect to a constant equilibrium position, because they represent the deflection from this equilibrium. Since the mode shapes are determined for a structure vibrating in vacuo (i.e. without aerodynamic forces), the equilibrium position is the shape of the wing on the ground. The reference plane for the mode shapes will be the plane in which the wing root chordline lies (the "rigid wing plane" treated in section 3-2-2). The mode shapes themselves represent the forward, downward and pitch up position of the elastic axis at the center of each wing section. Note that secondary motion, e.g. inward translation of the wing tip due to plunge, is ignored.

2-1-2 Motivation behind the Modal Approach

The use of mode shapes often leads to acceptable estimations of structural dynamics [38] and particularly aeroelastic analysis [28]. The approach is applicable to complex systems, such as aircraft wings [26] and is very efficient [31]. Once the mode shapes are determined in a pre-processing step, the aeroelastic simulations with the modal approach have been reported to be 17 times faster than those with a finite element approach [28]. This huge decrease in computational time can be accredited to the fact that a finite element approach simulates every node separately. The modal and LPM approach only uses generalized coordinates, creating a very compact model.

The modal approach is also faster and more accurate than the LPM approach, which is used in the current aeroelastic model at the TU Delft. As will become clear in the next section, the LPM approach introduces an inaccuracy, since bending moments are not correctly represented as a function of bending angles [26]. Furthermore, it is expected that the modal approach will be much faster. For stiff structures like a wing, SimMechanics will have to take a small time-step to accurately determine the high-frequency dynamic behavior of the wing. This increases the computational time for the LPM model, but less so for the modal approach, because of the use of a fast, uncoupled state-space system. This will be investigated in chapter 8.

The modal approach might introduce inaccuracies because it has constant modes and thus assumes structural linearity. Aeroelastic analyses using constant modal information can give inaccurate results for nonlinear structures, and may require a relatively large number of modes to obtain a reasonable level of accuracy [39].

Structural nonlinearities may be concentrated or distributed. Examples of concentrated structural nonlinearities are freeplay in a control surface hinge and concentrated loads [39, 28]. Distributed nonlinearities (e.g. wing buckling) are often caused by large local structural changes [28]. The concentrated nonlinearities are mainly a problem in stress analysis; in flight mechanics however, net loads are important and these can be adequately determined with the modal approach [28, 40].

Distributed nonlinearities do not seem to be a problem for the current research, since most aeroelastic analyses of flight vehicles have been performed under the assumption of small displacements and restoring forces proportional to the displacements [39]. This includes load prediction for certification purposes [41]. Literature suggests that structural nonlinearities due to large deformation primarily exist for very high aspect ratio wings (in the order of 35 [40]). Such wings are used for e.g. high-altitude long-endurance aircraft such as the HELIOS [42]. For relatively low-aspect-ratio conventional wings, however, the effects of structural nonlinearities seem to be small [43].

Because the main disadvantages of the modal approach are not relevant for flight mechanics applications, the advantages of the approach outweigh the disadvantages. Therefore the modal approach is chosen as the structural model.

2-1-3 The Lumped-Parameter Approach

The Lumped-Parameter Method (LPM) approach is a straightforward way of modeling the continuous wing by a set of rigid elements that are coupled by springs and dampers. The fact that rigid elements are used, makes this method easily compatible with the SimMechanics multibody dynamics environment [26]. Because of that reason, this method has already been implemented at the TU Delft. As was stated before, the goal of the current research is to improve on this model by using more effective methods. Since the LPM model forms the starting point of the research, it will be shortly described here.

With the LPM, the structure is discretized into a number of identical generalized beam elements, where each of these beam elements is a body-joint-body combination, as can be seen in figure 2-2. In this figure, each generalized beam element is connected to another beam element with a weld (W) and within each beam element there is a joint (J) between two bodies (B). Figure 2-3 shows a single generalized beam element. The characteristics of the joint, i.e. the stiffness and damping coefficients, are chosen to reflect the characteristics of the part of the beam it describes [26]. The equations of motion are constructed automatically in the SimMechanics multibody environment.

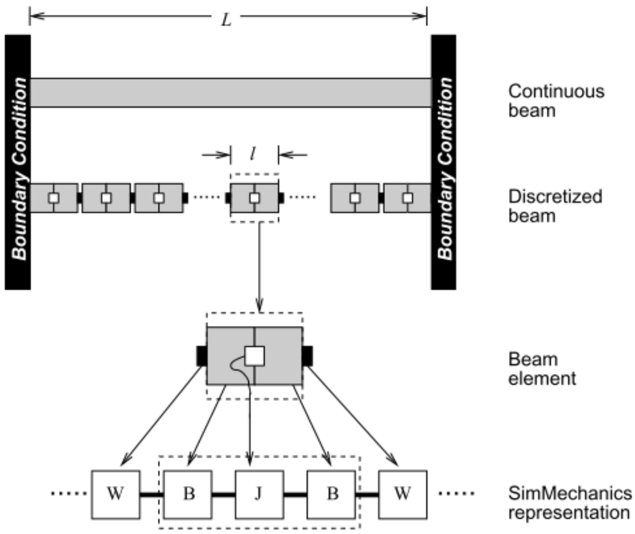

Figure 2-2: The lumped-parameter discretization of a beam [26].

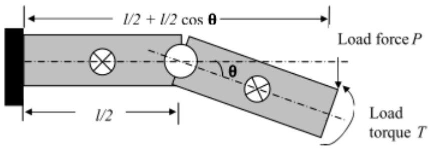

Figure 2-3: A single generalized beam element [26].

The method creates a compact model that can still capture the dynamic response of the structure, since it does not model every node, but instead uses generalized coordinates. These generalized coordinates are the degrees of freedom of the generalized beam elements (θ in figure 2-3).

The method can be extended to represent more complex geometry (e.g. aircraft wings), but this can better be modeled with other approaches (e.g. the modal approach) [26]. Furthermore, the bending moment is not correctly represented as a function of beam bending angles, since the bending moment at a particular beam element depends only on the deflection of that beam element. In reality, the bending moment also depends on the neighboring deflection angle [26]. This could be solved by building a custom-made joint that takes into account the deflection angles of multiple elements in order to determine the joint deflection and reaction force. Unfortunately, the beam elements are then interdependent, and simple determination of joint primitives is no longer possible. For these reasons, the LPM approach is not the most appropriate method to use for modeling aeroelastic wing deformation.

2-1-4 Load Prediction

After the current research, the aeroelastic model may be used in load alleviation systems. The goal of load alleviation is to decrease the extreme wing-bending moments and wing-tip accelerations [44]. Peak loads may occur in flight due to gusts or maneuvers and could be much higher than the loads during normal flight [4]. Control systems can be used to reduce the dynamic response to gusts and maneuvers. Critical design loads can thus be alleviated significantly: in the order of 10% [44]. Because of that, fatigue is potentially decreased, passenger comfort is increased and a more efficient wing may be designed [4].

The first step in load alleviation is good load prediction [4], which is treated here. Once the loads can be predicted, an active control algorithm may be used to alleviate the loads. Interesting variables to predict are the wing-tip acceleration and the wing-root shear force, bending moment and torsion moment. The first can be used as input for control algorithms, since it is a good indicator of an upcoming peak of the wing-root bending moment [44]. The other variables must be minimized in the load alleviation process. Most focus is usually on minimizing the wing-root bending moment without degrading the shear force and torsion moment [44].

Determination of net loads during maneuvers or extreme gusts is often the primary purpose of the response analysis. Two methods are widely used for calculating dynamic loads: the Mode-Displacement (MD) method and the Summation of Forces (SOF) method [44].

In the MD method, the loads are directly obtained from the modal displacements. Equation (2-18) represents the main assumption in the MD method. In this equation $\mathbf{P}$ is a vector containing the net loads. These net loads are determined by multiplication of the stiffness matrix K and the response (displacement) vector $\mathbf{s}$. The net loads $\mathbf{P}$ must be integrated to calculate e.g. the root bending moment. This is done using so-called "load modes", which can be determined from geometry or using fictitious masses [45].

$$\mathbf{P}(t) = K\mathbf{s} = K\Phi\mathbf{q}(t) \tag{2-18}$$

In the SOF method, loads are based on the summation of aerodynamic and inertial forces [45]. These would normally be determined in the frequency domain and then transformed to the time domain by Inverse-Fourier transforms [45]. In the Multibody System Dynamics (MSD) simulation that is used in the current research, the forces are already obtained in the time domain and integration of these forces can be done automatically in the MSD environment [26].

Although in general the MD method is better equipped to address the prediction of loads [44], the SOF method will be used here, because it exploits the advantages of the MSD environment in which the model is constructed.

2-2 Aerodynamics

In this section, the aerodynamic part of the aeroelastic wing model is discussed. Aerodynamic analysis can be a very demanding part of an aeroelastic analysis. It has been reported that for a high-fidelity aeroelastic analysis (using a Reynolds-Averaged Navier-Stokes approach), 60% of CPU time was spent on fluids, 38% on mesh deformation required for the aerodynamic analysis and only 2% on structures [46]. Another study showed that the total time required for aeroelastic analysis of a four-second maneuver using high-fidelity CFD methods is 35 hours on a 32-processor SGI Origin 2000 [21]. Indeed, the major limitations of applying complex CFD codes are the computational time and memory requirement [38]. On the other hand, the simple algebraic equations of (quasi-)steady methods require very little computational time.

As was stated in chapter 1, a main requirement of the program is that it should have low computational cost, so that it can be applied rapidly in preliminary design. Therefore, it is clear that choosing an appropriate aerodynamic model is paramount for the performance of the aeroelastic program. The typically high computational cost of aerodynamic analysis forces upon us the delicate choice of finding a method that is accurate enough for the prospected applications and requires a minimum amount of computational cost. This decision is made step by step in the following sections.

2-2-1 Linear or Nonlinear

The first decision that should be made is whether a linear model suffices for the prospected applications, or whether nonlinear aerodynamic effects should be included. Nonlinear models are based on e.g. the Navier-Stokes equations, the Euler equations or the full potential equation [47]. Linear models are much simpler and are based on, for instance, a Doublet-Lattice Method (DLM) or a (quasi-)steady method.

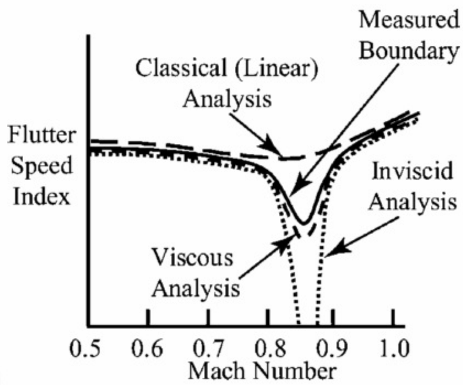

Figure 2-4: Flutter speed index prediction for different Mach numbers [48].

Figure 2-4 shows the flutter speed index as a function of Mach number. The flutter speed index is a non-dimensional form of speed at which flutter instability just occurs. From the figure it is clear that linear analysis can accurately describe the flutter speed index for subsonic Mach numbers below approximately 0.75. In the transonic regime however, figure 2-4 shows highly nonlinear aerodynamic effects, making aeroelastic analysis significantly more complicated. In this regime, shock waves can form and disappear as the aircraft undergoes structural deflection. Furthermore, regions of separated flow can appear and disappear as these shock waves strengthen and weaken [48].

Because the model is focused on aircraft in the subsonic speed range, linear aerodynamic models are accurate enough and will be used. Many authors agree that linear models can accurately describe subsonic aeroelasticity with attached flow [8, 10, 49, 50].

2-2-2 Steady, Quasi-Steady or Unsteady

The next choice that should be made is whether to use a steady, quasi-steady or unsteady aerodynamic model [7], which are explained next.

- **Steady models**: Aerodynamic forces and moments are only dependent on instantaneous position and orientation. In practice, they only depend on the instantaneous angle of attack. This dependency can be modeled in the form of a look-up table, or a simple algebraic equation.
- **Quasi-steady models**: Aerodynamic forces and moments are dependent on the instantaneous position, orientation and motion, which form an equivalent steady aerodynamic situation. This entails the assumption that motion occurs at a low frequency. Because second and higher order derivatives are omitted, inertial and history effects are neglected [51], as well as the influence of the wake [38]. Again a look-up table or a simple algebraic equation is used.
- **Unsteady models**: Aerodynamic forces and moments are dependent on the complete time history of the flow. The unsteady effects become clear when one looks at the wake of an oscillating profile, as is shown in figure 2-5. When vorticity develops around an airfoil (thus creating lift), a vortex of the same strength but opposite direction is shed into the wake. The downwash from this vortex changes the flow that impinges on the profile, which changes the effective angle of attack [52]. In a dynamic situation, the strength and direction of the shed vortex change with time as the profile oscillates, which can be observed in figure 2-5. Other unsteady effects are due to compressibility (e.g. time delays due to the presence of shocks), airfoil thickness, flow separation (e.g. dynamic stall) and viscosity [52]. An example of a linear, unsteady model is a DLM model.

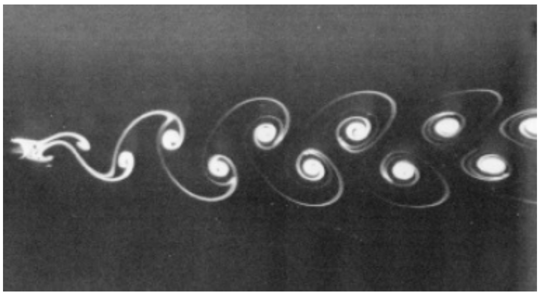

Figure 2-5: Wake vortices shed by an oscillating profile [53].

These three types of models are now compared to assess which performs best for the goals of the current research. The steady model has little advantages over the quasi-steady model. Both are easily applied and the difference in computational time is negligible. Quasi-steady models include aerodynamic damping, which may be important in determining aeroelastic responses [51]. For these reasons, the steady model will not be used.

Literature does not provide a definitive answer to the question whether a quasi-steady or an unsteady aerodynamic method should be used. Quasi-steady models are still very popular in early design stages because of their simplicity and low computational cost. They are accurate for low frequency motion [7, 51], which is one of the reasons that they are sometimes referred to as "low-frequency models". However, literature suggests that these models are not very reliable for flutter determination of subsonic flows, because unsteady aerodynamic terms are significant [38, 54].

As was stated in chapter 1, it is not the goal of this research to determine instability boundaries, but rather to determine the dynamic response in certification flight. It is mainly in aeroelastic instability situations that quasi-steady models are inaccurate [38, 54], so at this point it is decided to use a quasi-steady model. In order to justify the quasi-steady approach, it is assumed that the wing oscillations occur at low frequency.

2-2-3 Theory of Quasi-Steady Models

Now a closer look is taken at quasi-steady models, in which aerodynamic forces and moments are dependent on the instantaneous Position, Orientation and Motion (POM). Although this assumption might appear to be quite straight-forward, it is not unambiguous and there are several ways to apply the quasi-steady approximation [7].

The most extensive quasi-steady model reported in literature is based on an approximation of Theodorsen's function. Theodorsen's theory is developed for a thin airfoil undergoing small harmonic oscillations in incompressible flow. Equation (2-19) shows Theodorsen's equation for determining lift [52]. In this equation, L is the lift force, C_{l0} is the lift coefficient at zero angle of attack and $C_{l\alpha}$ is the lift curve gradient. Furthermore, ρ is the air density, b is the semichord, h is the plunge translation, a is the distance between the midchord point and the elastic axis as a fraction of the semichord, u is the air flow speed and α is the local angle of attack.

A very interesting variable in equation (2-19) is $\mathbf{C}(k)$, which is called Theodorsen's function. This function is determined separately and is used to describe circulatory effects. It is a complex-valued function of the reduced frequency k and is a ratio of Hankel functions [55]. Circulatory effects are dependent on motion history and the wake, while noncirculatory effects simply represent acceleration of fluid surrounding the oscillating body [38]. For the quasi-steady model, equation (2-19) can be used with $\mathbf{C}(k)$ constant and equal to one, which corresponds to a reduced frequency k of zero [56]. Thus, the equations become simple algebraic functions of the POM.

$$L = \rho b u^2 C_{l0} + \pi \rho b^2 \left(\ddot{h} - ba\ddot{\alpha} + u\dot{\alpha}\right) + C_{l\alpha}\rho b u^2 \mathbf{C}(k) \left[\frac{\dot{h}}{u} + b\left(\frac{1}{2} - a\right)\frac{\dot{\alpha}}{u} + \alpha\right] \tag{2-19}$$

Note that lift, drag and moment look-up tables can also be used for this quasi-steady model. In order to apply this approach, the effective angle of attack α_{eff} has to be used. This α_{eff} should be measured at the three-quarter-chord point [38]. As will become clear in the following, α_{eff} can be deduced from equation (2-19), noting that it is approximately the part between square brackets, as is shown in equation (2-20). The terms that are omitted because of this approach, i.e. the terms dependent on $\ddot{\alpha}$ and $\ddot{h}$, have a relatively small effect compared to other terms [7].

$$\alpha_{eff} \approx \frac{\dot{h}}{u} + b\left(\frac{1}{2} - a\right)\frac{\dot{\alpha}}{u} + \alpha \tag{2-20}$$

As is shown, α_{eff} depends on the regular angle of attack α, but also on motion-dependent terms based on plunge speed $\dot{h}$ and the time derivative of angle of attack, $\dot{\alpha}$. Note that α_{eff} depends on $\dot{\alpha}$, because it causes plunge of the three-quarter-chord point. In order to recognize this, first consider equation (2-21), which relates the three-quarter-chord point plunge due to pitch ($h_{\alpha,0.75c}$) to the angle of attack α. In the equation, $d_{ea,0.75c}$ is the chordwise distance between the elastic axis (about which the airfoil pitches) and the three-quarter-chord point. If equation (2-21) is now differentiated with respect to time, this yields equation (2-22). This equation shows the relation between the pitching velocity $\dot{\alpha}$ and the three-quarter-chord point plunge speed due to pitching velocity, i.e. $\dot{h}_{\dot{\alpha},0.75c}$. This relation was also present in equation (2-19), in which a small-angle approximation was used, so that the cosine was assumed to be equal to 1.

$$h_{\alpha,0.75c} = d_{ea,0.75c} \sin\alpha = b\left(\frac{1}{2} - a\right)\sin\alpha \tag{2-21}$$

$$\dot{h}_{\dot{\alpha},0.75c} = b\left(\frac{1}{2} - a\right)\cos\alpha\dot{\alpha} \tag{2-22}$$

In equation (2-20), another small-angle approximation was used to determine the effect of plunge speed on α_{eff}. In reality, the effect on the angle of attack is not the ratio of downward and forward speed, but the arctangent of that ratio. This is shown in equation (2-23), which presents the final form of the effective angle of attack, that will be used in the model. Note that removing small-angle approximations improves the accuracy of the model with respect to the quasi-steady models presented in literature, without much extra computational cost. In the multibody systems environment, the local velocities and angles can be measured or calculated, as will be discussed in section 3-2-2.

$$\alpha_{eff} = \tan^{-1}\left(\frac{\dot{h} + \dot{h}_{\dot{\alpha},0.75c}}{u}\right) + \alpha = \tan^{-1}\left(\frac{\dot{h} + b\left(\frac{1}{2} - a\right)\cos\alpha\dot{\alpha}}{u}\right) + \alpha \tag{2-23}$$

If a simple equation like equation 2-19 is used instead of look-up tables, lift has a proportional relation to α_{eff}. With look-up tables, however, a nonlinear relationship between α_{eff} and lift becomes possible. That is because a higher-fidelity aerodynamic code may be used to determine the entries of the look-up tables in a pre-processing step. Thus, various nonlinear effects, such as trailing-edge stall, can be included in the model. The higher-fidelity code also allows inclusion of compressibility effects and three-dimensional wing effects. Because of these advantages, look-up tables are used in the model, created for the current research.

A remark must be made regarding the compatibility of the aerodynamic model to the structural model. As was discussed in section 2-1, the wing is modeled as a number of spanwise sections that can move freely relative to each other (driven by the state-space system). Because of this, the strip theory assumption is made. In this approximation, each spanwise station of a wing is treated as though it were a portion of an infinite wing with uniform spanwise properties. Therefore, the lift and moment at one station are independent of what happens at other stations and two-dimensional aerodynamic theory can be used [7]. This greatly simplifies the coupling between structure and aerodynamics (also see section 2-3-3). Literature suggests that strip theory satisfies the main requirements for an aeroelastic model: sufficiently fast computation for time domain analysis with a small time step and compatibility with the frame in which structural forces and dynamics are defined [13]. The development of a more accurate aerodynamic model specifically suited to the needs of aeroelastic models still remains a challenge [13].

For lower aspect ratio wings, strip theory disagrees with higher-fidelity models, because of three-dimensional effects. However, when the static lift slope at sections near the tip is corrected to match higher-fidelity models, strip theory approaches the accuracy of unsteady panel methods, as long as the motion frequency is low [57]. In other words, strip theory with a tip correction is accurate in quasi-steady situations.

To conclude, the aerodynamic model that will be used consists of look-up tables with a quasi-steady model based on Theodorsen's theory, assuming strip theory with a tip correction.

2-3 Fluid-Structure Interaction

The subject of this chapter is the coupling of the structural and aerodynamic models treated in sections 2-1 and 2-2. In essence, Fluid-Structure Interaction (FSI) is a three-field problem which involves the fluid field, the structural field and the fluid mesh field [58]. The fluid mesh field deals with the fact that the mesh changes over time due to structural deformation. However, since it is not necessary to consider a changing mesh for a quasi-steady aerodynamic model [25], the following discussion will focus solely on combining the aerodynamic and structural models.

First, the difference between partitioned and monolithic approaches will be presented in section 2-3-1. Then, section 2-3-2 will treat several available partitioned simulation procedures. In these two sections, the choice of a specific method for the model is discussed. Lastly, in section 2-3-3 the effects of combining aerodynamic and structural models are discussed.

2-3-1 Partitioned and Monolithic Approaches

There are two approaches that can be used to model FSI. In the so-called partitioned approach, the aerodynamic and structural equations are integrated over time in an alternating manner and the interface conditions are enforced asynchronously. With the so-called monolithic approach, FSI is treated synchronously, meaning that all involved equations are in agreement within every time step [59].

In the partitioned approach separate models may be used, because of the modularity of the framework [46]. The data is transferred between the two models during the analysis. The monolithic method requires a different approach. If a completely linear aerodynamic model is employed (e.g. DLM or quasi-steady equations), this can be accomplished by including the aerodynamic equations in the structural state-space system forming a so-called aeroelastic state-space system. For aerodynamic models that are not completely linear (e.g. look-up tables or high-fidelity models), there are two options for the monolithic approach. First, the nonlinear model can be fit into a state-space system using indicial functions, based on superposition of aerodynamic effects due to step deformations (see [60, 61] for more information). Second, multiple fluid-structure iterations can be performed within one time step, until a converged solution is reached. This "converged co-simulation" approach is typically used for high-fidelity models.

The FSI approach must fit the methods used to model the structural behavior and aerodynamics of the system, i.e. a state-space modal superposition approach and a quasi-steady model based on Theodorsen's theory, assuming strip theory. The fact that a relatively simple aerodynamic model is used, makes the converged co-simulation method unnecessary. Converged co-simulation requires computational effort that is an order of magnitude higher than a partitioned or a monolithic state-space method [22]. Therefore, one of the latter two will be used in the model and these are compared in the next paragraph.

A great advantage of the partitioned approach over the monolithic state-space approach is the simplicity of its implementation, because of the modularity of the framework [46]. Another advantage is that it has a lower computational cost than monolithic state-space methods [59]. In addition, its accuracy will be close to that of a monolithic state-space approach [58]. However, for some problems the partitioned approach has been numerically unstable, where the monolithic approach appeared to be unconditionally stable [59]. The largest disadvantage of the monolithic state-space approach, is that it is only accurate for (approximately) constant airspeed, which cannot be generally assumed in flight dynamics. This is the case because aerodynamic forces are dependent on the product of the effective angle of attack and the square of the speed. The effect of the two cannot be (easily) decoupled, as is shown in the lift equation in equation (2-24). In this equation C', C'' and C''' are constant scalars and $C_{L_V}(V)$ represents the effect of speed on lift. The decoupling is not possible because the effect of α_{eff} and V cannot be decoupled into separate terms (hence the inequality sign). Furthermore, $C_{L_V}(V)$ will not be a linear function, but rather parabolic. Therefore an aeroelastic state-space system cannot be linear and time-invariant when speed is not constant.

$$L = \frac{1}{2}\rho V^2 S C_L(\alpha_{eff}) = C' \cdot V^2 C_L(\alpha_{eff}) \neq C'' \cdot C_{L_V}(V) + C''' \cdot C_L(\alpha_{eff}) \tag{2-24}$$

For the reasons mentioned above, the partitioned approach is chosen for the model. In the unlikely case that the partitioned approach proves to be numerically unstable, a more stable partitioned procedure (e.g. a predictor-corrector staggered procedure, see the next section) will be used. If numerical instability pursues, the monolithic approach could be used because of its unconditional numerical stability. The next section treats the available partitioned procedures.

2-3-2 Partitioned Procedures

To ensure time accuracy of a partitioned approach, i.e. consistency between aerodynamic loads and structural deformation, an appropriate method of solution exchange must be designed [46]. Several procedures exist, which are explained below.

The first procedure is the so-called conventional serial staggered procedure, depicted in figure 2-6a. In this procedure, the structural state at time n (U_n in the figure) is transferred to the aerodynamic discipline (1) which in turn advances the aerodynamic solution from time n to time $n+1$ (2). Then the aerodynamic forces and moments at time $n+1$ (P_{n+1} in the figure) are transferred to the structural discipline (3), which in turn advances the structural solution from time n to time $n+1$ (4). This procedure is attractive because of its simplicity and it is therefore the most popular among partitioned procedures [58]. In the presented procedure, the aerodynamic solution is updated before the structural solution. This could also be reversed.

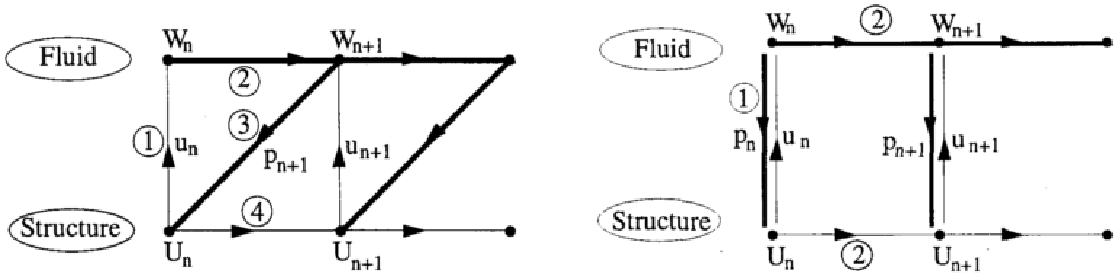

(a) Serial **(b)** Parallel

Figure 2-6: Conventional staggered procedures [58].

The second procedure is the so-called conventional parallel staggered algorithm, depicted in figure 2-6b. Firstly, the structural state at time n (U_n in the figure) is transferred to the aerodynamic discipline and the aerodynamic forces at time n (P_n in the figure) are transferred to the structural discipline (1). Secondly, both the aerodynamic and the structural solution are advanced from time n to time $n+1$ (2). Since this occurs simultaneously, this is a parallel procedure. This procedure is more efficient when the aerodynamic and structural models are run on separate processors, but the procedure has inferior stability properties [46].

The described procedures are the most well-known simple procedures. These procedures can be extended with predictor-corrector schemes, which are often used to seek near-second order accuracy [46]. Figure 2-7 shows such a predictor-corrector extension to the conventional serial staggered procedure. In this approach, first a prediction is made of the structural deformation at time $n+1$ (U^p_{n+1} in the figure). Subsequently, this predicted structural state is transferred to the aerodynamic model (2) and used to advance the aerodynamic state from time n to time $n+1$ (3). The forces obtained from the aerodynamic model at time $n+1$ are then transferred to the structural model (4), which functions as the corrector step. Lastly, the structural model is advanced in time (5). Using a predictor-corrector scheme enhances the accuracy of the model at limited additional computational cost [46].

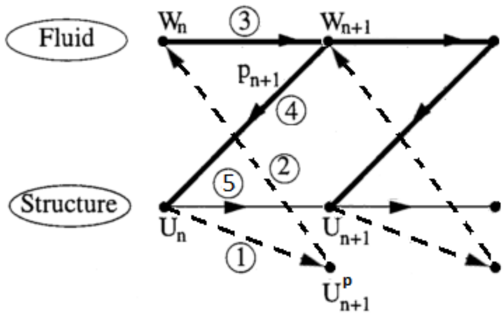

Figure 2-7: The predictor-corrector serial staggered procedure.

For the current research, the conventional serial staggered procedure will be used, because of its simplicity and better stability properties than the conventional parallel staggered procedure. If instabilities were to be found, a predictor-corrector scheme could be used in an attempt to create a stable simulation. However, as will become clear in chapter 4, this is not necessary, since computational instability does not occur.

2-3-3 Effects of Combining Aerodynamics and Structures

Although a partitioned approach will be used in the model, it is interesting to investigate the combined aerodynamic and structural equations. First, equations (2-2), (2-3) and (2-4) are combined to form the equation of vibration shown in equation (2-25).

$$M \begin{bmatrix} \ddot{h}_1 \\ \ddot{g}_1 \\ \ddot{\xi}_1 \\ \vdots \\ \ddot{h}_n \\ \ddot{g}_n \\ \ddot{\xi}_n \end{bmatrix} + C \begin{bmatrix} \dot{h}_1 \\ \dot{g}_1 \\ \dot{\xi}_1 \\ \vdots \\ \dot{h}_n \\ \dot{g}_n \\ \dot{\xi}_n \end{bmatrix} + K \begin{bmatrix} h_1 \\ g_1 \\ \xi_1 \\ \vdots \\ h_n \\ g_n \\ \xi_n \end{bmatrix} = \mathbf{F} = \begin{bmatrix} V_1 \\ H_1 \\ M_1 \\ \vdots \\ V_n \\ H_n \\ M_n \end{bmatrix} \tag{2-25}$$

The force vector $\mathbf{F}$ consists of forces due to gravity, aerodynamics and other sources, such as thrust. Note that because aerodynamic strip theory is employed, the forces on a section are related to the POM of only that section. Equations (2-26)-(2-28) show the effect that the Position, Orientation and Motion (POM) have on the forces V, H and the moment M for a single spanwise section. In these equations, $C_{V\ddot{\alpha}}$, $C_{V\dot{\alpha}}$, $C_{V\alpha}$, $C_{V\ddot{h}}$, $C_{V\dot{h}}$ are coefficients that represent the effect of angular acceleration $\ddot{\alpha}$, angular velocity $\dot{\alpha}$, angle of attack α, plunge acceleration $\ddot{h}$ and plunge speed $\dot{h}$ on the vertical force. Likewise, $C_{H\ddot{\alpha}}$, $C_{H\dot{\alpha}}$, $C_{H\alpha}$, $C_{H\ddot{h}}$, $C_{H\dot{h}}$ are coefficients that represent the effect these variables have on the horizontal force and $C_{M\ddot{\alpha}}$, $C_{M\dot{\alpha}}$, $C_{M\alpha}$, $C_{M\ddot{h}}$, $C_{M\dot{h}}$ represent the effect on the section pitching moment. One can see that the forces and moment depend on $\ddot{\alpha}$, $\dot{\alpha}$, α, $\ddot{h}$ and $\dot{h}$, reflecting Theodorsen's function (equation (2-19)). The vertical position h has no effect on the forces and moment, but there is an effect that is independent of the position and orientation variables (e.g. due to gravity or camber), which is captured in variables C_{V0}, C_{H0} and C_{M0}.

$$V = C_{V\ddot{\alpha}}\ddot{\alpha} + C_{V\dot{\alpha}}\dot{\alpha} + C_{V\alpha}\alpha + C_{V\ddot{h}}\ddot{h} + C_{V\dot{h}}\dot{h} + C_{V0} \tag{2-26}$$

$$H = C_{H\ddot{\alpha}}\ddot{\alpha} + C_{H\dot{\alpha}}\dot{\alpha} + C_{H\alpha}\alpha + C_{H\ddot{h}}\ddot{h} + C_{H\dot{h}}\dot{h} + C_{H0} \tag{2-27}$$

$$M = C_{M\ddot{\alpha}}\ddot{\alpha} + C_{M\dot{\alpha}}\dot{\alpha} + C_{M\alpha}\alpha + C_{M\ddot{h}}\ddot{h} + C_{M\dot{h}}\dot{h} + C_{M0} \tag{2-28}$$

Equations (2-26)-(2-28) can now be substituted in equation (2-25), to yield equation (2-29). This equation is the aeroelastic equation of vibration. In this equation it becomes clear that the aerodynamic force terms, on the right hand side of the equation, are dependent on the vector of response coordinates and its first and second derivative. Since this is similar to the mass, damping and stiffness matrices (M, C and K), the aerodynamic matrices in the equation are named the aerodynamic mass matrix M_{aero}, the aerodynamic damping matrix C_{aero} and the aerodynamic stiffness matrix K_{aero}. Note that since these matrices contain off-diagonal terms, the modes become coupled, but that is an inherent part of every aeroelastic system [7]. Also note that these matrices were not included in the determination of the modal data, because the modes were determined in vacuo. In equation (2-29) the benefit of employing aerodynamic strip theory becomes evident: the forces and moments acting on a spanwise section are dependent on the POM of that section only.

$$
\begin{aligned}
M\begin{bmatrix}\ddot{h}_1\\ \ddot{g}_1\\ \ddot{\xi}_1\\ \vdots\\ \ddot{h}_n\\ \ddot{g}_n\\ \ddot{\xi}_n\end{bmatrix} \quad + \quad C\begin{bmatrix}\dot{h}_1\\ \dot{g}_1\\ \dot{\xi}_1\\ \vdots\\ \dot{h}_n\\ \dot{g}_n\\ \dot{\xi}_n\end{bmatrix} + K\begin{bmatrix}h_1\\ g_1\\ \xi_1\\ \vdots\\ h_n\\ g_n\\ \xi_n\end{bmatrix} & \\
= \quad & \begin{bmatrix}
C_{V\ddot{h},1} & C_{V\ddot{g},1} & C_{V\ddot{\xi},1} & \dots & 0 & 0 & 0\\
C_{H\ddot{h},1} & C_{H\ddot{g},1} & C_{H\ddot{\xi},1} & \dots & 0 & 0 & 0\\
C_{M\ddot{h},1} & C_{M\ddot{g},1} & C_{M\ddot{\xi},1} & \dots & 0 & 0 & 0\\
\vdots & \vdots & \vdots & \ddots & \vdots & \vdots & \vdots\\
0 & 0 & 0 & \dots & C_{V\ddot{h},n} & C_{V\ddot{g},n} & C_{V\ddot{\xi},n}\\
0 & 0 & 0 & \dots & C_{H\ddot{h},n} & C_{H\ddot{g},n} & C_{H\ddot{\xi},n}\\
0 & 0 & 0 & \dots & C_{M\ddot{h},n} & C_{M\ddot{g},n} & C_{M\ddot{\xi},n}
\end{bmatrix}\begin{bmatrix}\ddot{h}_1\\ \ddot{g}_1\\ \ddot{\xi}_1\\ \vdots\\ \ddot{h}_n\\ \ddot{g}_n\\ \ddot{\xi}_n\end{bmatrix}\\
+ \quad & \begin{bmatrix}
C_{V\dot{h},1} & C_{V\dot{g},1} & C_{V\dot{\xi},1} & \dots & 0 & 0 & 0\\
C_{H\dot{h},1} & C_{H\dot{g},1} & C_{H\dot{\xi},1} & \dots & 0 & 0 & 0\\
C_{M\dot{h},1} & C_{M\dot{g},1} & C_{M\dot{\xi},1} & \dots & 0 & 0 & 0\\
\vdots & \vdots & \vdots & \ddots & \vdots & \vdots & \vdots\\
0 & 0 & 0 & \dots & C_{V\dot{h},n} & C_{V\dot{g},n} & C_{V\dot{\xi},n}\\
0 & 0 & 0 & \dots & C_{H\dot{h},n} & C_{H\dot{g},n} & C_{H\dot{\xi},n}\\
0 & 0 & 0 & \dots & C_{M\dot{h},n} & C_{M\dot{g},n} & C_{M\dot{\xi},n}
\end{bmatrix}\begin{bmatrix}\dot{h}_1\\ \dot{g}_1\\ \dot{\xi}_1\\ \vdots\\ \dot{h}_n\\ \dot{g}_n\\ \dot{\xi}_n\end{bmatrix}\\
+ \quad & \begin{bmatrix}
C_{Vh,1} & C_{Vg,1} & C_{V\xi,1} & \dots & 0 & 0 & 0\\
C_{Hh,1} & C_{Hg,1} & C_{H\xi,1} & \dots & 0 & 0 & 0\\
C_{Mh,1} & C_{Mg,1} & C_{H\xi,1} & \dots & 0 & 0 & 0\\
\vdots & \vdots & \vdots & \ddots & \vdots & \vdots & \vdots\\
0 & 0 & 0 & \dots & C_{Vh,n} & C_{Vg,n} & C_{V\xi,n}\\
0 & 0 & 0 & \dots & C_{Hh,n} & C_{Hg,n} & C_{H\xi,n}\\
0 & 0 & 0 & \dots & C_{Mh,n} & C_{Mg,n} & C_{M\xi,n}
\end{bmatrix}\begin{bmatrix}h_1\\ g_1\\ \xi_1\\ \vdots\\ h_n\\ g_n\\ \xi_n\end{bmatrix} + \begin{bmatrix}C_{V0,1}\\ C_{H0,1}\\ C_{M0,1}\\ \vdots\\ C_{V0,n}\\ C_{H0,n}\\ C_{M0,n}\end{bmatrix}\\
= \quad & M_{aero}\begin{bmatrix}\ddot{h}_1\\ \ddot{g}_1\\ \ddot{\xi}_1\\ \vdots\\ \ddot{h}_n\\ \ddot{g}_n\\ \ddot{\xi}_n\end{bmatrix} + C_{aero}\begin{bmatrix}\dot{h}_1\\ \dot{g}_1\\ \dot{\xi}_1\\ \vdots\\ \dot{h}_n\\ \dot{g}_n\\ \dot{\xi}_n\end{bmatrix} + K_{aero}\begin{bmatrix}h_1\\ g_1\\ \xi_1\\ \vdots\\ h_n\\ g_n\\ \xi_n\end{bmatrix} + \mathbf{F_0}
\end{aligned}
\tag{2-29}
$$

2-4 Control Surfaces

In the previous sections, control surfaces were ignored, but their inclusion in the model will be discussed in this section. Control surfaces are an important subject, because they form an

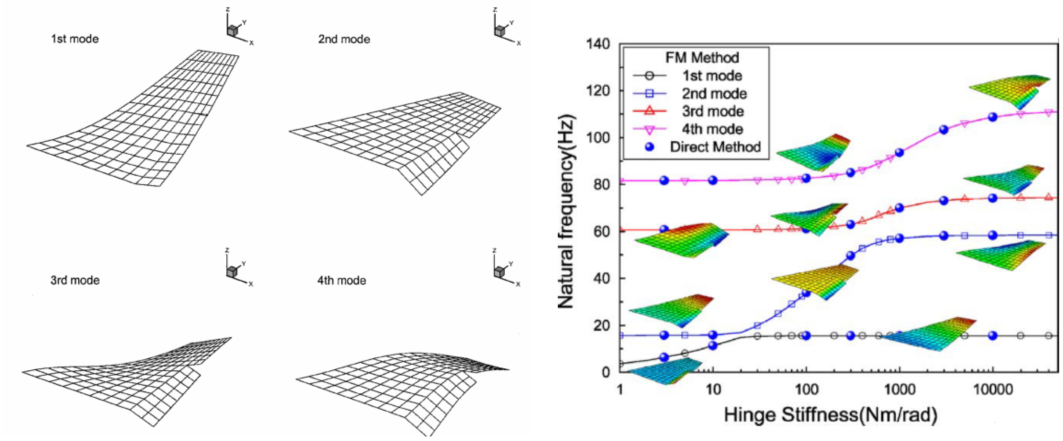

(a) Flapping modes **(b)** Dependency on hinge stiffness

Figure 2-8: Mode shapes of an airfoil with a control surface hinge spring [39].

important input for the flight mechanics described in chapter 5.

Several methods to include control surfaces in an aeroelastic model can be distinguished. An approach that is often used in the preliminary design phase of aircraft, is to assume that the presence of control surfaces can be represented by their aerodynamic contribution only [3]. By making this assumption, one neglects the inertia, dynamics and actuation systems associated with the control surface. From a structural point of view, this assumption entails that a control surface is driven by an infinitely stiff and infinitely powerful linear servo actuator, which is capable of exactly driving the position of the control surface.

Some inaccuracy might be introduced because of this assumption, as becomes evident from figure 2-8. In this figure, a control surface is connected to the wing model via a parameterized spring. Clearly, the possibility of a "flapping" control surface has effect on the modal data. Figure 2-8a shows the change of mode shapes due to flapping. The first mode is a pure bending mode as was the case for a wing without a control surface. The second mode however, is a pure flapping mode. The third and fourth mode show a torsion-flapping mode and a bending-flapping mode. The natural frequencies are also affected by the presence of a control surface, as can be seen in figure 2-8b. In this figure, each line represents a natural frequency and the associated mode shape. When a line part is horizontal, the hinge stiffness has no effect on this mode shape, which implies that no flapping occurs in that mode shape. For the sloping line parts, flapping does occur. From the figure it becomes clear, that flapping occurs at different modes as the hinge stiffness changes. These effects are ignored when only the aerodynamic contribution is taken into account. For that reason, this assumption is typically only used for static or low-frequency aeroelastic problems [1].

With the above assumption, the control surface can be implemented by assuming that an idealized point force will act at the trailing edge of the wing section whenever a control surface is deflected. It is suggested that the force is determined with equation (2-30) [62]. In this equation, F_c is the idealized control force, q is the dynamic pressure and F_c^* is the control coefficient. On the basis of slender-wing theory, the control force may be altered by varying the control coefficient, without affecting the pressure distribution on the rest of the wing [62]. Using equation (2-30), one assumes that the control is irreversible so that F_c^* is constant during a perturbed motion. However, this does not necessarily result in a constant control force F_c, because that depends on the dynamic pressure as well. Although this approach is simple, it is a close representation of a flap-type control situated at the trailing edge of a wing [62].

$$F_c = qF_c^* \tag{2-30}$$

The magnitude of F_c^* can be altered during the trim algorithm (see chapter 5) and is an important output of the trim algorithm. The trim algorithm can either adjust F_c^* directly, or it can be done through the control surface deflection angle. For the latter, the value of F_c^* could be determined using algebraic relations (e.g. Theodorsen's extended model [63]) or a look-up table based on the control surface deflection angle and the main wing effective angle of attack. The mode shapes that were found with the methods in section 2-1, i.e. without a moving control surface, can still be used. The control deflection angle simply becomes an additional degree of freedom [1].

2-5 Summary

Many choices concerning the aeroelastic wing model were made in this chapter. Table 2-1 provides an overview of the models that are used for the different disciplines and the associated assumptions (in *italics*).

Table 2-1: The approaches taken for the various disciplines and the associated assumptions.

Discipline	**Approach & assumptions**
Structures	Modal approach in a linear time-invariant state-space system
	Free-free in vacuo mode shapes
	Neglect high frequency modes
	Small deformation
	No concentrated nonlinearities
	Rayleigh damping
Aerodynamics	Look-up tables using the quasi-steady α_{eff}
	Subsonic flight
	Low frequency motion
	Strip theory
	Corrected aerodynamic coefficients near wing tip
Control surfaces	Only consider aerodynamic contribution
	Neglect dynamics, inertia and actuation of control surface
	Idealized control force at trailing edge
Load prediction	Summation of forces (with MSD)
Fluid-structure interaction	Conventional serial staggered partitioned approach

Chapter 3

Aeroelastic Wing Methodology

In this chapter, the implementation of the aeroelastic wing model is treated, which is based on the theory discussed in the previous chapter. The model is created in the SimMechanics environment. This environment is readily compatible with MATLAB, thus making it easy to understand the model for many people at the faculty and paving the way for integration of the model into other programs (such as the Design and Engineering Engine of figure 1-3). Furthermore, SimMechanics allows the user to create multibody systems with relative ease. For the model of a single wing, this does not provide a big advantage, because the state-space system is at the center of the calculations and not a multibody system code (see section 2-1). However, as will become clear in chapter 6, the multibody system environment will be of great benefit when multiple wings are combined to form an Aeroelastic Flight Mechanics (AFM) model.

In the following, first the general concept of the model is discussed in section 3-1. Then, the SimMechanics model itself will be treated in section 3-2. Thereafter, simulation with this model using various MATLAB files is the subject of section 3-3. Lastly, a short summary is provided in section 3-4. The treatment of the implementation is kept concise in this report and the interested reader is invited to look into the model itself, where ample comments were used to provide new users with a thorough understanding of the model. Another option would be to read the user guide in appendix D or to use the interactive help environment presented to the user upon initialization of the model.

3-1 General Concept

The general concept of the model is that the flexible wing is modeled as a number of massless wing sections that can move independently from each other. These wing sections move with respect to a rigid wing basis. Figure 3-1 visualizes this concept, where they grey part is the rigid wing basis and the blue parts are the massless wing sections.

In the model both a rigid and a flexible wing exist alongside each other. On the one hand, the flexible wing describes the actual position of the aeroelastic wing. The state-space system determines the vertical, horizontal and pitch-up deflection of each aeroelastic node. The aeroelastic node of a section represents the elastic axis point at the spanwise center of that section. The input for the state-space model are the forces (both aerodynamic and gravitational) that act on the wing. On the other hand, the rigid wing basis allows translation and rotation of the wing root (due to flight dynamics). It also allows measurement of the root moments and forces via Summation of Forces (see section 2-1-4).

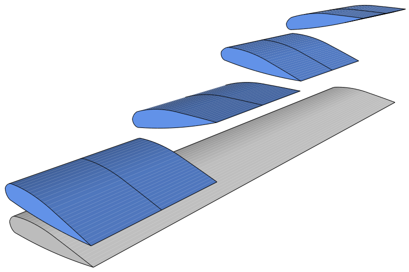

Figure 3-1: The general model concept: moving wing sections overlaid on a rigid wing basis.

3-2 Description of the SimMechanics Model

In this section, the SimMechanics wing model will be explained, based on the screenshot of the model given in figure 3-2. Five groups of blocks will be treated. Firstly, the blue blocks which form the general environment. Secondly and thirdly, the white blocks which form the aeroelastic and the special nodes (the difference between the two will be explained later). Fourthly, the grey blocks which represent the rigid wing basis. And lastly, the pink blocks which are related to the state-space system. Each of these groups will now be treated.

3-2-1 General Environment

The general environment blocks are fairly simple blocks that perform a variety of functions.

Time The "Time" block is used to save the time to the MATLAB workspace, so that figures can be created.

Atmosphere The "Atmosphere" block is used to determine the air density for the given flight altitude.

Gust The "Gust" block is used to create the gust that is used in the aeroelastic node blocks (treated later). The block can create a vertical gust speed with a "1 - cos" profile. This type of gust is used throughout literature [44, 45, 64] and in regulations, such as CS-23 and CS-25 [65, 66]. It is described in equation (3-1), in which w_g is the instantaneous gust vertical velocity, $\bar{w}_g$ is the maximum gust vertical velocity and L_g is the gust length in terms of the time for a point on the aircraft to travel across it [44].

$$w_g(t) = \frac{\bar{w}_g}{2}\left(1 - \cos\frac{2\pi}{L_g}\right) \tag{3-1}$$

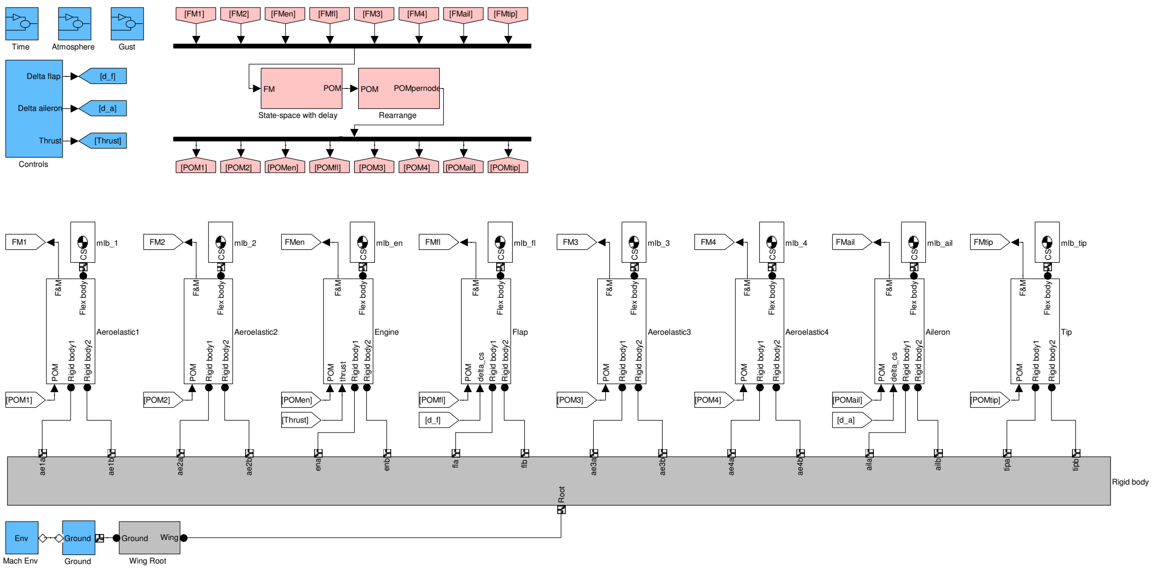

Figure 3-2: Screenshot of the SimMechanics wing model with eight nodes.

Controls The "Controls" block is used to determine the settings of the three controls of the wing: the flap deflection, the aileron deflection and the thrust. The thrust of a second engine (not shown) can also be included, and functions similarly to the thrust of the first engine. The values of the controls are a trim value plus a user-specified input of certain magnitude. This input can be a step function, a frequency sweep, an impulse, a 2-3-1-1 input or zero input. Note that the user specifies the deflection angles of the flap and aileron and the thrust force directly, and not as pilot input. This corresponds to the assumption of neglecting the control surface inertia, dynamics and actuation systems (as described in section 2-4).

The "Goto" tags "d_f", "d_a" and "Thrust" are used to transfer the control settings to the specific special node blocks (treated later).

Machine environment The machine environment ("Mach Env") block defines the mechanical simulation environment for the model. In this block, the gravity vector is defined. Note that for this model it is a zero vector, because gravity should not be included here, but should be modeled as input for the state-space system [26]. Weights are therefore included in the aeroelastic and special node blocks.

Ground The "Ground" block couples the model to the machine environment.

3-2-2 Aeroelastic Nodes

The aeroelastic nodes are at the core of the aeroelastic wing model. First, consider figure 3-3, which schematically shows how different blocks work together. In this figure, only two wing sections are shown, but the numer of sections can be higher in the model. At the bottom is the rigid wing basis, which consists of bodies connected with welds. These bodies, or rigid body parts, represent wing sections with mass m and mass moment of inertia J. Connected to each rigid body part is an actuatable joint capable of vertical and horizontal translation and pitch up rotation. Connected to these joints are massless bodies, which represent the flexible wing position. In turn, sensors determine the Position, Orientation and Motion (POM) of these massless bodies. Subsequently,the aerodynamic and gravitational forces and moments that work on the section are calculated with aerodynamic analysis. Lastly, a state-space system receives these forces and moments and determines the POM of the massless bodies. This information is used to actuate the previously mentioned joints, which completes the system. This approach is an indirect way of modeling a flexible wing in the SimMechanics environment. This workaround must be used, since SimMechanics can only model rigid bodies [26].

The determination of forces and moments, and the actuation of the massless bodies are the tasks that are performed by the aeroelastic node blocks. Both tasks are now discussed.

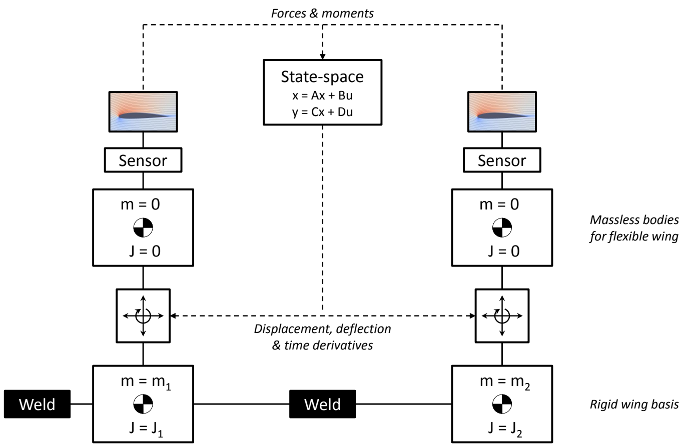

Figure 3-3: Schematic overview of the aeroelastic wing model.

Determination of forces and moments The "Aeroelastic" block receives the position, orientation and motion (POM) from the state-space group via a "From" tag. It then determines the forces and moments acting on the wing section and subsequently sends those forces and moments (FM) to the state-space group via a "Goto" tag.

As was described in section 2-2, the aerodynamic force and moment coefficients are determined based on look-up tables. The input for these look-up tables is the effective angle of attack. To understand the determination of this angle of attack, one must first gain an understanding of the various reference frames that are used. Figure 3-4 shows the X-axes as lines in the vertical plane for the used reference frames. The names of the reference frames are provided in the box, the angles between the reference frames on the left and the usage of the reference frames on the right.

Each of these reference frames has its own reasons for being included in the analysis. Firstly, the vehicle-carried normal Earth reference frame F_E, which includes the flat Earth horizontal, is used to define the weight W, the aircraft forward velocity u, and the aircraft downward velocity w. Note that the effective aircraft downward velocity also includes the effect of the gust velocity w_g. Secondly, the aerodynamic reference frame F_a is used to define the lift force L and the drag force D. Thirdly, the body-fixed reference frame F_b is of no importance for the single wing model, but will be important for the AFM model treated in chapter 6.

Fourthly, the rigid-wing reference frame F_{rw}, which includes the plane through the wing root chord line, is used for the definition of the mode shapes. Because the mode shapes are defined in this reference frame, also the forces must be defined in this plane (see section 2-1). These forces are the force orthogonal to the rigid-wing plane V and the force parallel to the rigid-wing plane H. Note that the pitching moment M and the side-force S also exist in the model. Fifthly, the flexible-wing reference frame F_{fw} is used to define the thrust force T. Lastly, the effective flexible-wing reference frame $F_{fw,eff}$ is used to determine the effective angle of attack.

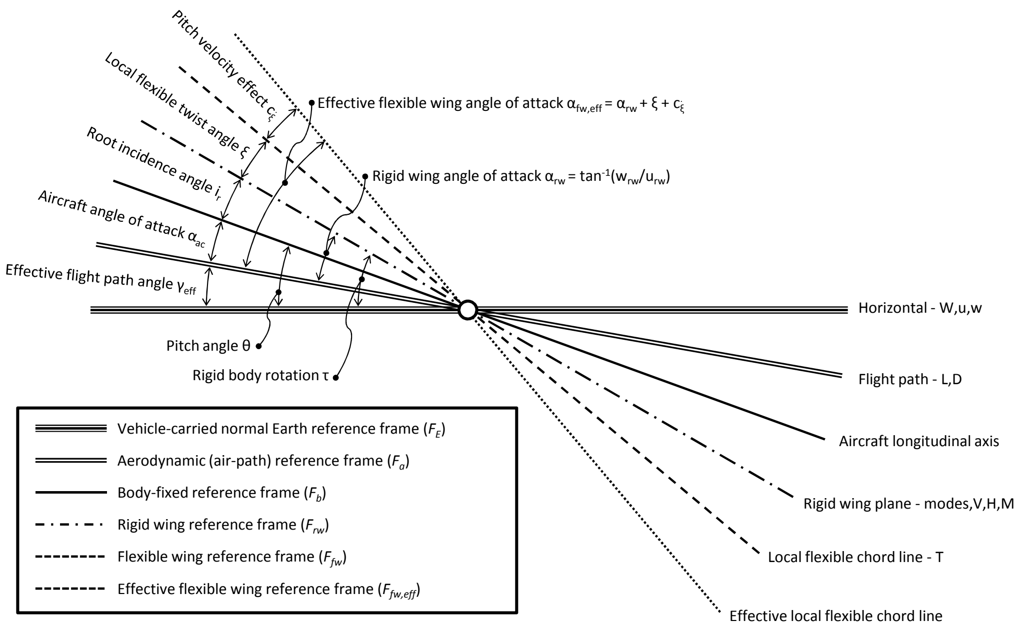

Figure 3-4: Definition of the used reference frames and twist angles.

Now that the reference frames are familiarized, the angles between the reference frames can be treated. Some of the angles are required to determine the input for the state-space group, i.e. V, H, S and M, which are in the F_{rw} frame. The first angle of interest is the angle τ, which is part of the rigid body rotation matrix. It is the transformation matrix between F_E and F_{rw}. This can be determined with a Body Sensor in SimMechanics. It is used to transform the section weight W from F_E to F_{rw}.

The second angle that must be determined is the effective flexible wing angle of attack $\alpha_{fw,eff}$. This is the effective angle of attack that is used to determine the aerodynamic force and moment coefficients. It can be determined using equation (3-2). In this equation α_{rw} is the rigid wing angle of attack, ξ is the aeroelastic twist deflection, $c_{\dot{\xi}}$ is the effect of the pitch velocity on the effective angle of attack. Furthermore, b is the semichord, a is the distance between midchord and elastic axis in semichords, u_{rw} is the forward velocity in the rigid-wing reference frame and w_{rw} is the downward velocity in the rigid-wing reference frame. This equation is similar to equation (2-23).

Everything on the right-hand side of the equation is available. From the state-space system we know ξ and $\dot{\xi}$, in which the dot represents a derivative with respect to time. Furthermore,

u_{rw} and w_{rw} can be determined from the velocity of the rigid wing body (treated in section 3-2-4) in the F_E frame. It should then be transformed from F_E to F_{rw} using the rotation matrix containing angle τ. Both the velocities and the rotation matrix can be sensed using a Body Sensor. Added to these velocities should be the gust velocity w_g, which is user input, and the aeroelastic plunge and sweep velocity, known from the state-space system. The remaining parameters a and b are user input, so this allows the calculation of $\alpha_{fw,eff}$ and thus the determination of the force and moment coefficients.

$$\alpha_{fw,eff} = \alpha_{rw} + \xi + c_{\dot{\xi}} = \tan^{-1}\left(\frac{w_{rw}}{u_{rw}}\right) + \xi + \tan^{-1}\left(\frac{b\left(\frac{1}{2} - a\right)\cos\xi\dot{\xi}}{u_{rw}}\right) \tag{3-2}$$

The last angle of interest is the rigid-wing angle of attack α_{rw}, which was defined in equation (3-2). This angle is used to transform the aerodynamic lift and drag force from F_a to F_{rw}.

Now that all forces and moments are known in the F_{rw} frame, the aerodynamic forces are translated from the aerodynamic center to the elastic axis and the gravitational force from the center of gravity to the elastic axis. At this point, the forces and moment, as working on the elastic axis and in the F_{rw} frame, are known (i.e. V, H, S and M). This is the output of the "Aeroelastic" block and is sent to the state-space system via a "Goto" tag.

Actuation of the massless body The "Aeroelastic" block is also responsible for the actuation of the massless body (mlb). Actuation is simply performed with "Joint Actuator" blocks connected to a planar joint that allows plunging and sweeping translation and pitching rotation (the three aeroelastic degrees of freedom). Actuation is done by motion (as opposed to forces) that comes from the state-space system via a "From" tag. The mlb has zero mass and inertia, in order to prevent that forces other than those fed to the state-space system work on the multibody system. If the mlb were to have mass or inertia, actuation by motion would cause additional root forces and moments, interfering with the load prediction capabilities of the model. Note that having bodies with zero mass and inertia causes no computational errors as long as they are actuated purely by motion [26], as is the case in this model.

3-2-3 Special Nodes

The special nodes share similarities with the aeroelastic nodes. They also receive the POM from the state-space system and send the forces and moments to the state-space system. Moreover, they also actuate a mlb. Such an mlb does not represent a wing section, but another object on the wing. These can be flaps, ailerons, engines or landing gear. In addition, a tip node is always present. These five special node types are now discussed.

Landing gear The landing gear ("LG") block essentially introduces the gravitational force due to landing gear weight. Just as with the wing section weight discussed in section 3-2-2, the landing gear weight is given in the F_E reference frame and must be transformed to the F_{rw} frame using the rigid body rotation matrix. Note that the landing gear weight may also cause a moment around the elastic axis, if the landing gear center of gravity does not lie on the elastic axis. In the current model, only landing gear weight is included, representing an aircraft in flight. An extension could easily be made in the future, where riding on the ground is simulated by introducing forces transferred to the wing through the landing gear.

Engine The "Engine" block introduces engine weight in a fashion similar to that of the landing gear. In addition, it introduces the thrust force to the model. It is assumed that the thrust works parallel to the local flexible chord line, so that when the wing section rotates, the engine and therefore the thrust rotate as well. In order to transform the thrust force from the F_{fw} frame to the F_{rw} frame, the local flexible twist angle ξ is used (see figure 3-4).

Flap The "Flap" block introduces the aerodynamic effect of flap deflection. As was discussed in section 2-4, the effect of flap deflection is modeled as an idealized point force working on the trailing edge of the spanwise center of the flap. Due to application at the trailing edge, downward flap deflection causes the wing to twist down, which is a close representation of reality [62]. The aerodynamic coefficients are determined using two-dimensional look-up tables based on the flap deflection angle δ_f and the effective angle of attack of the local flexible wing section $\alpha_{fw,eff}$. Both angles are available: δ_f comes from the "Controls" block and $\alpha_{fw,eff}$ is determined in the same way as with an aeroelastic node. The forces are then transformed to the F_{rw} frame, again in the same way as with the aeroelastic nodes.

Aileron The "Aileron" block works in a similar fashion as the flap block, but of course with different input parameter values.

Tip The "Tip" block must be included to allow measurements of tip deflection, so the primary function is simply to receive the POM of the tip from the state-space system and actuate the mlb that represents the tip node. During a regular simulation, there are no forces or moments that work on the tip. For verification purposes, however, tip forces and moments were included.

3-2-4 Rigid Wing Basis

The rigid wing basis is formed by the grey blocks in figure 3-2 and consists of the following parts.

Wing root The "Wing Root" subsystem connects the wing structure to the "Ground" block. It does this using a bushing joint (having 6 degrees of freedom), so that the user can specify the translation and rotation of the wing root and their time derivatives. Examples are the forward speed of the wing and the wing setting angle. The root moments and forces are measured at this bushing joint.

Rigid wing nodes The "Rigid Wing" subsystem consists of body blocks: one for every aeroelastic and special node. These body blocks are connected by welds, thus representing a rigid wing. The system of body blocks represents the actual geometry of the wing, including e.g. sweep and dihedral. This allows that the connections from the rigid wing to the aeroelastic and special node groups are at the correct locations, i.e. on the elastic axis of the wing. Because of that, the measurement of the rigid body velocity becomes accurate for every node, also in case of e.g. yawing motion where outboard nodes have a higher velocity than inboard nodes.

Another function of the rigid wing is force actuation. In order to be able to perform Summation of Forces (SOF), the forces and moments determined in the aeroelastic and special nodes should be applied to the system at some location. This cannot be on the massless bodies, since these massless bodies are already actuated with motion (described by the state-space system). For this reason the forces and moments are applied on the rigid wing.

The last function of the rigid bodies is that they introduce mass and inertia. Since there is no gravity, this does not cause gravitational forces, which are already defined in the aeroelastic and special nodes. It does, however, introduce inertial forces. This becomes important once the wing model is implemented in an AFM model as it affects the flight dynamics of the aircraft. It is not possible to give mass and/or inertia to the massless bodies, because that would create additional, erroneous forces in SimMechanics once these bodies are actuated with motion.

In the text above, two assumptions were implied. Wing deflection is ignored when it comes to, firstly, the force application locations, and secondly, the inertial properties of the wing. These assumptions must be made, but introduce little inaccuracy, since the deflection is small compared to the rigid wing geometry. Note that the largest effect of flexibility on flight mechanics, being the change in forces and moments, is not ignored.

3-2-5 State-space System

The state-space system is modeled using the pink blocks in figure 3-2. The function of this group of blocks is to determine the POM of the nodes from the forces and moments working on those nodes. The group consists of four parts which will be discussed now.

From tags The forces and moments working on each of the nodes were determined in the aeroelastic and special node blocks. To prevent clutter of the model, "Goto" and "From" tags were used for data transfer. The forces and moments vector $[VHSM]$ of each of the nodes arrives via the "From" tags and these are combined into a large input vector using a "Mux" block.

State-space with delay The "State-space with Delay" block holds the state-space system that was described in section 2-1 and is at the core of the model. Firstly, the input vector is adjusted so that it contains a concatenation of $[VHM]$, instead of $[VHSM]$, for all the nodes. Note that this could be achieved by altering the state-space system itself, but it was preferred to do this explicitly in SimMechanics, for the sake of clarity.

This adjusted input vector is then fed to a state-space block, which produces the output vector containing the POM of the nodes and the amplitude of the modes and their time derivatives. As was described in section 2-3, a partitioned approach is used in this model. This was achieved in SimMechanics using a "Unit Delay External IC" block. This means that the output of the state-space system is delayed one time step. Thus, it is prevented that model evaluation takes very long or even indefinitely trying to find a solution where forces and moments on the one hand and POM on the other are perfectly consistent within a single time step. The user may supply the initial conditions for the delayed state-space system in the form of an initial state vector and output vector.

The last step is adjusting the output vector, so that only the nodal information (POM) is sent to the following blocks and not the modal information (amplitudes and time derivatives). Note that both are sent to the workspace for possible inspection.

Rearrange The "Rearrange" block is used to rearrange the elements in the output vector from the "State-space with Delay" block. It makes it possible to split the output into separate pieces for the different nodes. Again, this is done explicitly in SimMechanics for clarity, but could just as well be done by adjusting the state-space system.

Goto tags Finally, the output is split using a "Demux" block and the various output vectors, containing the POM for the different nodes, are sent to the aeroelastic and special node blocks with "Goto" tags.

3-3 Simulation with the SimMechanics Model

Now, simulation with the model, described in the previous section, is treated. First, the input is discussed and then the build-up and simulation of the model. Note that the numerical integration parameters are discussed in chapter 6. Many lines of code were written, but the discussion here is kept to a high level. The interested reader is referred to the code itself or to the user guide in appendix D.

3-3-1 Input to the Model

The user can specify most of the input directly in the file *aircraft_description.m*. Table 3-1 shows the wing, flight and simulation parameters that the user should provide. Table 3-2 shows the parameters regarding objects on the wing that the user should provide if he wishes to include such an object. As can be seen, the elastic axis (e.a.), the aerodynamic center (a.c.) and the center of gravity (c.g.) must be specified (in chordwise direction) to determine the application point of the forces. As was discussed in section 2-2, the aerodynamic forces due to control surface deflection are assumed to work on the trailing edge (and the aerodynamic data should be provided accordingly).

Most model parameters are calculated from the given input parameters. Examples are the width of the sections (from the number of sections, assuming sections of equal width) and the local semichord (from root chord, taper and spanwise position). Parameters denoted by an asterisk in table 3-1 can either be provided directly by the user or they can be computed. The section mass and inertia, for instance, can be estimated from geometry in various ways and the initial deflection can be loaded from a previous simulation.

The parameter tables do not show perhaps the most important input: the modal and aerodynamic data. This data should be determined with external models in a pre-processing step and is discussed next.

Modal Input

The modal data forms the basis of the modal superposition method described in section 2-1. Several *.csv* files must be provided to the model. One containing the natural frequencies of the modes and one for each mode shape that is included in the analysis. The mode shapes are defined by the plunge (downward) translation, the sweep (forward) translation and the pitch (upward) rotation; all measured on the elastic axis of the wing. The MATLAB code imports the *.csv* files and uses the information to create the state-space system.

Table 3-1: Wing, flight and simulation input parameters.

Wing	**Section**	**Flight**	**Simulation**
Semispan	Location of e.a.	Velocity vector	Number of sections
Root chord	Location of a.c.	Altitude	Number of modes
Taper	Location of c.g.	Gust velocity	*Initial deflection
Sweep	Thickness ratio	Gust length	Simulation time
Dihedral	*Mass	Gust start time	
Setting angle	*Inertia		
Twist			

Table 3-2: Input parameters regarding objects on the wing.

Engine	**Landing gear**	**Control surface**
Location of e.a.	Location of e.a.	Location of e.a.
Spanwise location	Spanwise location	Spanwise location
Chordwise location	Chordwise location	Deflection angle
Mass	Mass	Control input
Inertia	Inertia	
Trim thrust		
Thrust input		

Note that the modal (structural) damping ratio must provided separately by the user. It is assumed that it is equal for all modes and has a value of 0.02. This appears to be a valid assumption, because it is used for aircraft wings throughout literature [7, 67, 68].

The user has various possibilities to determine the modal data. For simple geometries, this could be done in MATLAB, as is discussed in sections 4-2 and 4-4. For most wings however, modal analysis should be performedin a pre-processing step. A Finite Element Analysis (FEA) program or experimental data could be employed. It is also possible to use EMWET for mode determination [69]. EMWET is a medium-fidelity wing weight estimation method and finite beam element model, which uses consistent shape function of a 3D 2-node Timoshenko beam for modal analysis [70]. EMWET is coupled to the current model and is specifically suited for the earlier design phases, in which not much information about the wing is known.

For the test case of the model, an A320-like wing [71], MSC PATRAN and MSC NASTRAN were used to determine the mode shapes. This choice was made because of the availability of the model, experience of the author and because it is a standard for the aerospace industry [25]. Figure 3-5 shows the first, second, third and fifteenth mode of the wing. Higher modes are more complex than lower modes and typically have a lower amplitude due to their higher generalized stiffness, i.e. natural frequency. Modal data of the first nine modes can be found in appendix B in a more readable format.

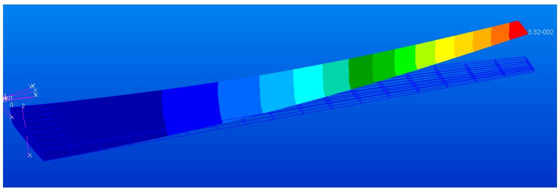

(a) Mode 1: 1st bending mode.

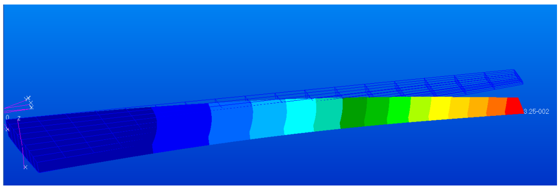

(b) Mode 2: 1st sweeping mode.

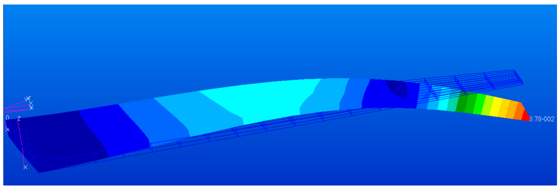

(c) Mode 3: 2nd bending and 1st twisting mode.

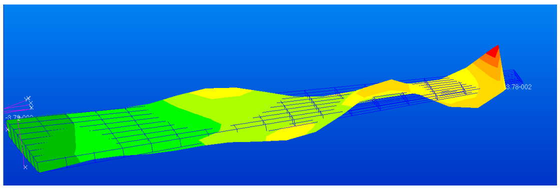

(d) Mode 15: a higher mode.

Figure 3-5: Modes 1, 2, 3 and 15 found using MSC PATRAN and MSC NASTRAN.

Aerodynamic Input

The aerodynamic data is used to fill the look-up tables in SimMechanics. For the clean wing, the user must supply a vector of angles of attack α and corresponding lift coefficient C_L, drag coefficient C_D and moment coefficient C_M vectors. The model allows the definition of different coefficient values at different spanwise sections. This allows the implementation of a tip correction (discussed in section 2-2-3), in which the aerodynamic coefficients are reduced near the tip, compared to the rest of the wing. The section lift force L_i, drag force D_i and pitching moment M_i can then be determined using equations (3-3). Here q is the dynamic pressure, S_i is the section surface area and c_i is the section midchord.

$$L_i = qS_iC_L(\alpha) \qquad D_i = qS_iC_D(\alpha) \qquad M_i = qS_ic_iC_M(\alpha) \tag{3-3}$$

If the flap and aileron are included in the model, the user must also provide the associated aerodynamics. C_L and C_D are the idealized trailing edge force coefficients. They should be provided in the form of matrices, since they are dependent on both the clean wing angle of attack α and the control surface deflection angle δ. For these latter variables, the user should provide input vectors. For control surfaces, equation (3-4) shows how one can obtain forces and moment from the coefficients. Note that these equations were deduced from the control coefficient equation (2-30).

$$L = qC_L(\alpha, \delta) \qquad D = qC_D(\alpha, \delta) \tag{3-4}$$

The aerodynamic data must also be determined in a pre-processing step with an external program. For the test case, an A320-like wing, a DATCOM model was used to determine this data [72]. DATCOM consists of a very large collection of equations used in aircraft design. A tailless aircraft was modeled, to focus on purely the aerodynamics of the wing. Clean wing aerodynamic data was readily available in the DATCOM output, but the aerodynamic data for the control surfaces required manipulation in MATLAB before it was usable. For instance, the effect of aileron deflection on lift could be determined by evaluating the aircraft rolling moment due to opposite deflection of ailerons on both wings. All aerodynamic data of the A320-like wing is presented in appendix A.

3-3-2 Build-up and Simulation of the Model

With the input described in the previous section, a SimMechanics model is constructed in *aircraft_generator.m*. This generator selects, places and connects the various blocks described in section 3-2 using MATLAB expressions. Some of these blocks are standard SimMechanics blocks, but most have been created by the author and located in the "block library". This library contains masked blocks, of which the contents are covered (i.e. masked) and only the required input is visible. These masked blocks can be used multiple times, each time with different input. For instance, each wing section is represented by the same block, but with different input.

Generation of the SimMechanics model is a fully automated process, which gives great flexibility to the code. At literally the touch of a button, a new SimMechanics model can be created reflecting changes in for instance the number of nodes or the inclusion of a control surface. The resulting program both functions properly and looks clear, as if it was hand-made for that specific input. Because the model is flexible enough to reflect any conventional aircraft input, it can easily be adopted in an automatic design framework (such as the one shown in figure 1-3).

Finally, the simulation is performed in *time_domain_simulation.m*. This executes the SimMechanics model, based on the MATLAB input to create the results. These results can then be saved and used to create figures for interpretation. If desired, a three-dimensional animation can be presented, showing the behavior of the wing.

3-4 Summary

This chapter showed how the theory presented in chapter 2 was implemented to form the aeroelastic wing model. It was explained that the model exists of a rigid wing basis on which a flexible wing is overlaid, in the form of independently moving massless bodies. The position, orientation and motion of these massless bodies, i.e. the deformation of the flexible wing, are determined by a state-space system. The input for this state-space system are the aerodynamic and gravitational forces and moments.

The SimMechanics blocks that represent this concept were treated in detail, as well as the input to the model. Lastly, automated model build-up and simulation were treated.

Chapter 4

Aeroelastic Wing Verification

In this chapter, the verification of the aeroelastic wing model is treated. This is of vital importance, since it gives credibility to the results of the model. Unfortunately, validation data is scarce for models used to determine the dynamic response of an aeroelastic wing [73]. Even for a broader scope, i.e. aeroelasticity in general, no comprehensive benchmarking validation standard currently exists [49]. Most validation data presented in literature is about flutter analysis, to which this model is not optimized (see section 2-2-2). In some articles, validation data about the dynamic response was given, but either the required aerodynamic data or the required modal data was missing. For these reasons, the focus will lie on verification, which will therefore be done extensively.

Verification and validation of the Aeroelastic Flight Mechanics (AFM) model will be treated in chapter 7. It will be of a less extensive nature than that of the aeroelastic wing model because of three reasons. Firstly, because the aeroelastic wing model is at the core of the AFM model. Secondly, because the aeroelastic wing model forms the main novelty created in the current research. And thirdly, because of scarcity of AFM verification methods and validation data, which is the case because of the rarity of such a model. These reasons are discussed more extensively in chapter 7.

In the following sections, the verification analyses of the aeroelastic wing model will be treated. Before these analyses were performed, all calculations in the model were checked by hand, to make sure that separate parts of the model functioned correctly (which was the case). The analyses treated in this report can therefore focus on the functioning of the model as a whole. In all analyses that were performed, no computational instability was encountered. This justifies the choice of using a simple partitioned procedure for fluid-structure interaction (see section 2-3).

Verification of the aeroelastic wing model was split up in four parts, which will be discussed one by one. They are a qualitative assessment, an assessment of the steady-state predictions, an assessment of the transient behavior of the model, and a comparison with the lumped-parameter model.

4-1 Qualitative Assessment

The first integral analysis of the model is a qualitative assessment of the response following a gust, flap, aileron, and thrust input. This gives a general idea of the functioning and capabilities of the model. The wing that is modeled is the A320-like wing treated in chapter 3 and of which detailed information is available in appendices A and B. For all analyses, the wing is moving forward at a constant speed of 133 m/s and at zero angle of attack, so that the local angle of attack of wing sections is defined only by the wing setting angle and the wing twist.

Figure 4-1 shows the tip deflection following a "1-cos" upward gust prescribed by CS regulations [66]. Vertical deflection is positive upwards, horizontal deflection is positive forwards and twist deflection is positive for pitch-up. The gust is defined as equation (3-1) with parameters gust length $L_g = 1\ s$ and maximum gust velocity $\bar{w}_g = 11.15\ m/s$, starting after 1 second. One can see that at the start of the analysis, the tip is at rest at its steady-state position (found in an earlier analysis). During the gust, i.e. between 1 and 2 seconds, the vertical and horizontal deflection in figure 4-1 are as expected. An upward gust increases the effective angle of attack α_{eff}, thus increasing the lift and drag. This causes the tip to move upwards and backwards. However, the twist deflection is unexpected. The simulation shows a pitch-down deflection, where one would expect pitch-up, since a higher α_{eff} causes a higher aerodynamic pitch-up moment. This discrepancy can be explained with the mode shapes. It is known that the first mode shape primarily couples an upward vertical deflection with a pitch-down twist deflection. The fact that this mode was predominant in the simulation, explains why the tip pitches down. After the gust, the tip vibrates towards is steady-state position again.

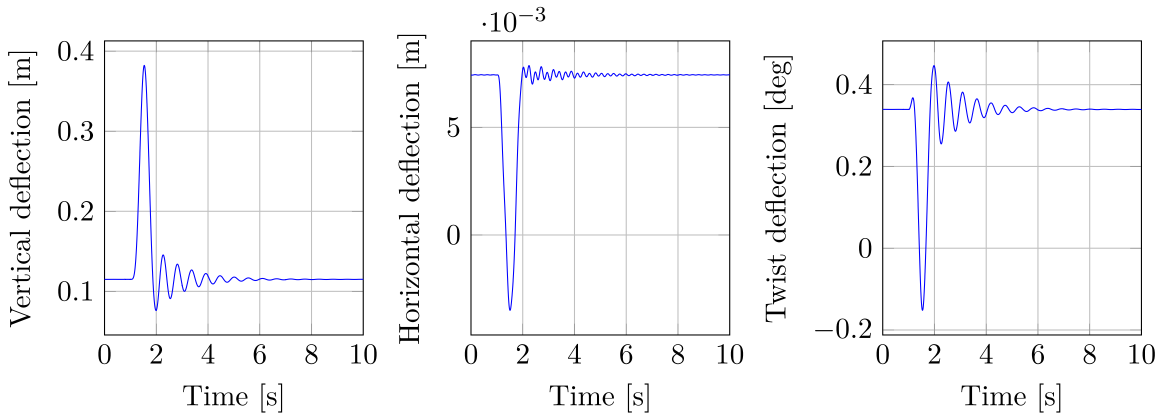

Figure 4-1: Tip deflection following a "1-cos" upward gust for a forward-moving wing.

Figure 4-2 shows the tip deflection following a flap deflection of 10 degrees applied between 1 and 4 seconds into the simulation. The behavior is as expected. When the flap deflection is applied, lift and drag increase and a pitch-down moment is created. This causes the tip to deflect upwards and backwards and to twist pitch-down, as is shown in the figure. Figure 4-3 shows the tip deflection following a downward aileron deflection. Since downward aileron deflection resembles flap deflection, one expects similar results for the two. Indeed, the deflections in figures 4-2 and 4-3 have the same direction.

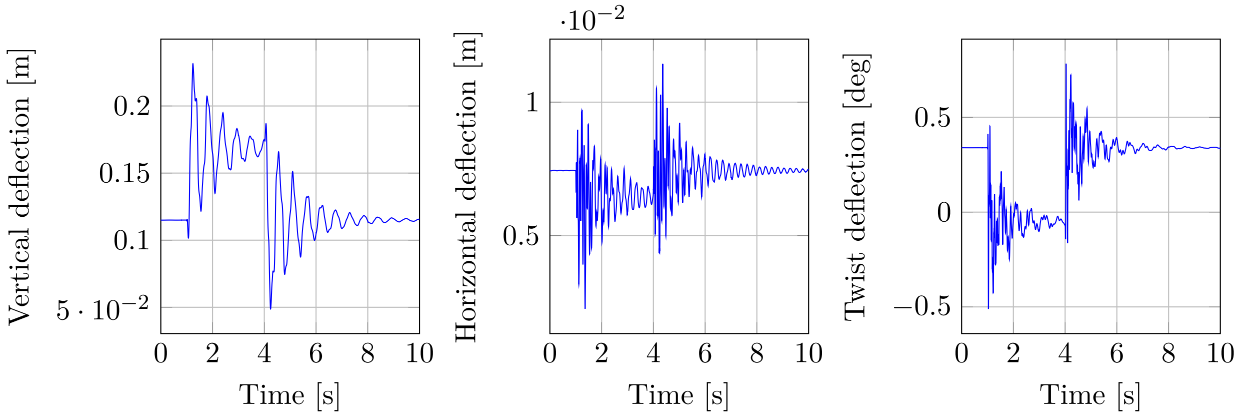

Figure 4-2: Tip deflection following a $10\,^\circ$ flap deflection for a forward-moving wing.

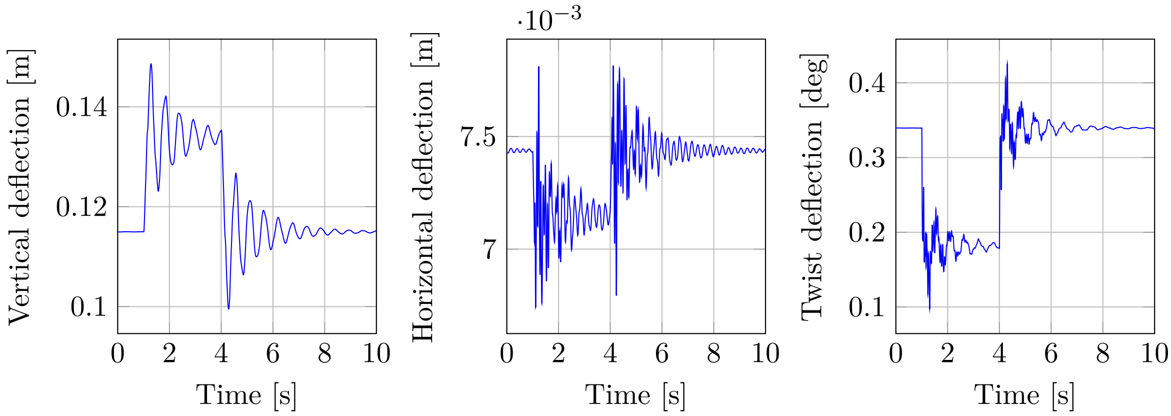

Figure 4-3: Tip deflection following a $10\,^\circ$ aileron down deflection for a forward-moving wing.

Lastly, figure 4-4 shows the tip deflection following a thrust increase from 118 kN to 268 kN during 1 and 4 seconds. The figure shows that there is little effect on the vertical deflection and that the tip moves forward, as expected. The twist deflection shows high-frequency vibration, corresponding to the typically higher frequencies of twist modes (see appendix B). The steady-state twist deflection during the period of increased thrust does not differ much from that for the normal thrust level. This could be expected, because the thrust force is aligned with the local chord, and can therefore not create a twist moment around the elastic axis, which lies on that chord line.

4-2 Steady-State Assessment

In this section, the steady-state position of the wing is verified by comparing it to theoretical calculations. Since a wing is too complex to verify with simple calculations, use is made of a rectangular cantilever beam. This beam is the same as the A320-like wing treated before (and in appendices A and B), but with some exceptions. First, the structural modal damping ratio is set to 0.2, to decrease the time to arrive at the steady-state position. Second, the chord is assumed to be equal to the tip chord along the whole semispan. Third, the wing

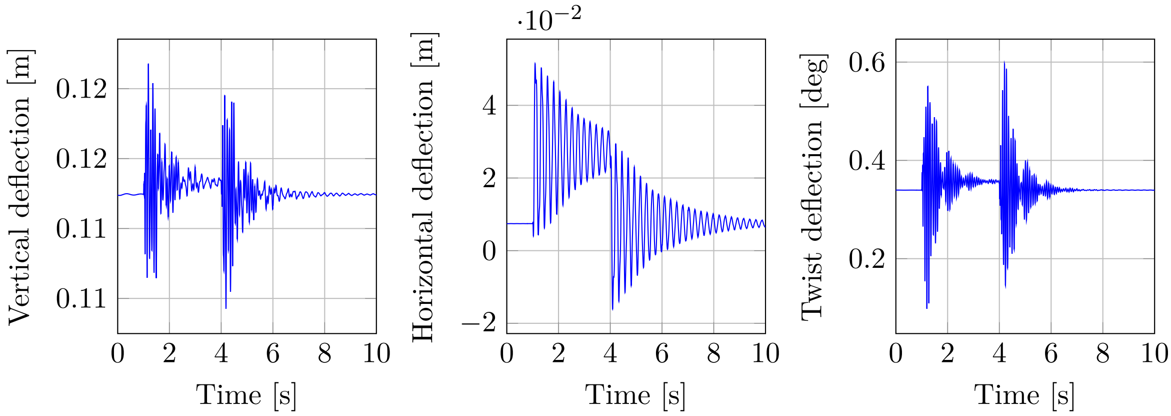

Figure 4-4: Tip deflection following a thrust increase for a forward-moving wing.

thickness is assumed to be 1 m everywhere. Fourth, the wing is assumed to be solid 2014-T6 aluminium. And fifth, the sweep, dihedral and setting angle are all zero. This creates a wing with a constant rectangular cross-section with a height of 1 m and a rectangular planform of 17.1 m by 1.6 m. Note that this beam has no physical significance, because the aerodynamic data and the wing weight are not changed, even though the airfoil shape obviously changed.

4-2-1 Rectangular Beam Modal Analysis

In order to analyze the rectangular beam, the mode shapes and natural frequencies should be determined. Assuming that deflection in one direction does not affect the cross-sectional properties, deflections in other directions are not affected by that deflection. Because of this, the modes are uncoupled.

There are several steps that must be taken to determine the plunge modes [74]. The process is analogous for the sweep modes, so that will not be shown here. The governing differential equation for plunge deflection is given in equation (4-1), in which E is the elastic modulus, I is the area moment of inertia, h is the plunge deflection, y is the coordinate from root to tip, ρ is the material density and A is the cross-sectional area. Substitution of the ansatz in equation (4-2) into the differential equation yields equation (4-3). Here, ϕ is the plunge mode shape and ω is the corresponding natural frequency.

$$EI\frac{\partial^4 h}{\partial y^4} + \rho A \frac{\partial^2 h}{\partial y^2} = 0 \tag{4-1}$$

$$h(y,t) = \phi(y) \sin(\omega t + \epsilon) \tag{4-2}$$

$$\frac{d^4\phi}{dy^4} - \frac{\rho A \omega^2}{EI}\phi(y) = 0 \tag{4-3}$$

Equation (4-3) is a fourth-order differential equation having the general solution in equation (4-4). Wavenumber λ is defined in equation (4-5), called the characteristic equation. The coefficients C_1-C_4 must be determined from the boundary conditions of the cantilever beam, given in equation (4-6). At the fixed end ($y = 0$), there is zero displacement and slope. At the free end ($y = L$), there is zero bending moment and shear force. Using this yields the frequency equation (4-7). This equation is solved in MATLAB using an optimization routine, in order to obtain the values of λL that solve the equation. With equation (4-5), the natural frequencies ω can then be determined.

$$\phi(y) = C_1 \sin \lambda y + C_2 \cos \lambda y + C_3 \sinh \lambda y + C_4 \cosh \lambda y \tag{4-4}$$

$$\lambda^4 = \frac{\rho A \omega^2}{EI} \tag{4-5}$$

$$\begin{aligned} \phi|_{y=0} &= 0 & \left.\frac{d\phi}{dy}\right|_{y=0} &= 0 \\ \left.\frac{d^2\phi}{dy^2}\right|_{y=L} &= 0 & \left.\frac{d^3\phi}{dy^3}\right|_{y=L} &= 0 \end{aligned} \tag{4-6}$$

$$\cos \lambda L \cosh \lambda L + 1 = 0 \tag{4-7}$$

One can also obtain the mode shape from the information above. The mode shape is given in equation (4-8) in which k_r is the constant described in equation (4-9). The subscripts r denote the different mode shapes related to the different natural frequencies. The first factor of equation (4-8) is used to perform mass normalization. The above derivation gives the rectangular beam mode shapes and natural frequencies in plunge and sweep. Appendix B presents them for the rectangular beam that is considered in the next sections.

$$\phi_r(y) = \left(\frac{1}{\sqrt{\rho A L}}\right) \left[\cosh(\lambda_r y) - \cos(\lambda_r y) - k_r \left(\sinh(\lambda_r y) - \sin(\lambda_r y)\right)\right] \tag{4-8}$$

$$k_r = \frac{\cos(\lambda_r L) + \cosh(\lambda_r L)}{\sin(\lambda_r L) + \sinh(\lambda_r L)} \tag{4-9}$$

The torsion modal information must still be determined. This is less covered in textbooks, but can be done in a similar way as for plunge and sweep. The general torsional vibration equation is given in equation (4-10). Here G is the shear modulus, γ is the torsional constant of the cross-section, ξ is the twist, ρ is the material density and J_p is the polar moment of area. Substitution of the ansatz in equation (4-11) into the differential equation yields a differential equation to which the general solution is given in equation (4-12) [7]. Here ϕ_T is the torsional mode shape, ω_T is the torsional natural frequency and λ_T is the torsional wavenumber. The latter is defined in equation (4-13).

$$G\gamma \frac{\partial^2 \xi}{\partial y^2} - \rho J_p \frac{\partial^2 \xi}{\partial t^2} = 0 \tag{4-10}$$

$$\xi(y,t) = \phi_T(y) \sin(\omega t + \epsilon) \tag{4-11}$$

$$\phi_T(y) = C_1 \sin \lambda_T y + C_2 \cos \lambda_T y \tag{4-12}$$

$$\lambda_T^2 = \frac{\rho J_p \omega_T^2}{G\gamma} \tag{4-13}$$

The coefficients C_1 and C_2 must be determined from the boundary conditions given in equation (4-14). At the fixed end ($y = 0$), there is zero twist and at the free end ($y = L$) there is zero moment. Using these boundary conditions results in equation (4-15), which is the frequency equation. As its name suggests, it can be used to find the natural frequency, in combination with equation (4-13).

$$\begin{aligned} \phi_T\big|_{y=0} &= 0 \\ \left.\frac{d\phi_T}{dy}\right|_{y=L} &= 0 \end{aligned} \tag{4-14}$$

$$\cos \lambda_T L = 0 \tag{4-15}$$

The solution to the frequency equation is given in equation (4-16). The mode shapes are given in equation (4-17). Again, the subscripts r denote the different mode shapes related to the different natural frequencies.

$$\lambda_{T,r} = \frac{(2r-1)\,\pi}{2L} \tag{4-16}$$

$$\phi_{T,r}(y) = \sin\left(\frac{(2r-1)\,\pi}{2L} y\right) \tag{4-17}$$

4-2-2 Simple Loading

Using the modal data defined in the previous section, the first steady-state analysis can be performed. This is a simple analysis, in which aerodynamic forces and the mass of the wing and landing gear are ignored so that the engine is the only force-producing object. For illustrative purposes, the engine center of gravity is placed halfway along the semispan with the regular chordwise offset (0.94 chords in front of the local elastic axis). Furthermore, it is given a mass of 10 kg and a thrust of 100 N. This creates a vertical force (due to weight), a horizontal force (due to thrust) and a pitch-down moment (due to static unbalance related to the chordwise offset), all acting at the middle of the beam.

The steady-state deflection can now be calculated using mechanics of materials equations. Equations (4-18) and (4-19) [75] are the well-known "forget-me-nots" for a cantilever beam with a force at half its length, used for the calculation of the tip plunge h_{tip} and forward deflection g_{tip}. Here V and H are the vertical and horizontal force, respectively. The twist of a rectangular section can be determined with equation (4-20) [76], in which ξ_{tip} is the tip twist deflection and M is the pitching moment. k_2 is a constant that can be determined trough a look-up table based on the ratio between width and height [77]. Equations (4-21)-(4-23) [75, 76] show the equations to determine the deflections at stations along the semispan, i.e. the length of the beam. In these equations, η is the dimensionless semispan. Note that these equations only hold for spanwise stations up to half the semispan.

$$h_{tip} = \frac{5VL^3}{48EI_{plunge}} \tag{4-18}$$

$$g_{tip} = \frac{5HL^3}{48EI_{sweep}} \tag{4-19}$$

$$\xi_{tip} = \frac{ML}{2k_2GI_{plunge}} \tag{4-20}$$

$$h(y) = \frac{V\,(\eta(y)L)^2}{6EI_{plunge}}\left(\frac{3}{2}L - \eta(y)L\right) \tag{4-21}$$

$$g(y) = \frac{H\,(\eta(y)L)^2}{6EI_{sweep}}\left(\frac{3}{2}L - \eta(y)L\right) \tag{4-22}$$

$$\xi(y) = \frac{M\eta(y)L}{k_2GI_{plunge}} \tag{4-23}$$

At this point, the results from a simulation can be compared to theoretical calculations based on the above equations. This is done in table 4-1, where the deflections at the tip and at 45% of the semispan are shown. The errors are very small, indicating correspondence between theory and model. The errors for twist are a bit larger than those for plunge and sweep, because of the approximate nature of the twist equations [76].

Table 4-1: Comparison of simulation and theory for midspan forces and moment.

Variable	**Simulation**	**Theory**	**Error**
h_{tip}	$5.241 \cdot 10^{-6}$	$5.241 \cdot 10^{-6}$	0.00%
g_{tip}	$2.087 \cdot 10^{-6}$	$2.088 \cdot 10^{-6}$	-0.01%
ξ_{tip}	$-1.434 \cdot 10^{-7}$	$-1.437 \cdot 10^{-7}$	-0.15%
$h(.45L)$	$1.783 \cdot 10^{-6}$	$1.783 \cdot 10^{-6}$	0.00%
$g(.45L)$	$7.101 \cdot 10^{-7}$	$7.102 \cdot 10^{-7}$	-0.00%
$\xi(.45L)$	$-1.295 \cdot 10^{-7}$	$-1.293 \cdot 10^{-7}$	0.16%

4-2-3 Multiple Loading

As was shown, the model generates accurate results when forces and a moment are applied on one location of the wing. Now, the steady-state position for a multiply loaded rectangular beam is assessed. All forces that act on a wing, i.e. aerodynamic forces, thrust and mass of the wing, landing gear and engine, are included. As was stated before, these forces are not related to the solid rectangular beam, but to the original A320-like wing.

In order to capture the deflection of a multiply loaded beam in a single expression and to make automated integration possible, discontinuity functions will be used [75]. Consider the beam in figure 4-5, on which several downward forces V_i act on several distances from the root d_i. These forces create a reaction moment M_R and force V_R at the root. In order to determine the deflections, the elastic formula in equation (4-24) may be used [75]. This equation relates the fourth-order derivative of plunge h to the distributed loading along the semispan w.

$$EI_{plunge}\frac{d^4h}{dy^4} = w(y) \tag{4-24}$$

Using discontinuity functions, the equivalent distributed loading may be determined for a multiply loaded beam, such as the one in figure 4-5. Equations 4-25 and 4-26 show a type of discontinuity function, called a singularity function, that relates vertical force V or moment M to the equivalent distributed loading. Another type of discontinuity function, called a

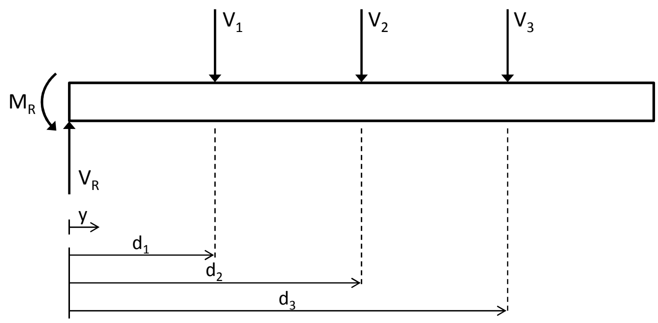

Figure 4-5: The multiply loaded rectangular beam.

Macaulay function, is shown in equation (4-27). This function is applied when the part in angle brackets is raised to a power m equal to or greater than zero.

$$w = V\langle y-d\rangle^{-1} = \begin{cases} 0 & \text{for } y \neq d \\ V & \text{for } y = d \end{cases} \tag{4-25}$$

$$w = M\langle y-d\rangle^{-2} = \begin{cases} 0 & \text{for } y \neq d \\ M & \text{for } y = d \end{cases} \tag{4-26}$$

$$w = \langle y-d\rangle^{m} = \begin{cases} 0 & \text{for } y < d \\ (y-d)^m & \text{for } y \geq d \end{cases} \quad m \geq 0 \tag{4-27}$$

Using equations (4-25) and (4-26) to describe the equivalent distributed loading for the multiply loaded in figure 4-5 and combining this with equation (4-24), yields equation (4-28). This equation may now be integrated four times, following integration rules for discontinuity functions stated in equations (4-29) and (4-30) [75]. Performing this integration yields equation (4-31). Because the left side of the beam is clamped, integration coefficients C_1 and C_2 are zero. Note that in this equation, the discontinuity functions are Macaulay functions, described in equation (4-27).

$$EI\frac{d^4h}{dy^4} = w(y) = V_R\langle y-0\rangle^{-1} - M_R\langle y-0\rangle^{-2} + \sum_{i=1}^{n} V_i\langle y-d_i\rangle^{-1} \tag{4-28}$$

$$\int \langle y-d\rangle^{m} = \langle y-d\rangle^{m+1} \qquad \text{for } m = -1, -2 \tag{4-29}$$

$$\int \langle y-d\rangle^{m} = \frac{\langle y-d\rangle^{m+1}}{m+1} + C \qquad \text{for } m \geq 0 \tag{4-30}$$

$$h = \frac{1}{EI_{plunge}}\left(\frac{V_R}{6}\langle y-0\rangle^3 - \frac{M_R}{2}\langle y-0\rangle^2 + \sum_{i=1}^{n}\frac{V_i}{6}\langle y-d_i\rangle^3 + C_1 y + C_2\right) \tag{4-31}$$

Using equation (4-31), the plunge deflection may be determined. This equation may also be used to determine the sweep deflection with some obvious adjustments: the forces should be horizontal, the moment should work in the horizontal plane and the area moment of inertia should be I_{sweep}.

Determination of the twist is much easier. It may be determined for each of the spanwise sections separately using equation (4-32), which looks like equation (4-23). Here, L_i is the length of the section and T_{int} is the internal torsion moment, which is equal to cumulative torsion going from root to tip.

$$\xi_i = \frac{T_{int,i} L_i}{k_2 G I_{plunge}} \tag{4-32}$$

Now, theoretical calculations can be performed, in order to verify the steady-state deflection of the model. Table 4-2 show the deflection of the tip and at 55% semispan, found with the simulation and with theory. Again, the errors are very small, which indicates that the model can correctly determine steady-state deflections. Note that the assessment was performed at 55% semispan instead of 45% like before. This was done, because at 45% semispan, the twist deflection crosses zero and in that case a small absolute error would yield a large percentage error, which blurs the assessment.

Table 4-2: Comparison of simulation and theory for distributed forces.

Variable	Simulation	Theory	Error
h_{tip}	$3.668 \cdot 10^{-3}$	$3.668 \cdot 10^{-3}$	0.01%
g_{tip}	$1.175 \cdot 10^{-3}$	$1.174 \cdot 10^{-3}$	0.01%
ξ_{tip}	$7.814 \cdot 10^{-6}$	$7.809 \cdot 10^{-6}$	0.07%
$h(.55L)$	$1.646 \cdot 10^{-3}$	$1.646 \cdot 10^{-3}$	0.01%
$g(.55L)$	$5.809 \cdot 10^{-4}$	$5.810 \cdot 10^{-4}$	-0.01%
$\xi(.55L)$	$2.775 \cdot 10^{-6}$	$2.771 \cdot 10^{-6}$	0.12%

4-3 Dynamic Assessment

In the previous section the steady-state behavior of the model was verified. In this section, the transient behavior of the model is treated. It will be verified in two ways. Firstly, the damping of the model will be verified using a decay envelope analysis. After that, the dynamic aeroelastic behavior of the model is verified by assessing the dynamic response following periodic gust input.

4-3-1 Decay Envelopes

The transient part of the deflection is governed by oscillatory decay, caused by damping. The user can provide the model with the structural modal damping ratio, which is usually set to 0.020 (see section 3-3-1). However, there are also other sources of damping as will become evident later. One can analyze the time history of the modal amplitudes in order to check whether the decay is as expected. In this section, the decay envelope method is explained and used.

Once the simulation is performed, the locations of local maxima can be determined. Then a curve fit of the exponential form in equation (4-33) is made through these maxima. In this equation, q_r is the modal amplitude of mode r and A and B are curve fit constants. Once this fit is made, equation (4-34) can be used to determine the modal damping ratio ζ_r from the curve fit constant B and the natural frequency of the mode ω_r.

$$q_r(t) = A\mathrm{e}^{Bt} \tag{4-33}$$

$$\zeta_r = -\frac{B}{\omega_r} \tag{4-34}$$

Three different load cases were simulated. The first load case includes all forces, i.e. weights, aerodynamic forces and moments, and thrust. In the second load case the aerodynamics are absent and in the third case both the aerodynamics and the thrust are absent. The results are shown in table 4-3. If only structural damping exists, the modal damping ratio for all modes should be 0.020. As one can see from the table, this is only true in the case where aerodynamics and thrust are absent, i.e. when there is only structural damping. Since the damping ratio is 0.020 for all modes in this load case, the transient analysis is simulated as expected.

Table 4-3: Modal damping ratios of the first ten modes.

Mode	All forces	Aerodynamics absent	Aerodynamics and thrust absent
1	0.076	0.022	0.020
2	0.020	0.020	0.020
3	0.059	0.020	0.020
4	0.023	0.020	0.020
5	0.024	0.020	0.020
6	0.020	0.020	0.020
7	0.019	0.003	0.020
8	0.025	0.020	0.020
9	0.020	0.020	0.020
10	0.021	0.020	0.020

An example of such a decay envelope analysis is shown in figure 4-6, which shows the first mode without aerodynamics and thrust. As one can see, the modal damping ratio is equal to 0.02 and the decay envelope nicely captures all local maxima. Clearly, structural damping is the only source of damping.

An important source of damping, besides structural damping, is aerodynamic damping. When a quasi-steady aerodynamic model is used, damping increases. This is because plunge velocity increases the effective angle of attack, thus increasing the lift force, which opposes the plunge motion. This effect is indeed displayed in the decay analysis of figure 4-7. This figure shows the first mode (a plunge mode) subject to all forces, including aerodynamic ones. The decay envelope again nicely captures all local maxima, but because of aerodynamic damping, the modal damping ratio is almost 4 times as high as with only structural damping.

Besides aerodynamic and structural damping, the thrust force influences damping, even when it has constant magnitude. The effect on damping is complex, because it involves multiple degrees of freedom and multiples modes. Figure 4-8 shows the analysis for the seventh mode subject to weights and thrust. Clearly, this mode is affected by the thrust, especially since

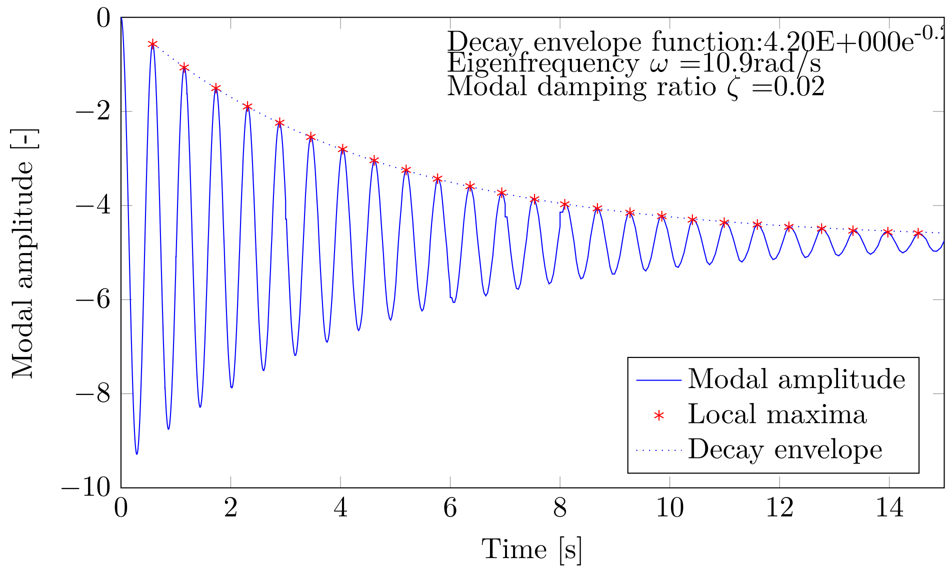

Figure 4-6: Decay envelope analysis for the first mode without aerodynamics and thrust.

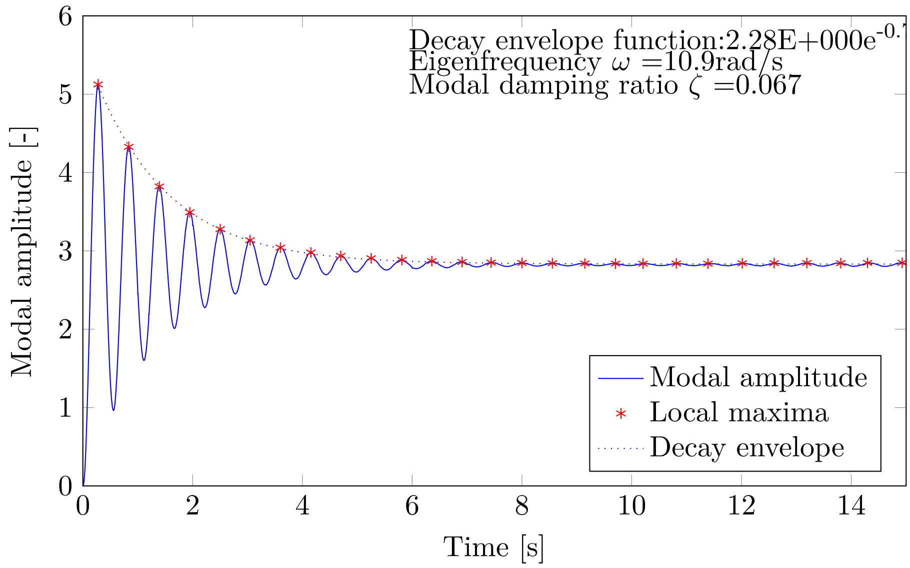

Figure 4-7: Decay envelope analysis for the first mode with all forces.

it shows perfectly clean behavior when the thrust force is absent (see table 4-3). This mode is a complex mode that combines pitch-up twist with backwards sweep (see appendix B). Whenever the wing pitches up, the thrust force rotates as well, since the engine is connected to the wing. Therefore, the forward-acting component of thrust decreases. This decrease stimulates the backwards motion that is also present in the mode, instead of opposing it. The thrust force thus causes negative damping. This can also be seen in figure 4-8, where the modal damping ratio is lower than the structural modal damping ratio of 0.02. Note that the figures does not show clean transient behavior, but oscillations at two different frequencies instead. This is the case because it is a complex mode that interacts with the effects of another mode.

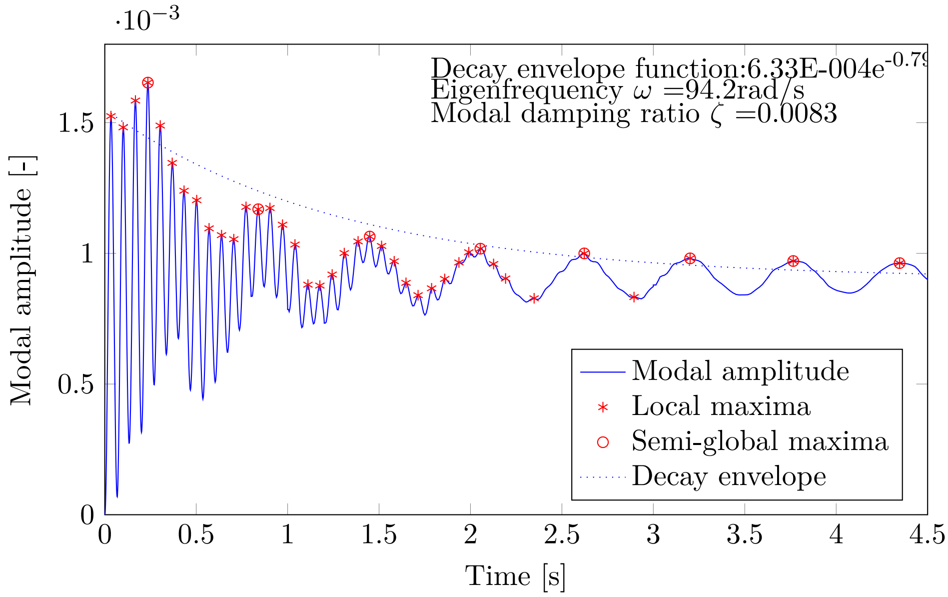

Figure 4-8: Decay envelope analysis for the seventh mode without aerodynamics.

4-3-2 Mode Excitation with Gusts

Another way of verifying the dynamic behavior of the model is by examining the dynamic response following periodic gusts of various frequencies. If the frequency of a gust coincides with the frequency of a particular mode, it can be expected that that mode dominates the response [44].

Multiple simulations were performed in which a wing that is at its steady-state encounters a sinusoidal gust. From the response that follows, one can calculate the range of the mode amplitude for each mode, i.e. the difference between the maximum and minimum mode amplitude. The results of this investigation are shown in figures 4-9 and 4-10. Each subfigure shows the amplitude range of a different mode (on the vertical axis), for varying gust frequencies (on the horizontal axis). The red lines indicate the location of the natural frequencies of the modes. Indeed, the mode amplitude ranges are maximum when the gust frequency coincides with the natural frequency of the mode, thus verifying the dynamic behavior of the model.

4-4 Comparison with Lumped-Parameter Model

In this section, the modal model is compared to the Lumped-Parameter Method (LPM) model. An LPM model was already created by Mark Voskuijl. For the current research, it was created again so that it completely corresponds to the modal model. The theory behind it will not be treated in detail here, but the interested reader is referred to literature [26].

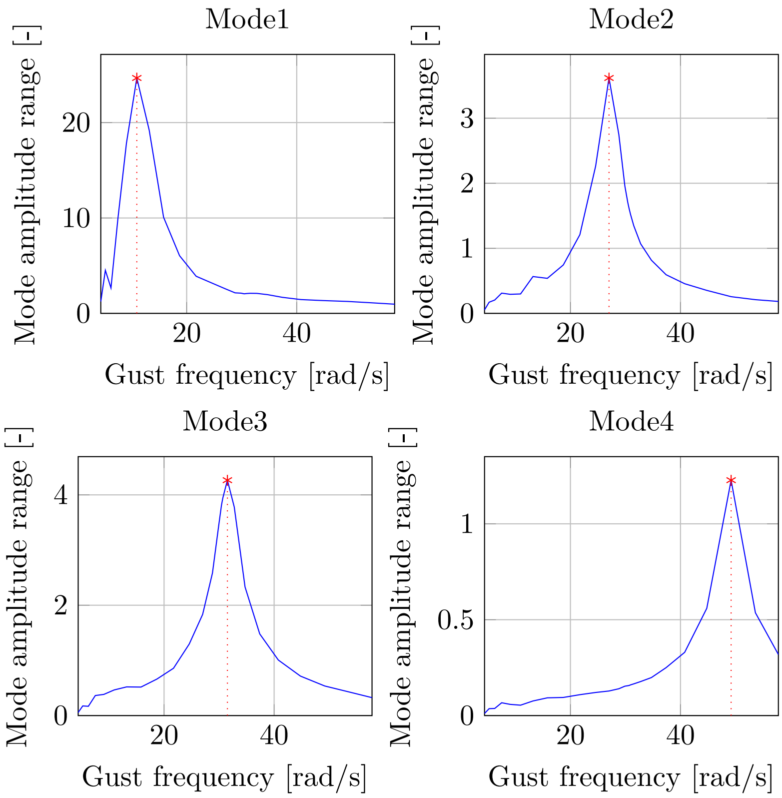

Figure 4-9: Mode amplitude ranges of modes 1-4 due to gusts of different frequencies.

4-4-1 Mode Determination

The first step that should be taken is to determine the mode shapes of the LPM model, so that a comparable modal model can be created. For this, consider the LPM representation in figure 4-11. This figure shows four body blocks, with torsion mass moment of inertia J_{ti} and bending mass moment of inertia J_{bi}. Note that the user can specify the number of body blocks, as long as it is an even number. Connections are present, which introduce degrees of freedom in torsion and bending. For the springs, the torsional stiffness k_{ti} and the bending stiffness k_{bi} are determined by the geometry of the surrounding bodies [26]. For the welds (the black squares), they are set to values that are many orders of magnitude higher.

The modal information can be determined using the following approach [78]. The torsion mass matrix M_t is defined in equation (4-35) and the torsion stiffness matrix K_t is defined in equation (4-36). The bending mass matrix M_b and bending stiffness matrix K_b are defined in a similar way. Now the equation of vibration is given in equation (4-37), in which $\ddot{\theta}_\mathbf{t}$ is a vector containing the torsion rotations and $\ddot{\theta}_\mathbf{b}$ is a vector containing the bending rotations. Note that no bending-torsion coupling occurs here.

$$M_t = \text{diag}\left(J_{t1}, J_{t2}, J_{t3}, J_{t4}\right) \tag{4-35}$$

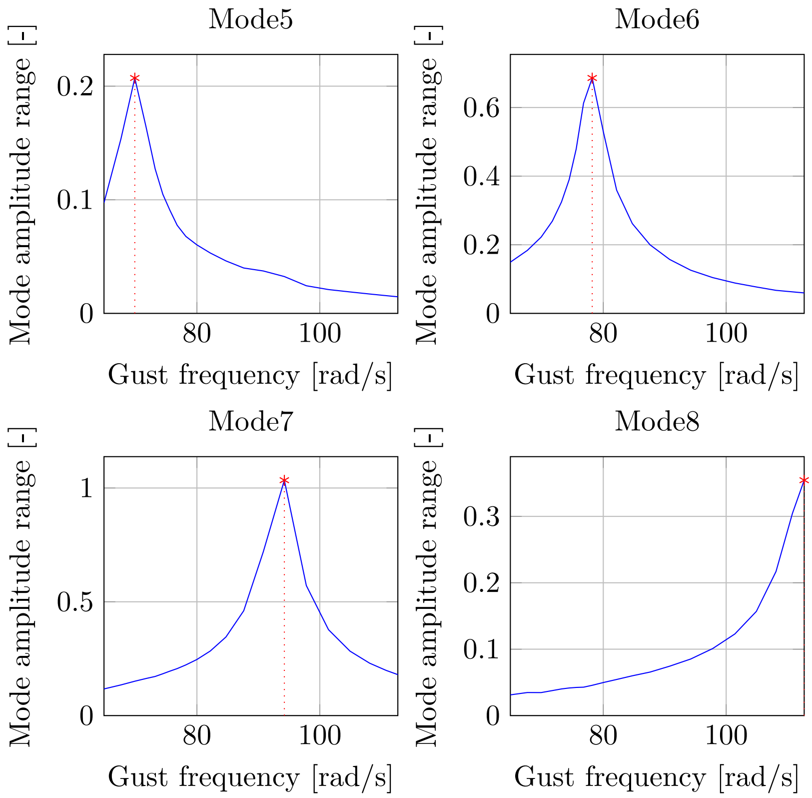

Figure 4-10: Mode amplitude ranges of modes 5-8 due to gusts of different frequencies.

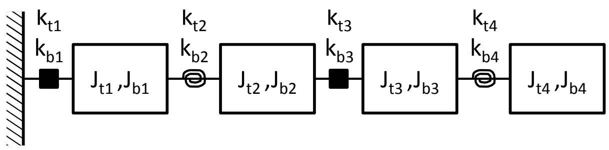

Figure 4-11: Lumped-parameter model configuration.

$$K_t = \begin{bmatrix} k_{t1} + k_{t2} & -k_{t2} & 0 & 0 \\ -k_{t2} & k_{t2} + k_{t3} & -k_{t3} & 0 \\ 0 & -k_{t3} & k_{t3} + k_{t4} & -k_{t4} \\ 0 & 0 & -k_{t4} & k_{t4} \end{bmatrix} \tag{4-36}$$

$$\begin{bmatrix} M_t & 0 \\ 0 & M_b \end{bmatrix} \begin{bmatrix} \ddot{\theta}_{\mathbf{t}} \\ \ddot{\theta}_{\mathbf{b}} \end{bmatrix} + \begin{bmatrix} K_t & 0 \\ 0 & K_b \end{bmatrix} \begin{bmatrix} \theta_{\mathbf{t}} \\ \theta_{\mathbf{b}} \end{bmatrix} = \begin{bmatrix} \mathbf{0} \\ \mathbf{0} \end{bmatrix} \tag{4-37}$$

Using the above information, the mass-normalized stiffness matrix $\tilde{K}$ can be determined from equation (4-38). In this equation, L is the Cholesky decomposition of the mass matrix M. Using the built-in eigensolver of MATLAB, an eigenvalue analysis on $\tilde{K}$ can be performed, yielding the natural frequencies and the matrix of eigenvectors P. The non-normalized mode shape vector S is then calculated from equation (4-39), after which the mass-normalized mode shape vector Φ is calculated using equation (4-40). Finally, the bending rotations can be transformed to plunge translations using trigonometry. Note that the welds were treated as very stiff springs, and that the natural frequencies of mode shapes that include weld rotation are therefore very large compared to the other natural frequencies.

$$\tilde{K} = L^{-1} K \left(L^T\right)^{-1} \tag{4-38}$$

$$S = M^{-\frac{1}{2}} P \tag{4-39}$$

$$\Phi = \left(S^T M S\right)^{-\frac{1}{2}} S \tag{4-40}$$

4-4-2 Steady-State Comparison

At this point, the steady-state position of the rectangular beam discussed in section 4-2-3 can be assessed. Three models are compared to each other: the LPM model, the modal model based on theoretical modes derived in section 4-2-1, and the modal model based on LPM-deduced modes, which were just described. All contain twelve spanwise sections. The LPM-modes have an accuracy comparable to the LPM model, which is worse than modes determined with a finite element program or with exact theory. Note that the rectangular beam that is assessed here does not include an engine or landing gear, since the created LPM cannot model these.

Figure 4-12 shows the vertical and twist deflection of the rectangular beam subjected to gravitational and aerodynamic forces. Two conclusions can be drawn from this figure. Firstly look at the LPM model and the LPM-based modal model. Both models predict the same deflections, meaning that the LPM modes were accurately determined and again verifying the steady-state prediction capability of the modal model.

The second conclusion that can be drawn is that the LPM and the LPM-based modal model provide relatively inaccurate predictions of the deflections, even though twelve LPM body blocks were used here. Note that accuracy is measured with respect to the theoretical model. Accuracy could be improved by increasing the number of body blocks, but that comes at a relatively steep cost for the LPM model, because the problem size, i.e. the number of generalized coordinates, increases just as much. For the modal model, the number of generalized coordinates does not increase when more nodes are added, since the number of modes stays the same.

This second conclusion aptly uncovers a main advantage of the modal method over the LPM method. Increasing accuracy of the LPM model is a costly affair, compared to that of the modal model. For the latter, improving accuracy is effectively only a matter of increasing the accuracy of the mode determination step, performed in the pre-processing phase. When the simulations were performed, it was found that the modal model was approximately 18 times faster than the LPM model, when twelve body blocks were included. This low computational cost is another great advantage of the modal model.

Only the steady-state position of the LPM and the modal model will be compared. It is not possible to compare the transient behavior, because it is not possible to model constant modal damping with the LPM model. Recall equation (2-11), which defined Rayleigh Damping and which is repeated below. Damping matrix C defines the damping coefficients for the LPM model, i.e. for each degree of freedom. The Rayleigh constants c_1 and c_2 are defined by

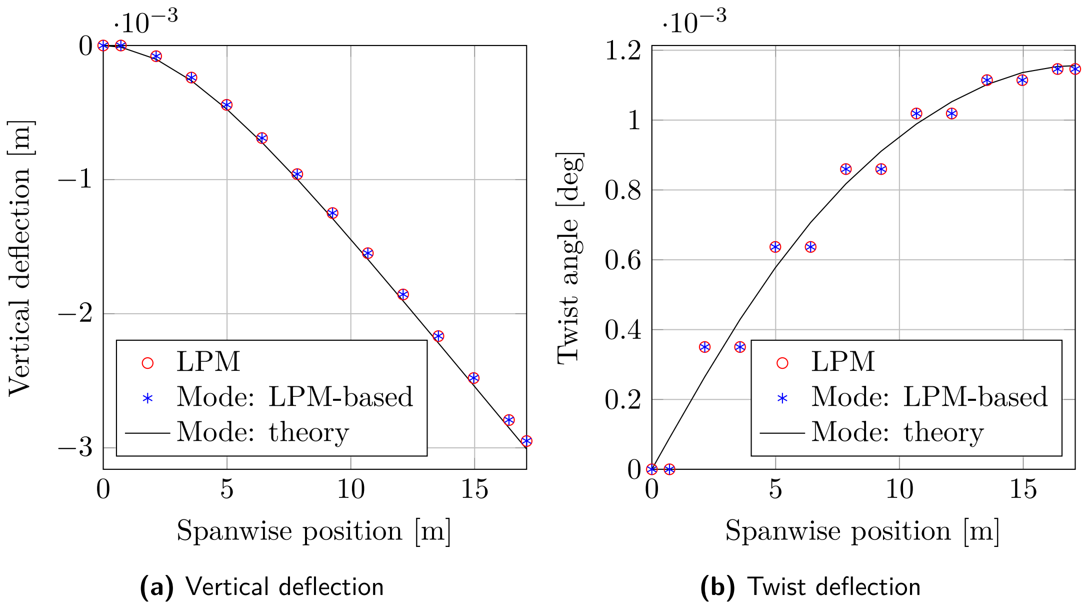

Figure 4-12: Comparison of rectangular beam deflection predicted by three different models.

the user and can be used to determine the modal damping ratio for mode r, i.e. ζ_r, using equation (4-41) [34].

$$C = c_1 M + c_2 K \tag{2-11}$$

$$\zeta_r = \frac{c_1}{2\omega_r} + \frac{c_2\omega_r}{2} \tag{4-41}$$

The problem is that, for constant c_1 and c_2, it is generally impossible to have an equal modal damping ratio ζ_r for every mode r. This is shown in figure 4-13, which shows the modal damping ratio for the twelve included modes. The Rayleigh constants were determined using three different approaches. One approach focuses on the significant modes (the first four here), one on all twelve modes and one on the average of the two [34]. None of these approaches achieved a modal damping ratio of 0.02 for every mode, which is the general way of modeling wing structural damping (see section 3-3-1). Therefore, constant Rayleigh Damping cannot be modeled with the LPM approach.

4-5 Summary

This chapter treated the verification of the aeroelastic wing model, in order to give credibility to the results of the model. Verification of the wing model was done extensively, since the wing model is at the core of the AFM model and because it contains the main novelties of this research.

First, a qualitative analysis showed that the wing reacts to gust and control input as one would expect. Thereafter, it was shown that static deformation is modeled correctly, since it closely agrees with theoretical calculations. In addition, the dynamic response of the wing was verified. Firstly, decay envelope analysis proved that damping of the wing corresponds to the provided structural damping ratios, as long as aerodynamic and thrust (i.e. non-structural)

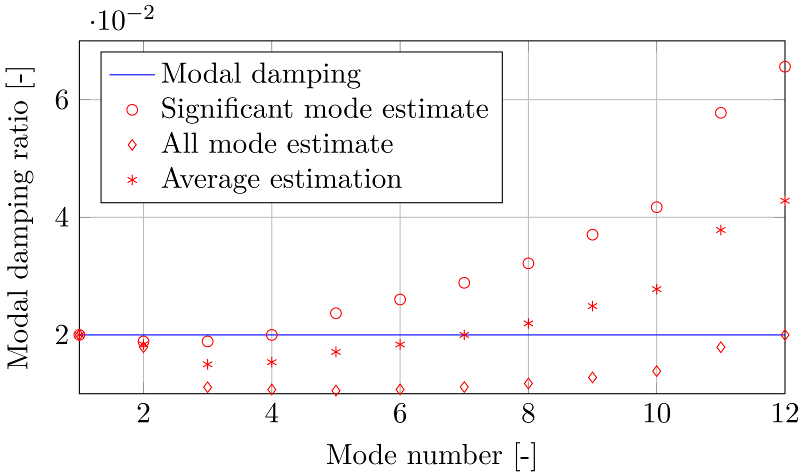

Figure 4-13: Modal damping ratios calculated from Rayleigh damping constants.

forces are absent. And secondly, mode excitation with gusts showed that wing deformation is largest for gust frequencies that are close to the natural frequencies of the modes. The last analysis showed that the lumped-parameter model finds similar, but less accurate, static deformation than the modal model.

All in all, the aeroelastic wing model was investigated with a multitude of analyses. Satisfying results were found for all analyses, which positively concludes the verification of the wing model.

Part II

The Flight Mechanics Model

Chapter 5

Flight Mechanics Theory

In this chapter the remaining theory behind the Aeroelastic Flight Mechanics (AFM) model will be treated. The theory behind the aeroelastic wing model, which is at the core of the AFM model, has already been discussed in chapter 2.

Generally, there are three main functionalities that are necessary for flight simulation and flight control purposes [19]. The first is simulation of the flight dynamics, i.e. the numerical integration of the equations of motion. The second is trimming, which is the determination of suitable input values to obtain a desired flight condition. The third is linearization and stability analysis around the trimmed position. These three functionalities are the subject of sections 5-1 to 5-3.

5-1 Flight Dynamics

The goal of the current research is to simulate the dynamic behavior of the whole aircraft due to control input, gusts and turbulence, together with structural deformation of the wing and empennage. As stated in chapter 1, attempts have been made to create an AFM model in which flight mechanics and structural dynamics are decoupled. Unfortunately, this has turned out to be too limiting, as aerodynamic coupling cannot be eliminated [3]. Two types of models are usually employed to simulate coupled flight mechanics and aeroelasticity: unified models and Multibody System Dynamics (MSD) models. Both will be discussed in this chapter.

5-1-1 Unified Models

In a unified model, flight mechanics, structural dynamics and aerodynamics are all combined into a single model. The starting point of the model is an aeroelastic state-space system, in which aerodynamics and structural dynamics are combined (see section 2-3). Flight dynamics is then introduced to this state-space system by means of rigid body modes. These rigid body modes are included in addition to the structural deformation modes which together describe the translation and orientation of the moving and deforming body [79]. In order to do this, the rigid body motion and forces are projected onto the deformation axis [1]. Note that by using rigid body modes in the linear state-space system, it is assumed that the rigid body modes are linear, i.e. that the deviation from the rectilinear flight path is small [62].

Equation (5-1) shows the matrix equation of motion for the aircraft [79]. In this equation $\mathbf{q}_r$ is the vector of generalized rigid body coordinates and $\mathbf{q}_e$ is the vector of generalized elastic coordinates. Furthermore, M_{rr} is the mass matrix of the rigid body modes, M_{ee} is the mass matrix of the elastic deformation modes, M_{re} is the mass matrix that couples the rigid body motion to the elastic deformation and M_{er} is the mass matrix that couples the elastic deformation to the rigid body motion. C_{ee} is the damping matrix of the elastic deformation modes and K_{ee} is the stiffness matrix of the elastic deformation modes. Lastly, Q_r and Q_e represent the generalized forces affecting the rigid body modes and structural deformation modes, respectively.

$$\begin{bmatrix} M_{rr} & M_{re} \\ M_{er} & M_{ee} \end{bmatrix} \begin{bmatrix} \ddot{\mathbf{q}}_r \\ \ddot{\mathbf{q}}_e \end{bmatrix} + \begin{bmatrix} 0 & 0 \\ 0 & C_{ee} \end{bmatrix} \begin{bmatrix} \dot{\mathbf{q}}_r \\ \dot{\mathbf{q}}_e \end{bmatrix} + \begin{bmatrix} 0 & 0 \\ 0 & K_{ee} \end{bmatrix} \begin{bmatrix} \mathbf{q}_r \\ \mathbf{q}_e \end{bmatrix} = \begin{bmatrix} \mathbf{Q_r} \\ \mathbf{Q_e} \end{bmatrix} \tag{5-1}$$

The main advantage of this type of model is that flight mechanics and aeroelasticity are solved simultaneously, since the whole model is cast into a single state-space system. This allows the model to be used for solving a large set of stability and response problems [1]. There are, however, two large disadvantages. Firstly, the rigid body modes can take into account rigid-body translations, but are not sufficient to describe large rigid-body rotations, because of the inherent nonlinearities [79]. Larger deviations from the flight path, such as during a pull-up, can therefore not be sufficiently described [62]. The second disadvantage relates to the fact that a partitioned aeroelastic approach, which was found to be optimal in chapter 2, cannot be employed in this kind of model.

Note that in the approach described above, the flight mechanics were included in the aeroelastic system by introducing rigid body modes. Another approach does the opposite; it introduces aeroelasticity in the flight mechanics model by modifying the stability derivatives usually associated with flight mechanics. The lowest-order derivatives are modified by an allowance for flexibility based on the steady-state aeroelastic deformation of the structure. This approach, however, cannot represent dynamic aeroelasticity and is outdated [62].

A more inclusive unified model was created by Meirovitch and Tuczu [13]. Their model includes coupling effects between flight mechanics and structural deformation and allows nonlinear flight mechanics and dynamic aeroelasticity. The model is clearly and completely explained in the paper by the creators [13]; that explanation will not be repeated here, for the sake of brevity. It can be stated, however, that the model conflicts with the research objective (see section 1-2), since it is not compatible with the SimMechanics environment.

5-1-2 Multibody System Dynamics Models

Multibody System Dynamics (MSD) can be used to model multiple bodies that can undergo large and complex translations and rotations relative to each other and the environment [23]. This is the case for the interaction of aeroelasticity and flight dynamics [22].

An MSD model allows natural and straightforward coupling of aeroelasticity and flight mechanics [3]. It is especially suitable for preliminary design of flight mechanics and aeroelasticity and can include the structural modal superposition method [3]. In other words, it can efficiently simulate small elastic deformation, which is superposed on large overall motions [27]. All this implies that the MSD approach is well suited for the goals of this thesis.

The equations of motion used in flight mechanics are highly nonlinear [3]. These equations are created in the MSD environment, where the bodies are constrained by and coupled with the motion of other components through a set of nonlinear constraint equations [79]. The structural deformation is assumed to be linear, as was stated in section 2-1. MSD codes automatically generate the equations of motion of the model as a nonlinear set of equations and provide a variety of solvers for numerical integration [23]. Because of this, the extensive material on the construction of the equations of motion is not treated here and the interested reader is referred to literature on this subject [80, 81].

As was stated in section 3-1, structural deformation is superposed on the movement of the rigid wing (which represents the flight dynamics). Therefore, two sets of coordinates are required in the equations of motion. Firstly, a set of Cartesian coordinates and rotational parameters to describe the flight mechanics motion, i.e. the motion of the reference frame. Secondly, the generalized coordinates that represent the structural deformation with respect to the moving reference frame [3].

For the approach used in the current research (described in chapter 3), massless bodies describe the deformed shape of the wing with respect to the rigid wing basis, which does have mass and inertia. Consequently, the inertia and mass distribution of the complete wing does not change when deformation occurs. This introduces some inaccuracy, but the accuracy loss is only significant for aircraft with a large flexibility, such as aircraft with very high aspect ratios [82]. The current model is not capable of accurately modeling those aircraft anyway, because the assumption of structural linearity made in the current research does not hold for these aircraft.

5-2 Trim

In the previous section, the flight dynamics model was described. This chapter discusses the trim of the aircraft based on this flight dynamics model.

The trim problem for elastic aircraft can be described as finding a set of suitable input values to satisfy a set of conditions [22]. The suitable input values are the control surface deflections, the thrust setting and the aircraft attitude. The set of conditions are the aircraft accelerations and the wing deformation accelerations. A pilot usually trims his aircraft to attain steady flight, in which all these accelerations are zero. Trimming in an MSD environment is broader, and can also be used to determine the required input values for non-zero accelerations, e.g. representing a pull-up maneuver.

Trimming is an important part of the AFM model, because of three reasons. Firstly, because it is generally necessary to first solve the trim problem when simulating a free flying aircraft [23, 83]. This provides the initial condition for the flight simulation. Secondly, when comparing different aeroelastic flight mechanics models, it is logical to compare the aeroelastic deformations for similar maneuvers (found with trim), instead of for similar control inputs. Similar control inputs could lead to completely different flight mechanics behavior in the different models, which prevents a clear view on the similarities and differences between

Table 5-1: Classification of the trim variables.

Objective variables	**Control variables**	**Flight condition**
Forward acceleration $\dot{u}$	Elevator deflection δ_e	True airspeed
Downward acceleration $\dot{w}$	Thrust T	Flight path angle γ
Angular accel. about Y_b-axis q	Pitch angle θ	Pitch attitude rate $\dot{\theta}$
*Rightward acceleration $\dot{v}$	*Aileron deflection δ_a	*Yaw angle ψ
*Angular accel. about X_b-axis p	*Rudder deflection δ_r	*Roll attitude rate $\dot{\phi}$
*Angular accel. about Z_b-axis r	*Roll angle ϕ	*Yaw attitude rate $\dot{\psi}$
*Sideslip angle β	*Flight track angle χ	
†Mode acceleration $\ddot{\mathbf{q}}$	†Mode amplitudes $\mathbf{q}$	

several models. Lastly, trim is important because linearization and stability analysis, treated in section 5-3, are mostly performed around a trimmed position [82].

5-2-1 Rigid Trim

In this section, the Jacobian trim approach is described, which is the preferred method for rigid aircraft, but also for more complex systems such as tilt rotors [84]. The Jacobian method is robust, since trim convergence is likely to occur even with rough estimates of the Jacobian and a rough first guess [33]. Furthermore, it generally requires less than 10 iterations when the modal structural representation is used [3]. This also implies that the Jacobian approach is the method of choice for elastic aircraft [19, 33]. Note that in general, any optimization routine could be used to solve the trim problem, as long as it is robust enough.

The variables associated with the trim problems can be divided into three categories: the objective variables, the control variables and the flight condition variables. Table 5-1 shows the variables that fall into these categories. The variables denoted with an asterisk are only required for three-dimensional trim, i.e. when describing both symmetric and asymmetric aircraft motion. The variables denoted with an obelisk are related to wing deformation and are only required for explicit trim (the subject of section 5-2-2).

The objective variables need to be driven towards the specified values, often zero (i.e. steady flight with zero sideslip). The objective parameters are combined in the objective vector $\mathbf{o}$, shown in equation (5-2). The accelerations are all defined in the body-fixed reference frame F_b. The sideslip angle β is also included, since for most cases, there are multiple solutions to the trim problem, each with a different sideslip angle. In the desired solution the sideslip angle should be zero. In that case, the drag is at a minimum and the turn will be most comfortable for passengers [85].

The control parameters are adjusted in order to drive the objective parameters to their specified values. Together, they form the control vector $\mathbf{c}$, described in equation (5-3). The control variables describe the trimmed pilot control and the aircraft attitude. Lastly, the flight condition parameters specify the desired flight condition and are not changed during the trim process.

$$\mathbf{o} = \begin{bmatrix} \dot{u} & \dot{v} & \dot{w} & \dot{p} & \dot{q} & \dot{r} & \beta \end{bmatrix}^T \tag{5-2}$$

$$\mathbf{c} = \begin{bmatrix} \delta_e & \delta_a & \delta_r & T & \phi & \theta & \chi \end{bmatrix}^T \tag{5-3}$$

Now that the associated variables are known, the Jacobian approach can be explained. It is based on the assumption that the change of the objective vector is linearly related to the change in the control input, which is shown in equation (5-4) [84]. In this equation, J_i is the Jacobian matrix evaluated near control input $\mathbf{c}_i$. The Jacobian matrix is shown in equation (5-5). Its entries are first order partial derivatives and represent the effect of changes in each control input on each acceleration.

$$\mathbf{o}_{i+1} - \mathbf{o}_i = J_i \left[\mathbf{c}_{i+1} - \mathbf{c}_i\right] \tag{5-4}$$

$$J_i = \left.\frac{\partial \mathbf{o}}{\partial \mathbf{c}}\right|_{\mathbf{c}_i} = \begin{bmatrix} \frac{\partial \dot{u}}{\partial \delta_e} & \frac{\partial \dot{u}}{\partial \delta_a} & \frac{\partial \dot{u}}{\partial \delta_r} & \frac{\partial \dot{u}}{\partial T} & \frac{\partial \dot{u}}{\partial \phi} & \frac{\partial \dot{u}}{\partial \theta} & \frac{\partial \dot{u}}{\partial \chi} \\ \frac{\partial \dot{v}}{\partial \delta_e} & \frac{\partial \dot{v}}{\partial \delta_a} & \frac{\partial \dot{v}}{\partial \delta_r} & \frac{\partial \dot{v}}{\partial T} & \frac{\partial \dot{v}}{\partial \phi} & \frac{\partial \dot{v}}{\partial \theta} & \frac{\partial \dot{v}}{\partial \chi} \\ \frac{\partial \dot{w}}{\partial \delta_e} & \frac{\partial \dot{w}}{\partial \delta_a} & \frac{\partial \dot{w}}{\partial \delta_r} & \frac{\partial \dot{w}}{\partial T} & \frac{\partial \dot{w}}{\partial \phi} & \frac{\partial \dot{w}}{\partial \theta} & \frac{\partial \dot{w}}{\partial \chi} \\ \frac{\partial \dot{p}}{\partial \delta_e} & \frac{\partial \dot{p}}{\partial \delta_a} & \frac{\partial \dot{p}}{\partial \delta_r} & \frac{\partial \dot{p}}{\partial T} & \frac{\partial \dot{p}}{\partial \phi} & \frac{\partial \dot{p}}{\partial \theta} & \frac{\partial \dot{p}}{\partial \chi} \\ \frac{\partial \dot{q}}{\partial \delta_e} & \frac{\partial \dot{q}}{\partial \delta_a} & \frac{\partial \dot{q}}{\partial \delta_r} & \frac{\partial \dot{q}}{\partial T} & \frac{\partial \dot{q}}{\partial \phi} & \frac{\partial \dot{q}}{\partial \theta} & \frac{\partial \dot{q}}{\partial \chi} \\ \frac{\partial \dot{r}}{\partial \delta_e} & \frac{\partial \dot{r}}{\partial \delta_a} & \frac{\partial \dot{r}}{\partial \delta_r} & \frac{\partial \dot{r}}{\partial T} & \frac{\partial \dot{r}}{\partial \phi} & \frac{\partial \dot{r}}{\partial \theta} & \frac{\partial \dot{r}}{\partial \chi} \\ \frac{\partial \beta}{\partial \delta_e} & \frac{\partial \beta}{\partial \delta_a} & \frac{\partial \beta}{\partial \delta_r} & \frac{\partial \beta}{\partial T} & \frac{\partial \beta}{\partial \phi} & \frac{\partial \beta}{\partial \theta} & \frac{\partial \beta}{\partial \chi} \end{bmatrix}_{\mathbf{c}_i} \tag{5-5}$$

Reordering equation (5-4) results in equation (5-6). This equation represents the approach that is taken during the trim algorithm. It can be used to determine the new control input $\mathbf{c}_{i+1}$. Note that $\mathbf{o}_{i+1}$ was replaced by $\mathbf{o}_{desired}$ in this equation. This is done because it represents a numerical approximation to get as close to the desired accelerations $\mathbf{o}_{desired}$ as possible with a linear model. Equation (5-6) is used iteratively until the accelerations are close enough to the desired accelerations.

$$\mathbf{c}_{i+1} = \mathbf{c}_i + J_i^{-1} \left[\mathbf{o}_{desired} - \mathbf{o}_i\right] \tag{5-6}$$

The Jacobian matrix has not been determined yet. This is usually done with a finite difference method for every control input variable [25]. A central difference method is preferred in most cases, except near bounds on the control inputs, in which case a forward or backward difference method is more appropriate [84].

In the Jacobian approach, the nonlinear relation between the control input and the accelerations is estimated by a linear relation. This approximation is only accurate on a small segment around the control input at which it is evaluated. If the control input is changed, the Jacobian should be evaluated again near the new control input. A new simulation of the flight mechanics model is usually required for this [23].

Using a good initial guess for the control vector speeds up the trim calculation and makes it more robust. This first guess can be based on the trim situation of the rigid aircraft, the determination of which requires relatively little computational effort [3].

Two additional measures may be taken to improve the trim calculation. Firstly, a relaxation factor can be used to avoid excessive overshoots in the trim calculation. A relaxation factor of 0.75 for instance means that the trim corrections are only 75% of those calculated with the Jacobian [33]. Secondly, it is advised to scale the control parameters during the trim calculation, because some trim parameters may be numerically much larger than others [22].

5-2-2 Extension to Flexible Aircraft

There may be notable differences between the trim results for the flexible case versus the rigid case. That is because stability derivatives can be substantially different for these two cases [25]. For flexible aircraft, it is also required that the elastic deformation is in its steady state, so the second derivatives of the modal (i.e. generalized) coordinates should be zero [23]. In theory, these could also be non-zero in the trimmed situation, but that is hardly ever used. Flexibility can be included in the trim process in an implicit and in an explicit manner, as will be discussed in the following.

Implicit manner In the implicit way of approaching flexible aircraft trim, two levels are used [33]. First, there is an inner level that contains the AFM model which converges to the steady state solution. Above that is the outer level, which contains the trim algorithm, as described in section 5-2-1.

In the inner level, the control input is set to the values suggested by the trim algorithm. The initial shape of the structure is guessed, e.g. based on the final shape of the previous trim iteration. Then the simulation is run for a sufficient amount of time, until the structure is at its steady state. At this point, the flight mechanics accelerations and the sideslip angle, i.e. the objective parameters, are measured. These form the output of this level.

The measured flight mechanics accelerations are the input for the outer (trim) level. Here, the approach described in section 5-2-1 is used to select new control input. This will drive the objective parameters towards their prescribed values, whilst the accelerations associated with deformation are zero at every trim iteration.

Note that because some time is required for the structure to reach its steady-state, the aircraft will not be flying at the exact flight condition that was specified. For an unstable flight condition, this deviation can become large, which is the reason that this method is not suitable for unstable aircraft. For stable aircraft, the method does work and the described error can be reduced by artificially increasing the structural damping ratio during the trim process.

Explicit manner In the explicit way of approaching flexible aircraft trim, the accelerations associated with aeroelastic deformation are handled directly in the trim algorithm. Therefore, the objective vector will be of the form shown in equation (5-7). The second order derivatives of the modal coordinates, $\ddot{\mathbf{q}}$, are included and must be driven to their prescribed values, i.e. to zero. The vector of control inputs must be adjusted as well and is shown in equation (5-8), in which the shape of the structure, $\mathbf{q}$, was added. This means that the trim algorithm also tries to determine the steady-state shape of the structure. The Jacobian is then of the form shown in equation (5-9), similar to before.

In the explicit manner, the flying flexible aircraft only has to be simulated for a short duration, after it is clear what the accelerations associated with flight mechanics and flexibility are. This is in contrast with the implicit manner, where some time was required for the structure to reach its steady-state. The explicit approach will therefore find a trimmed condition that better reflects the desired flight condition than the implicit approach. Because of this, the explicit approach is used in the model to determine the final trim condition. A given number of implicit approach iterations can be performed in order to determine the initial guess for the explicit model.

Note that the Jacobian used in the explicit manner has more entries (due to the addition of $\mathbf{q}$ and $\ddot{\mathbf{q}}$), which requires more computational effort to evaluate. In other words, when the Jacobian is determined in the explicit manner, more entries must be evaluated, but less time is required for each entry evaluation.

$$\mathbf{o_{flex}} = \begin{bmatrix} \dot{u} & \dot{v} & \dot{w} & \dot{p} & \dot{q} & \dot{r} & \beta & \ddot{\mathbf{q}} \end{bmatrix}^T \tag{5-7}$$

$$\mathbf{c_{flex}} = \begin{bmatrix} \delta_e & \delta_a & \delta_r & T & \phi & \theta & \chi & \mathbf{q} \end{bmatrix}^T \tag{5-8}$$

$$J_i = \left. \frac{\partial \mathbf{o_{flex}}}{\partial \mathbf{c_{flex}}} \right|_{\mathbf{c}_i} \tag{5-9}$$

5-3 Linearization

Once the trimmed condition is determined, the nonlinear AFM model can be linearized around this condition. The obtained linearized model can be used for various purposes. Firstly, it can be used for stability analysis of the trimmed position, which allows the determination of stability derivatives and of the flight dynamics modes (not to be confused with the modes related to structural deformation). Secondly, it is often required for control systems. For instance, in order to perform load alleviation with most control system techniques, the nonlinear flight dynamics model needs to be transformed into a linear and controllable one [86]. Lastly, the linearized model may be used for fast time domain simulation. This is reasonably accurate as long as the deviations from the trimmed position are not too large.

With linearization, a nonlinear model is basically approximated by a linear one. There is a multitude of approaches that can be used to linearize flight mechanics models. The reader that is interested in the variety of approaches is referred to literature [86, 87]. Here, only Jacobian linearization will be discussed. For this, consider the nonlinear system given in equation (5-10). Here $\mathbf{x}$ is the state vector, $\dot{\mathbf{x}}$ is its time derivative, $\mathbf{u}$ is the input vector and $\mathbf{y}$ is the output vector. This nonlinear system has an equilibrium point, representing the trimmed condition.

Now, Jacobian linearization is a commonly used approach that assumes that the local linear behavior of the nonlinear system can be cast into the state-space form of equation (5-11) [88]. Here, $\mathbf{z}$ is a vector containing the deviation of the states from their equilibrium position, $\dot{\mathbf{z}}$ is its time derivative, $\mathbf{v}$ is a vector containing the deviation of the inputs from their equilibrium position and $\mathbf{w}$ is a vector containing the deviation of the outputs from their equilibrium position. The matrices A, B, C and D are defined in equation (5-12), and are determined at the equilibrium point. They are Jacobian matrices, hence the name of the approach. The entries of these Jacobian matrices may be determined using finite difference methods, similar to the determination of the Jacobian matrix in section 5-2-1.

$$\begin{aligned} \dot{\mathbf{x}} &= f(\mathbf{x}, \mathbf{u}) \\ \mathbf{y} &= h(\mathbf{x}, \mathbf{u}) \end{aligned} \tag{5-10}$$

$$\begin{aligned} \dot{\mathbf{z}} &= A\mathbf{z} + B\mathbf{v} \\ \mathbf{w} &= C\mathbf{z} + D\mathbf{v} \end{aligned} \tag{5-11}$$

$$\begin{aligned} A &= \frac{\partial f(\mathbf{x}, \mathbf{u})}{\partial \mathbf{x}} & B &= \frac{\partial f(\mathbf{x}, \mathbf{u})}{\partial \mathbf{u}} \\ C &= \frac{\partial h(\mathbf{x}, \mathbf{u})}{\partial \mathbf{x}} & D &= \frac{\partial h(\mathbf{x}, \mathbf{u})}{\partial \mathbf{u}} \end{aligned} \tag{5-12}$$

The important question that remains, is which variables should be in the state, input and output vectors. The input vector of a flight mechanics model contains the pilot inputs, i.e. the control surface deflections and the throttle. The state vector consists of the variables that define longitudinal and lateral-directional flight [85]. For longitudinal motion, these are the forward speed, the downward speed, the pitch angle and the pitch attitude rate. For lateral-directional motion, these are the rightward speed, the roll angle, the roll attitude rate, the yaw angle and the yaw attitude rate. The output vector can hold multiple variables of interest. If the linearized model is used for a load alleviation system, the output variables are the values that will be controlled, i.e. the wing root bending moment and/or variables that are used as a proxy for the wing root bending moment, e.g. modal or wing-tip accelerations. The input variables include the primary controls, but could also include secondary controls (e.g. trim tabs), broadening the capabilities of the load alleviation algorithm [9].

With these state, input and output vectors, the linear AFM model is defined. Eigenanalysis of matrix A provides information about the flight dynamics modes [85], and the Jacobian matrices hold information about the stability and control derivatives of the flexible aircraft.

5-4 Summary

This chapter discussed the theory about a broad range of subjects. Table 5-2 provides an overview of the models that are used for the different disciplines and the associated assumptions (in *italics*).

Table 5-2: The approaches taken for the various disciplines and the associated assumptions.

Discipline	**Approach & assumptions**
Flight Dynamics	Multibody System Dynamics
	Neglected changes in inertia and mass distribution due to deformation
	Structural deformation superposed on flight dynamics
Trimming	Combined implicit and explicit Jacobian approach
Linearization	Jacobian linearization

Chapter 6

Flight Mechanics Methodology

In this chapter, the implementation of the Aeroelastic Flight Mechanics (AFM) model is treated, which is based on the theory discussed in chapter 5. At the core of this model is the aeroelastic wing model, discussed in chapter 3. Just like in the previous chapter, the three main functionalities of flight simulation and control models form the basis for this chapter. They are the simulation of the flight dynamics, the trimming of the aircraft, and linearization and stability analysis. These three functionalities are the subject of sections 6-1 to 6-3.

6-1 Aircraft Model

Multibody System Dynamics (MSD) will be used to model the aircraft, as was stated in chapter 5. In this approach, the various parts of the aircraft are connected to each other and placed in the flight environment. The model lay-out will now be treated in further detail. Thereafter, the numerical integration method used for the time domain simulation is discussed.

6-1-1 Model Lay-out

Figure 6-1 shows a screenshot of the AFM model in SimMechanics. The blue blocks represent the general environment, which is the same as that discussed in section 3-2-1. The general environment is only defined once, so these blocks only reside at the level shown in figure 6-1.

The "Aircraft DOF" block (in green) is used to define the degrees of freedom of the aircraft. This block connects the aircraft reference point (near the aircraft center of gravity) to the "Ground" block, through a "Bushing" joint. Such a joint has six degrees of freedom. The first three are translations and represent the position of the aircraft in the Earth reference frame. The second three are rotations and represent the attitude of the aircraft with respect to the Earth reference frame, i.e. the Euler angles ψ, θ and ϕ. The initial values of the translations and rotations must be provided by the user, as well as those of their time derivatives, i.e. the velocities. This is important input, because it specifies the initial flight condition.

Although six degrees of freedom are required to model the complete behavior of a free-flying aircraft, the user can also choose to block some of the degrees of freedom. In that case, the user must still provide the initial values for the blocked translations or rotations and their time derivatives, i.e. the velocities. The velocity will stay constant throughout the time domain simulation and the translation or rotation will deviate from its initial condition according to this velocity. In such a way, the user can create a two-dimensional model (all lateral and directional degrees of freedom blocked), a wind tunnel model (all translational degrees of freedom blocked), or a fixed model (all degrees of freedom blocked).

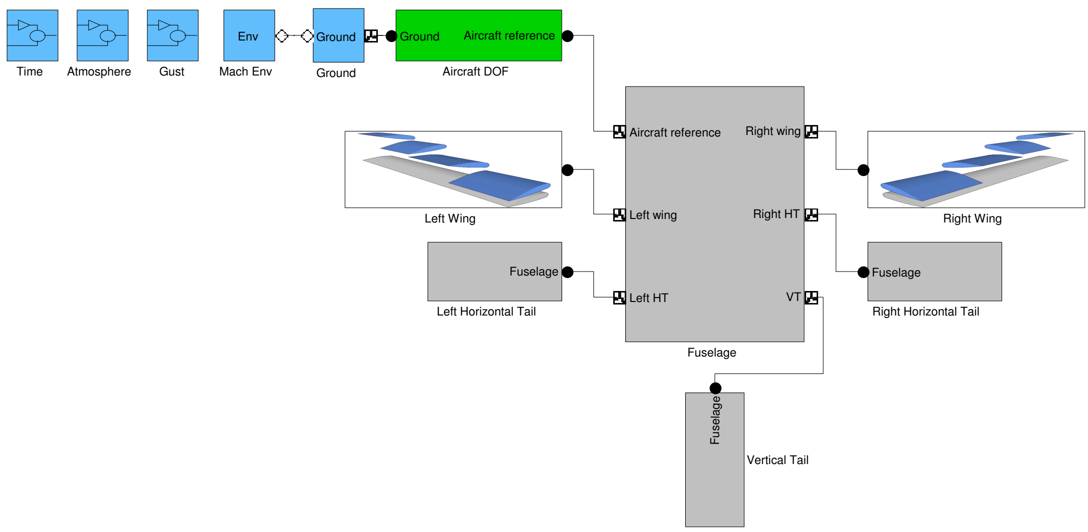

Figure 6-1: Screenshot of the SimMechanics aircraft model.

The remaining blocks are all actual aircraft parts. They represent the fuselage, the vertical tail, the horizontal tail and the wings. Commonly, an aeroelastic flight mechanics model will assume that the fuselage and empennage are rigid, and that the wings are flexible [89]. This is assumed because of two reasons. Firstly, because the deformations of the wing will be much larger than those of the fuselage and empennage. Secondly, because the effect of wing deformation on the forces acting on the aircraft will be the largest. In the model created for the current research, the fuselage is always rigid, but the wings and tail surfaces may be either rigid or flexible, whatever is desired by the user. Note that including flexibility of the fuselage is a relatively easy task, but it was chosen not to model this, because no associated mode shapes or natural frequencies were available. The different aircraft parts will now be treated in more detail.

The fuselage is modeled as a rigid body, to which all other parts are connected. The fuselage body also contains the aircraft reference point, which is connected to the "Aircraft DOF" block, in order to correctly specify the position, attitude and velocity of the aircraft. Moreover, a virtual sensor is connected at this reference point, and is used to make several measurements, in both the Earth and the body reference frames. In the Earth reference frame, the sensor measures the aircraft position (x_E, y_E and z_E), Euler angles (ψ, θ and ϕ), and the translational velocity (u_E, v_E and w_E) and accelerations ($\dot{u}_E$, $\dot{v}_E$ and $\dot{w}_E$). In the body reference frame, it measures the translational velocites (u, v and w) and accelerations ($\dot{u}$, $\dot{v}$ and $\dot{w}$), and the angular velocites (p, q and r) and accelerations ($\dot{p}$, $\dot{q}$ and $\dot{r}$). Besides that the fuselage forms a connection between aircraft parts and that it allows measurement of flight conditions, there are also forces that work on the fuselage. These are the weight, lift and drag. The lift and drag are determined using look-up tables based on the angle of attack and sideslip angle of the fuselage. Note that weight must be included explicitly, since the gravitational acceleration is zero in the model (see section 3-2-1). The required input parameters are shown in the first column of table 6-1. Parameters denoted by an asterisk can either be provided directly or they can be estimated. The estimation of mass is based on Raymer's method [90], the estimation of inertia is based on the DATCOM method [91] and the estimation of fuselage aerodynamics is based on Roskam's method [92]. The estimated aerodynamic data for the A320-like aircraft under consideration is presented in appendix A.

The wings are modeled according to the method described in chapter 3. The associated input parameters were given in table 3-1. A few parameters in this table are defined for the entire aircraft in the AFM model, instead of for the wing alone. These are the flight parameters and the simulation time. If the user chooses to neglect flexibility of the wing (e.g. for verification purposes), not much changes to the wing model. Only the state-space system is removed, such that the output variables of the state-space system (deformation and its time derivatives) are always zero.

When flexible tail surfaces are included in the model, they too are modeled in the way that was described in chapter 3. When rigid tail surfaces are assumed, they are modeled as a single section represented by a single body. The aerodynamic forces and weight are then determined for the tail surface as a whole. The aerodynamic forces and moment are dependent on the effective angle of attack through look-up tables. The control surfaces that are present on the tail surfaces are modeled in the same way as the ailerons and flaps on the main wing (see section 3-2-3). Thus, the control surface aerodynamic effect is modeled as an idealized point force on the trailing edge, which is dependent on the effective angle of attack and the control surface deflection angle. This aerodynamic data of the A320-like aircraft is presented in appendix A.

6-1-2 Numerical Integration Method

The aircraft model that was described in the previous section may be used for time domain simulation. Time domain simulation generally revolves around the integration of the Ordinary Differential Equations (ODEs) of the MSD system and those in the state-space system that represents deformation. In order to allow time domain simulation, the analysis mode in Simulink is set to "Forward Dynamics".

SimMechanics offers a multitude of numerical integration methods, each with its own advantages and disadvantages [93]. When deciding upon a solver, a variable step or a fixed step solver must be selected. For the current model, a variable step solver will be more efficient. That is the case, because the wing will oscillate with a high frequency just after an excitation, which requires a very small time step. Since high-frequency modes are heavily damped (see section 2-1-1), wing oscillations will soon occur at lower frequencies, for which a larger time step is sufficient. When the wing is at rest, only the natural frequencies related to flight mechanics are of interest, which are even lower and for which an even larger time step would suffice. If a fixed-step solver were to be used, these latter two situations would still be solved

Table 6-1: Fuselage, rigid tail surface and rigid tail control surface input parameters.

Fuselage	Rigid tail surface	Rigid tail control surface
Length	Semispan	Spanwise location
Wetted area	Root chord	Location of e.a.
Location of reference point	Taper	Deflection angle
*Mass	Sweep	Control input
*Inertia	Dihedral	Aerodynamic look-up tables
Location of aircraft c.g.	Setting angle	
Location of left wing apex	Location of e.a.	
Location of right wing apex	Location of a.c.	
Location of left HT apex	Location of c.g.	
Location of right HT apex	Thickness ratio	
Location of VT apex	*Mass	
*Aerodynamic look-up tables	*Inertia	
	Aerodynamic look-up tables	

with the small time step associated with high-frequency deformation vibration, which is very inefficient.

Furthermore, a continuous solver (instead of a discrete one) is required for this model, because SimMechanics blocks always have a continuous sample time [94]. In addition, the numerical stiffness of the model should be taken into account. A system is numerically stiff when it has very different timescales. This is the case for AFM models, since the time scales related to elastic deformation and flight mechanics are very different [89]. For numerically stiff problems, an implicit solver is required. Implicit solvers require more computational effort than explicit solvers, but they have greater stability for oscillatory behavior [93].

Because of the above reasons, an implicit, continuous, variable-step solver must be chosen. SimMechanics offers three: ODE15s, ODE23s and ODE23st. ODE15s is the least efficient of these three [93], and will therefore not be used. Of the remaining two, ODE23s is tailored to problems with constant mass matrices. This is the case for the current model, since the assumption is made that deformation has no effect on mass distribution and mass moments of inertia (see section 5-1-2). Therefore, the ODE23s solver will be used for the model. This solver is based on a modified Rosenbrock formula of the second order. The interested reader is referred to literature about this subject [95].

6-2 Trim

As discussed in section 5-2, trimming of the AFM model is important, because it is commonly used to find the starting point for time domain simulation and stability analysis. Trimming is based on the model described in the previous section, and will be done using a combined implicit and explicit Jacobian approach. The user may choose whether to perform two-dimensional trim, in which lateral and directional degrees of freedom are blocked, or full three-dimensional trim.

The trim algorithm that was created, is described in the flow chart shown in figure 6-2. In this figure, twelve rows can be distinguished, which will now be discussed.

In the first row, the general trim parameters are declared first. These are the trim type (2D or 3D), the number of implicit iterations (N_{impl}), the finite-difference used for Jacobian determination (ϵ) and the stoptime for the implicit and explicit simulations (t_{impl} and t_{expl}). Thereafter, the desired flight condition, the desired objective parameter values ($\mathbf{o}_{des}$ and $\ddot{\mathbf{q}}_{des}$) and the initial control vector ($\mathbf{c}_1$) are declared. Table 5-1 showed the variables that fall into these categories. Subsequently, the aircraft input parameters are created (with *aircraft_description.m*) and the SimMechanics model is created (with *aircraft_generator.m*).

In the second row, an initial simulation of the model is performed, and the initial objective vector ($\mathbf{o}_1$) and the final wing position ($\mathbf{q}_{final}$) are stored. These are used later, respectively for determination of the new control vector (row 6) and for the initial wing position of a subsequent simulation (row 4).

Rows three to six represent the implicit part of the trim algorithm, i.e. where wing deformation is not in the control and objective vector, but is handled by allowing the aeroelastic vibrations to damp out. In row three, the implicit trim loop is started and it will run for N_{impl} iterations. In each of these iterations, the Jacobian is constructed and a new control vector is determined, in an attempt to drive the objective variables to their desired values.

In rows four and five the Jacobian column for a control ($J_{col}(k)$) is determined. This is done iteratively, until all controls are treated. Each column of the Jacobian describes the linear effect of a change in a control variable on each of the objective variables. This is determined using a finite-difference method, in which the control is first slightly increased (by $\frac{\epsilon}{2}$) in row four and then slightly decreased (by $\frac{\epsilon}{2}$) in row five. The found objective vectors, respectively $\mathbf{o}^+$ and $\mathbf{o}^-$, are then subtracted and divided by ϵ to calculate the Jacobian column.

In row six, these columns are combined to form the complete Jacobian J, which is used to find the new control vector (using equation (5-6)). Then a simulation is performed, and the new objective vector ($\mathbf{o}_{i+1}$) and the final wing position ($\mathbf{q}_{final}$) are stored.

Row seven is used as a preparation for the explicit trim part. The final wing position of the last implicit trim iteration is included in the control vector as an initial guess. Moreover, the objective vector is appended with the desired modal accelerations ($\ddot{\mathbf{q}}_{des}$). Also, the simulation time is decreased to t_{expl}, since for explicit trim, it is not necessary to allow the elastic vibrations to damp out. Then, an initial simulation is performed and the objective vector $\mathbf{o}_{i+1,flex}$ is stored. objective Rows eight to eleven represent the explicit part of the trim algorithm. It is similar to the implicit part, but there are a few differences. Firstly, this part runs until all variables in the objective vector $\mathbf{o}_{i+1,flex}$ are closer to the objective values than the objective tolerance tol_{obj} (as is shown by the rhombus in this row). Secondly, there are more control variables ($N_{control,flex}$), more objective variables, and a larger Jacobian matrix, because the modal amplitudes and accelerations associated with wing deformation are included (see equations (5-7) to (5-9)).

Finally, after the objective variables are close enough to their prescribed objective values, i.e. trim is achieved, the trimmed condition is saved and the algorithm ends (row twelve).

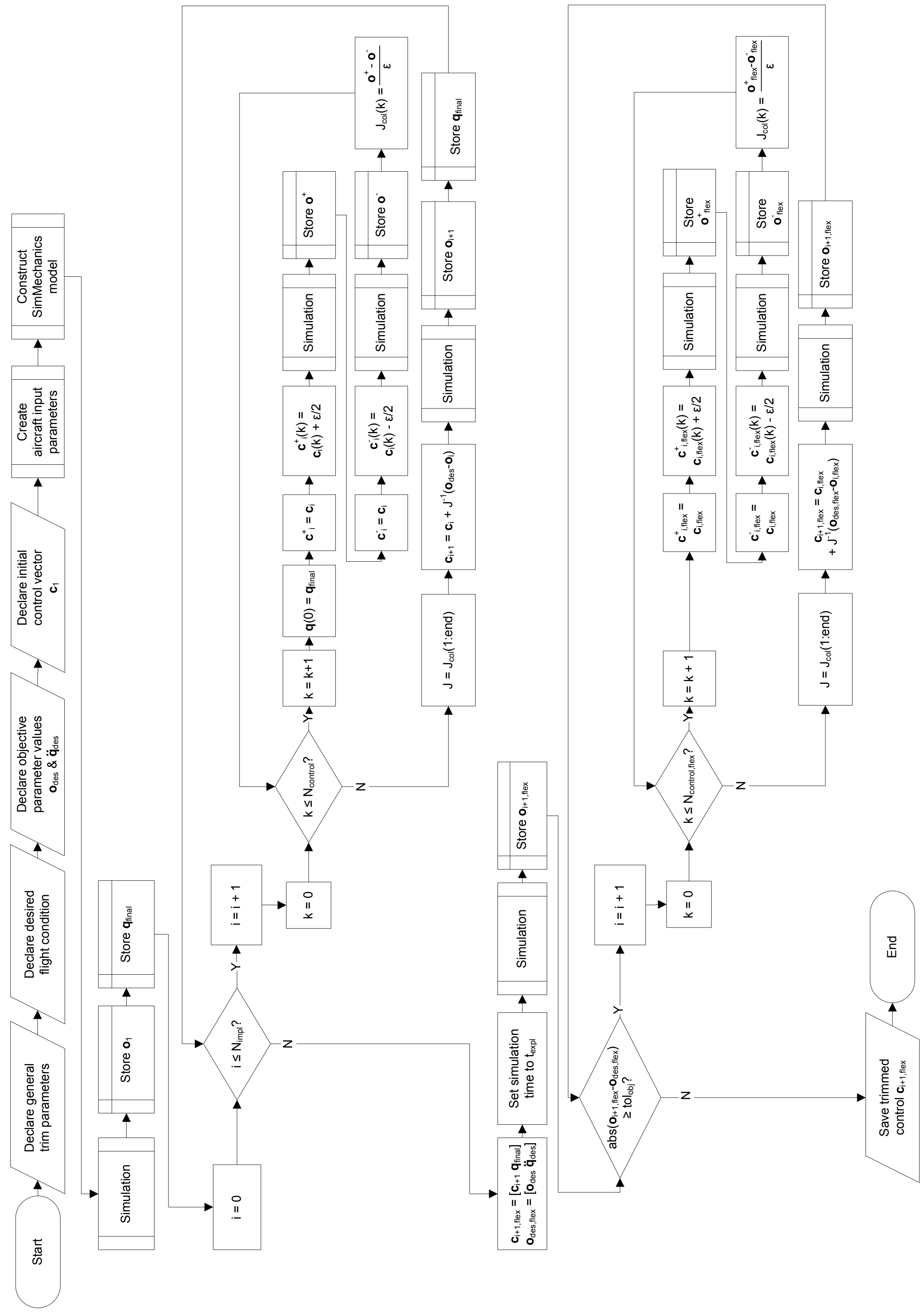

Figure 6-2: Flow chart of the trim algorithm.

6-3 Linearization and Stability Analysis

Linearization of the nonlinear AFM model is important, because it leads to an efficient state-space system, which is ideally suited for multidisciplinary integration, stability analysis and control integration [89]. As was discussed in section 5-3, the main goal of linearization is finding a state-space system that represents the behavior of the nonlinear system around a trimmed condition. The state vector $\mathbf{x}$ is shown in equation (6-1) and consists of the degrees of freedom of the aircraft and their time derivatives (discussed in section 6-1-1). The control vector $\mathbf{u}$ is shown in equation (6-1) and was discussed in chapter 5. In the following sections, flight mechanics mode analysis and the determination of stability and control derivatives will be discussed.

$$\mathbf{x} = \begin{bmatrix} x_e & y_e & z_e & \psi & \theta & \phi & u_e & v_e & w_e & \dot{\psi} & \dot{\theta} & \dot{\phi} \end{bmatrix}^T \tag{6-1}$$

$$\mathbf{u} = \begin{bmatrix} \delta_a & \delta_e & \delta_r & T \end{bmatrix}^T \tag{6-2}$$

6-3-1 Flight Mechanics Mode Analysis

When aircraft flight mechanics modes are to be determined, the output vector $\mathbf{y}$ would be of the form shown in equation (6-3). The variables described in this equation were all described earlier. For these state, input and output vectors, linearization can be performed. This could be done using Jacobian linearization (discussed in section 5-3), but since this model is developed in the SimMechanics environment, it is more appropriate to use the embedded functionalities for linearization. The *linmod* command can be used to extract a continuous-time linear state-space model (described in equation (5-11)) around an operating point, by linearizing each block in the model individually [96]. Note that this state-space system is very large, because in addition to the states of equation (6-1), it also contains wing deformation states, control system states (if present) and states related to SimMechanics blocks without a physical meaning. When for instance ten modes and ten wing sections are used for each wing, there will be a total of 444 states. For flight mechanics analysis, the *linmod* command can be configured, so that only the states in equation (6-1) are taken into account.

$$\mathbf{y} = \begin{bmatrix} \phi & \theta & \psi & p & q & r & u & v & w \end{bmatrix}^T \tag{6-3}$$

The resulting state-space system can be analyzed to obtain the flight mechanics modes. For instance, an eigenanalysis of state-matrix A will yield all eigenvalues of the aircraft, which represent the flight mechanics modes. Closer analysis requires decoupling of the longitudinal and the lateral-directional behavior of the aircraft, which is a valid assumption for rigid aircraft [85] and flexible aircraft [97].

For the longitudinal modes, i.e. the phugoid and short-period mode, the rows and columns in the state-space matrices that relate to lateral-directional behavior can be discarded. The only variables that are considered are the states θ, u_e, w_e and $\dot{\theta}$, the input δ_e, and the outputs θ, q, u and w. From this reduced state-space system, the longitudinal natural frequencies and damping factors can be determined (using the *damp* command). The phugoid mode will always have the smaller natural frequency and damping factor, compared to the short-period mode [85].

For the lateral modes, i.e. the Dutch roll, roll subsidence and spiral mode, only the lateral-directional part of the state-space system is investigated. The only variables that are considered are the states ϕ, v_e, $\dot{\psi}$ and $\dot{\phi}$, the inputs δ_a and δ_r, and the outputs ϕ, ψ, p, r and v. The natural frequencies and damping factors can be determined from this reduced state-space system. The Dutch roll mode will be the only periodic mode, the spiral mode will be a lightly (or negatively) damped aperiodic mode and the roll subsidence will be a more heavily damped aperiodic mode [85]. Note that in the special cases where the spiral and roll mode are coupled, this mode would be periodic and would have a lower natural frequency than the Dutch roll mode [98].

6-3-2 Stability and Control Derivatives

Stability and control derivatives represent the effect of a change in, respectively, a state variable or a control variable on the aerodynamic forces and moments. Determination of these derivatives is strongly related to the flight mechanics mode analysis discussed in the previous section. Non-dimensionalized stability and control derivatives are of interest, since they allow easy comparison of stability characteristics of different aircraft [85].

Symmetric stability derivatives represent the effect of a change in longitudinal variables (u, α or q) on the forward aerodynamic force X, the downward aerodynamic force Z and the aerodynamic moment about the Y_b-axis M. Note that these variables are in the body reference frame and therefore differ from the state variables described section 6-1. Because of this, they are not determined with the *linmod* command, but by means of the finite-difference method [3]. This is done by increasing and then decreasing either u, α or q by a small perturbation value (half the finite-difference) from the trimmed condition. After a very short simulation time (0.01 s), the accelerations in the body reference frame are measured. The changes in the accelerations are then divided by the finite difference to yield the linear effect on the accelerations. Multiplying this by the aircraft mass (for translational accelerations) or the corresponding mass moment of inertia (for angular accelerations), yields the effect on the aerodynamic forces or moments. Finally, dividing by non-dimensionalization factors yields the dimensionless stability derivatives. There are different non-dimensionalization factors for different derivatives; they are presented in appendix C-1.

This procedure is summarized in equation (6-4). Here, C_{Z_u} is the stability derivative of Z due to a change in u, and m is the total mass of the aircraft. The last part of the equation represents the finite-difference method, where a "+" superscript represents the simulation where u was increased and a "−" superscript represents the simulation where u was decreased.

$$C_{Z_u} = \frac{1}{\frac{1}{2}\rho V S}\frac{\partial Z}{\partial u} = \frac{1}{\frac{1}{2}\rho V S}\frac{m\partial \dot{w}}{\partial u} = \frac{1}{\frac{1}{2}\rho V S}\frac{m\left(\dot{w}^{+} - \dot{w}^{-}\right)}{u^{+} - u^{-}} \tag{6-4}$$

Asymmetric stability derivatives represent the effect of lateral-directional variables (β, p or r) on the rightward aerodynamic force Y, the aerodynamic moment about the X_b-axis L and the aerodynamic moment about the Z_b-axis N. Control derivatives are determined just like stability derivatives, but by perturbing the control variables instead of the state variables.

6-4 Summary

In this chapter, the implementation of the AFM model was explained, which is based on the theory discussed in chapter 5. The three sections of this chapter explained the three main functionalities of the AFM model. First, the aircraft model lay-out was presented. Moreover, the motivation behind the ODE23s numerical integration method, used for time-domain simulation, was explained. Second, the trim algorithm was treated, based on the associated flow chart. Third, linearization and stability analysis were explained. It was shown that the model can be linearized (with *linmod*) and that flight mechanics modes can be determined. Furthermore, the calculation of non-dimensionalized stability and control derivatives (using the finite-difference method) was treated.

Chapter 7

Flight Mechanics Verification

In this chapter, the verification of the Aeroelastic Flight Mechanics (AFM) model is treated. This is of vital importance, since it gives credibility to the results of the model. The aeroelastic wing model, which is at the core of the AFM model, was already verified in chapter 4.

In chapter 4, it was found that validation data is scarce for aeroelastic wing models. Unfortunately, validation data is even more scarce for AFM models [99]. Creating a representative wind tunnel model for a single aeroelastic wing is hard, because of scaling effects [100]. Creating an AFM wind tunnel model would be even harder, because the model becomes even more complex. Another reason why validation data is scarce, is the rarity of AFM models.

Indeed, actual validation of AFM models is only performed a few times in literature. Some low-fidelity models were compared to high-fidelity (NASTRAN) analyses [3, 99]. Unfortunately, the required NASTRAN license (FlightLoads) is not available at the TU Delft. Another model was compared to detailed aircraft and flight test information, which was obtained from an aircraft manufacturer [13]. Lastly, the University of Michigan is currently creating an actual aircraft for validation of AFM models [101]. For the current research, this is not an option because of time and financial constraints.

Because of the above reasons, the AFM will only be verified, which will be done on a qualitative and semi-quantitative basis. First, the qualitative behavior of the AFM model is investigated in section 7-1, by looking at the deviations from steady, horizontal flight due to control input. Second, in section 7-2, a stability analysis is performed for a rigid aircraft and the results are compared to values for other aircraft. This is done to verify the behavior of the flight mechanics layer of the model. Lastly, the combination of aeroelasticity and flight mechanics is investigated in section 7-3, by looking at the trim control variables that are required to fly at various flight conditions. In all sections, the A320-like aircraft is considered, which is described in appendices A and B.

Table 7-1: Trim control variables for steady, horizontal flight found with 3D and 2D trim.

Control variable	Three-dimensional trim	Two-dimensional trim
δ_a	$0.12\,^\circ$	$0\,^\circ$
δ_e	$4.84\,^\circ$	$4.84\,^\circ$
δ_r	$2.71\,^\circ$	$0\,^\circ$
T	38.54 kN	38.54 kN
ϕ	$-0.07\,^\circ$	$0\,^\circ$
θ	$0.72\,^\circ$	$0.72\,^\circ$
χ	$0.00\,^\circ$	$0\,^\circ$

7-1 Qualitative Analysis

Here the qualitative behavior of the AFM model is analyzed, which provides insight in the functioning of the aeroelastic wing model, the flight mechanics model layer and the trim algorithm.

First, the control variables that are required for steady, horizontal flight are determined using the trim algorithm. The aircraft should fly at an altitude of 11 km and at a speed of 150 m/s in northward (u_e) direction. Both three-dimensional (3D) trim, i.e. with six degrees of freedom, and two-dimensional (2D) trim, i.e. with only longitudinal degrees of freedom, have been performed. The results are shown in table 7-1 and figure 7-1, representing an aircraft that flies at a small pitch angle and with a small elevator deflection, for pitch moment balance. Both Three-dimensional (3D) and Two-dimensional (2D) trim yield the same longitudinal control variables (δ_e, T and θ). In case of 3D trim, the lateral control variables have small, non-zero values. Nonetheless, the total set of control variables leads to steady, horizontal flight. In this case, because a negative (left-wing down) roll angle ϕ is combined with positive rudder deflection angle (rudder to the right) and a slightly positive aileron deflection angle (right aileron down), providing yaw and roll moment balance. This 3D trim condition is not optimal in terms of trim drag. However, trim minimization is not the subject of the current research and will not be discussed further here. Note that trim control variables can also be determined for other flight conditions, as will be shown in sections 7-3 and 8-2.

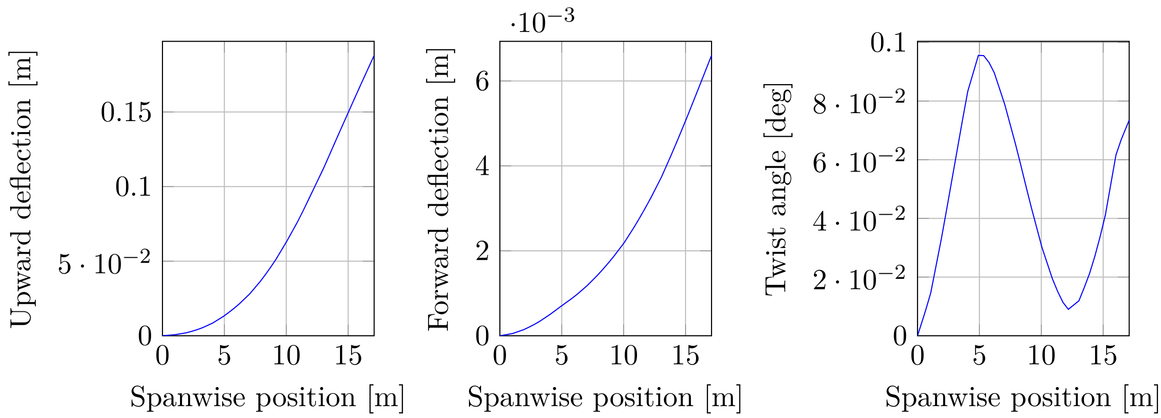

Figure 7-1: Trimmed position of the wing for steady, horizontal flight.

At this point, the effect of an impulse control surface deflection can be simulated. In the following analyses, each control surface deflection is increased by 10 degrees after five seconds, with a duration of half a second. First, consider figure 7-2, which shows the aircraft Euler angles, the elevator input, the flight speed and the altitude.

In the first five seconds, these variables are constant with time, reflecting steady, horizontal flight. As expected, directly after the elevator deflection, the aircraft pitches down, the flight speed increases, and the altitude decreases. Subsequently, the aircraft starts to oscillate. The pitch angle θ shows one high-frequency, heavily damped oscillation (the short-period) and one low-frequency, lightly damped oscillation (the phugoid). The phugoid is also apparent from the repeated exchange of flight speed and altitude. This is exactly the behavior that is expected after an elevator deflection. Note that the lateral variables ϕ, v_e and ψ remain approximately constant for roughly 40 seconds, which reflects the fact that longitudinal and lateral behavior are largely decoupled [97]. After many seconds, the lateral variables start to deviate, mainly caused by small symmetric-asymmetric coupling and very small numerical perturbations, which grow due to slight spiral instability (see section 8-1).

Figure 7-3 shows the tip deflection and the right wing root bending moment (WRBM) for the elevator impulse deflection. Clearly, the wing deformation and wing loads are affected by the short-period and the phugoid. Directly after the control input, the downward speed of the aircraft causes an increase of the effective angle of attack for the wing. Because of this, the lift, drag and pitch moment increase. This causes the wing to deflect upwards, backwards and pitch-up. This is expected behavior.

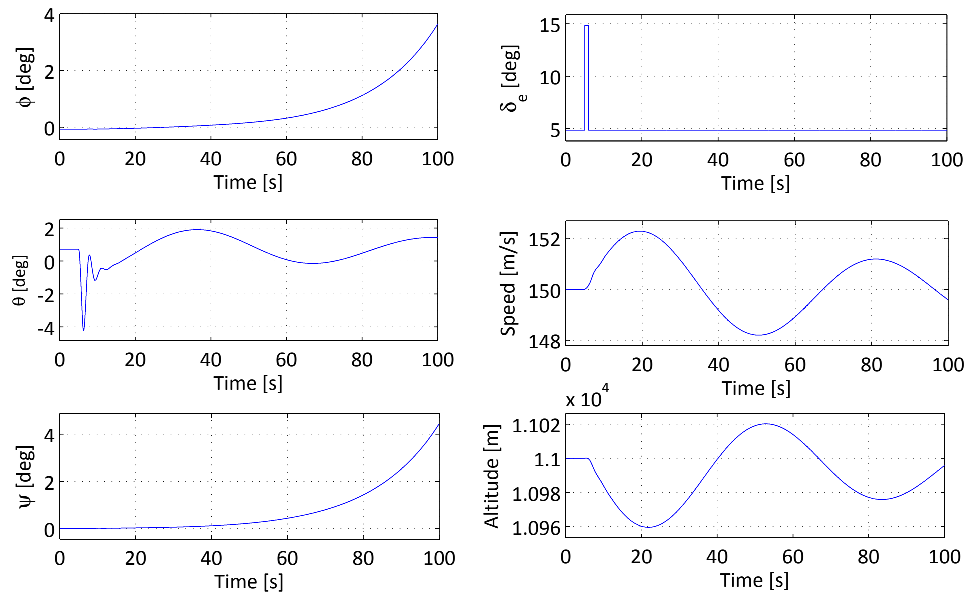

Figure 7-2: Aircraft behavior after an elevator 0.5 s impulse at t = 5 s in steady, horizontal flight.

Figure 7-4 shows the aircraft behavior after a positive aileron input (right aileron down). This causes the roll angle ϕ to become negative (right wing up) and the yaw angle to become negative (turn left), as expected. At first, the speed and altitude are not affected much. As time passes, the rotated lift vector (due to roll) causes the altitude to decrease, and as a result

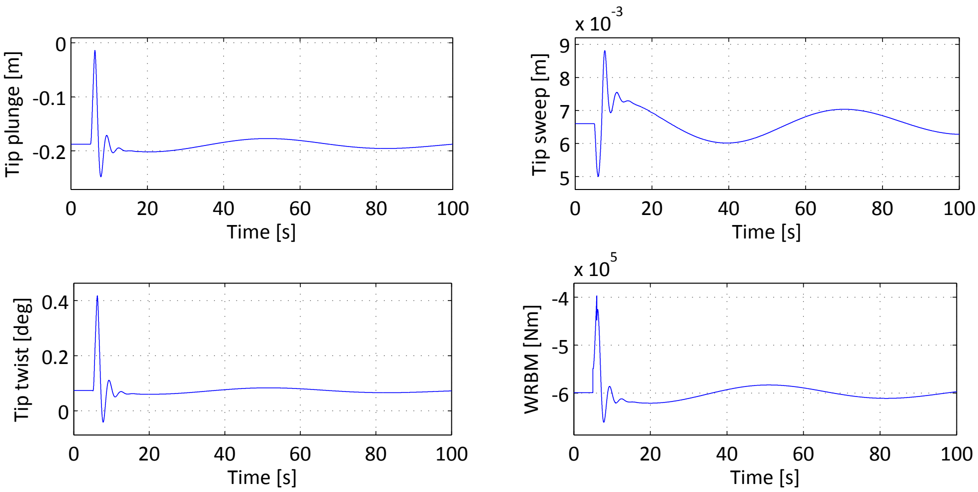

Figure 7-3: Deflection and load after an elevator 0.5 s impulse at t = 5 s in steady, horizontal flight.

the flight speed increases. The leftward spiral is also apparent from the figure, since the roll and yaw angle decrease, the speed increases and the altitude decreases, all at an increasing rate.

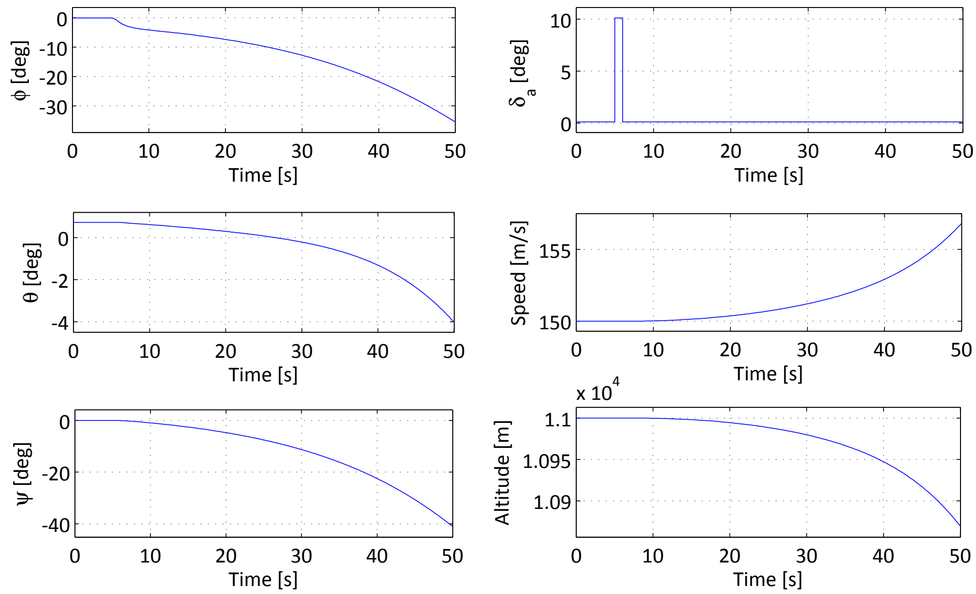

Figure 7-4: Aircraft behavior after an aileron 0.5 s impulse at t = 5 s in steady, horizontal flight.

Lastly, figure 7-5 shows the aircraft behavior after a positive rudder input (rudder right). Directly after the control input, the aircraft turns right (positive ψ) and oscillations of ϕ and ψ commence, which represents the Dutch roll mode. Note that θ also shows a small oscillation, because of the initial roll angle. Therefore, the rudder deflection force causes a moment around the axis about which θ is defined. In the long run, the aircraft gets into a rightward spiral, similar, but opposite to the one shown in figure 7-4.

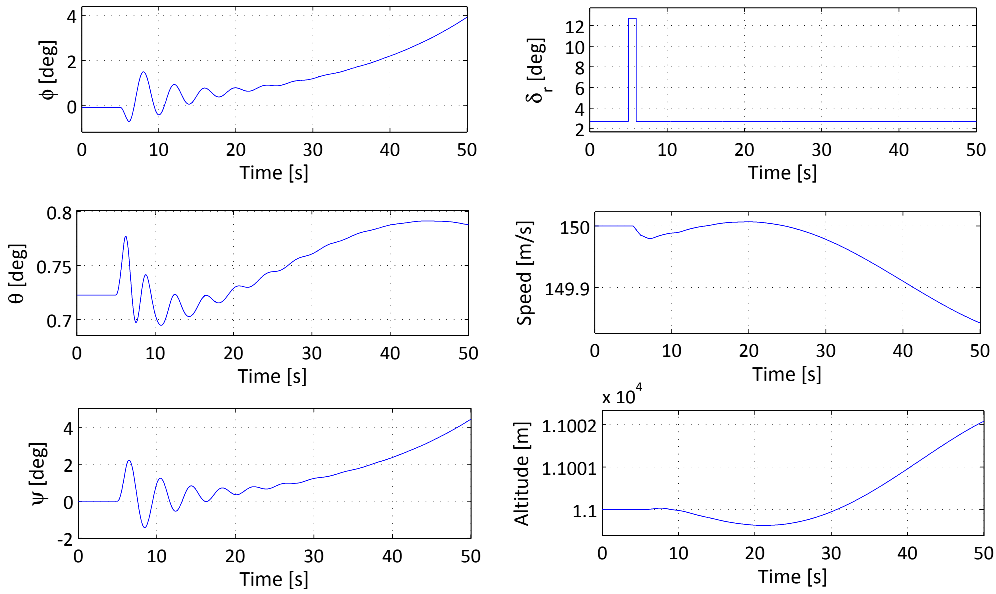

Figure 7-5: Aircraft behavior after a rudder 0.5 s impulse at t = 5 s in steady, horizontal flight.

7-2 Stability Derivatives Analysis

In this section, the flight mechanics behavior will be analyzed in more detail. For this analysis, the stability and control derivatives were determined for the rigid A320-like aircraft. In this manner, the flight mechanics layer of the model are investigated, and not on the elasticity part. Again, the reference condition is steady, horizontal flight, at an altitude of 11 km and a flight speed of 150 m/s. All results discussed in this section are presented in appendix C-2 in numerical form.

Figure 7-6 shows the symmetric stability and control derivatives, i.e. those related to longitudinal motion. The values for the A320-like aircraft are compared to those of other aircraft found in literature [85]. These derivatives were determined in flight tests, except for values that are very small, which were not measured but were assumed to be zero [102]. This comparison is possible because they are dimensionless (see section 6-3-2). All derivatives related to the effect on either X, Y or M share the same axis, in order to show the relative importance of the derivatives. Except for C_{X_q}, all derivatives are in the correct range when compared to other aircraft. After thorough investigation of the model and the results, the reason for this discrepancy was found. When determining derivatives with respect to q, the flight condition called "q-motion" is considered. It is shown in figure 7-7a, and causes a curvature of the flow field at all points except at the aircraft center of gravity. This flow field primarily increases the effective angle of attack at the horizontal tail, which is the prime contributor to C_{X_q}.

At this point, the large positive value of C_{X_q} can be explained using figure 7-7b, by looking at the projections of the lift and drag of the horizontal tail on the aircraft longitudinal axis (horizontal in the figure). In the trimmed condition (the upper figure), these almost cancel out (since $d_L \approx d_D$). However, when the effective angle of attack increases due to q-motion (the lower figure), the lift and drag force rotate and increase. This causes an effective force in the direction of the aircraft longitudinal axis (since $d_L > d_D$), which causes the value of C_{X_q} to be non-zero and positive.

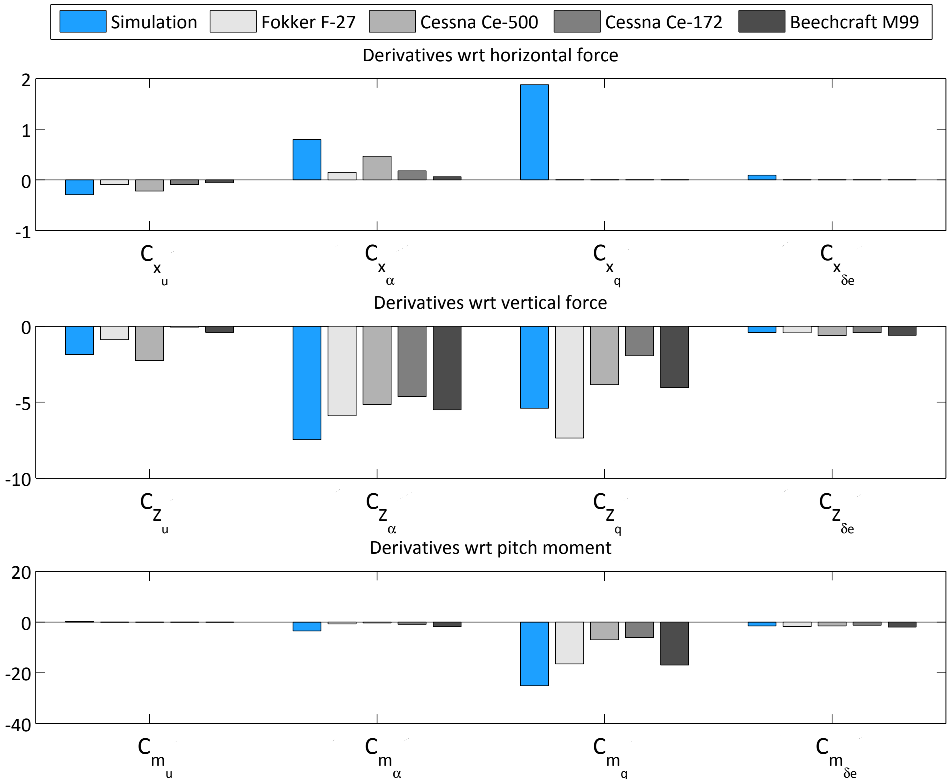

Figure 7-6: Symmetric stability and control derivatives of the rigid model and other aircraft.

Figure 7-8 shows the asymmetric stability and control derivatives, i.e. those related to lateral and directional motion. Here, all derivatives are in the correct range.

It is also interesting to verify the stability and control derivatives by assessing whether symmetric and asymmetric behavior are indeed uncoupled, as literature suggests [97]. First, the effect of asymmetric state and control variables on symmetric state variables is investigated (presented in appendix C-2). Analysis shows that the largest asymmetric-to-symmetric derivative (C_{X_β}) has an effect that is roughly one hundred times smaller than the smallest symmetric-to-symmetric derivative ($C_{X_{\delta_e}}$). When looking at the opposite, a similar result is obtained. The largest symmetric-to-asymmetric derivative (C_{n_q}) has an effect that is more than 10 times smaller than the smallest asymmetric-to-asymmetric derivative ($C_{l_{\delta_a}}$). This excludes the derivatives that are typically very close to zero ($C_{Y_{\delta_a}}$, $C_{n_{\delta_a}}$ and C_{n_p}). Indeed, symmetric and asymmetric behavior are uncoupled.

The effect of a change in a state or control variable on the wing root bending moments (presented in appendix C-2) is interesting as well. For symmetric input, it was found that the wing root bending moment of both wings changed by the same amount. For asymmetric input, it was found that the change was equal in magnitude, but opposite in sign for the left and right wing. This is expected behavior, again showing the existence of uncoupled symmetric and asymmetric behavior.

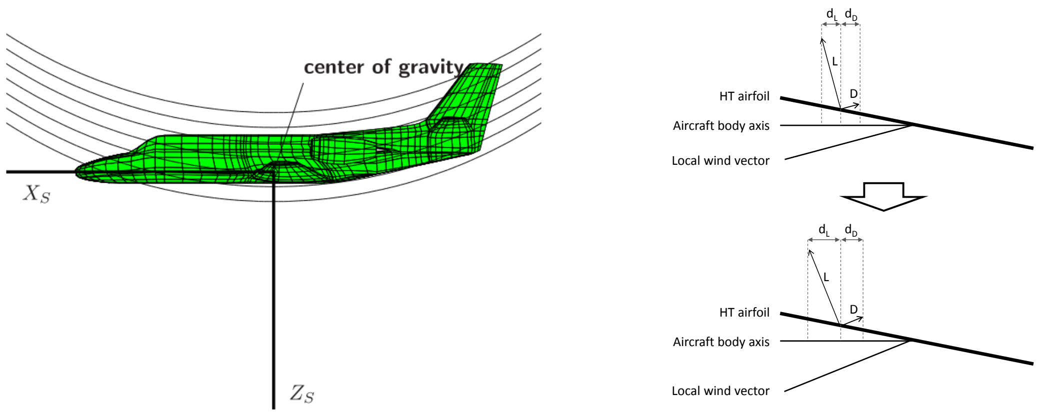

(a) Q-motion [85] **(b)** Rotation of forces at horizontal tail

Figure 7-7: Q-motion as the cause for discrepancy in C_{X_q}.

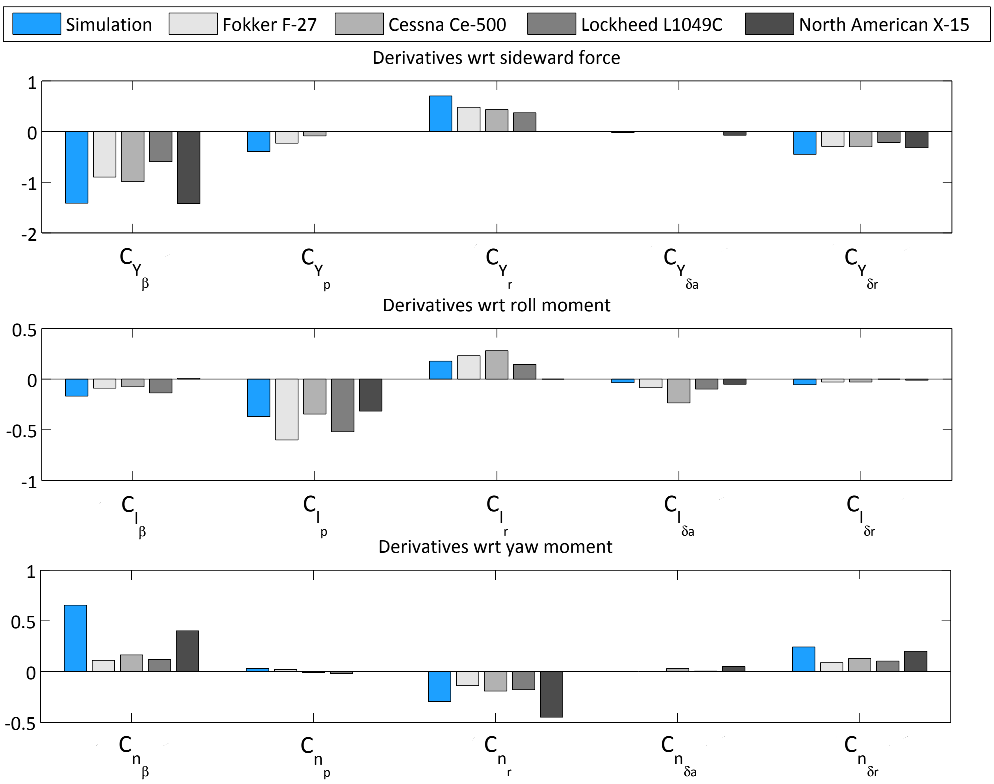

Figure 7-8: Asymmetric stability and control derivatives of the rigid model and other aircraft.

7-3 Trim Analysis

In this section, the trim conditions of the full, elastic AFM model are analyzed. The relation between mass configurations and flight conditions one the one hand, and trim control variables on the other hand will be investigated and compared to literature. In the following sections, the aircraft is trimmed for steady, horizontal flight at an altitude of 11 km and a northward speed of 150 m/s, unless explicitly stated otherwise.

7-3-1 Effect of Mass and Center of Gravity Location

When the mass or center of gravity location changes, different trim control variables are generally necessary to achieve steady, horizontal flight (or any other flight condition for that matter). This dependency is analyzed in this section, by trimming the aircraft for different payload values and different center of gravity locations.

The trim control variables were determined for payload masses ranging from 0 to 12000 kg. This was done for three different locations of the aircraft center of gravity (c.g.). At the regular location used in analysis (16.22 m behind the nose), 1.5 m in front of that and 1.5 m aft of that. The resulting trim variables for steady, horizontal flight are shown in figure 7-9.

The effect of increasing mass, for the middle c.g. location, is as expected. When mass increases, more lift is required for horizontal flight. This explains the increase of the pitch angle, and thereby the angle of attack of the aircraft. A higher lift also means a slight increase in drag, because the induced drag increases. Some extra thrust is therefore required when mass increases. Lastly, the elevator angle decreases when mass increases. The larger lift causes the wing to deform, mostly perpendicular to the aircraft longitudinal axis. Since the aerodynamic center of the wing lies in front of the aircraft center of gravity, the distance between these two points (i.e. the lift arm) decreases. The wing therefore creates a lower pitch moment, and less elevator deflection is required to have pitching moment balance. The above behavior also corresponds to literature [82, 99, 103].

The effect of the center of gravity location is also as expected. For a more forward center of gravity, the pitching moment caused by wing lift decreases, since the lift arm decreases. Less elevator deflection is then required for pitching moment balance. Because of this, the elevator creates less lift. In order to maintain horizontal flight, the pitch angle is increased. The thrust is slightly increased to negate the corresponding increase in drag.

7-3-2 Effect of Airspeed and Flight Path Angle

Now, the relation between the desired flight condition and the trim control variables is investigated. Figure 7-10 shows the effect that speed has on the three longitudinal trim variables that are required for steady, horizontal flight. When speed increases, less pitch angle is required to create the required lift for steady, horizontal flight. The thrust must be increased, in order to counteract the increased drag due to the higher speed. Lastly, the elevator deflection angle must increase, because of the decreased pitch angle. This is due to the same effect as with the varying mass analysis (section 7-3-1), where the elevator deflection angle was decreased, because of an increased pitch angle. The results that are predicted by the model correspond to the expectations, as well as with literature [82].

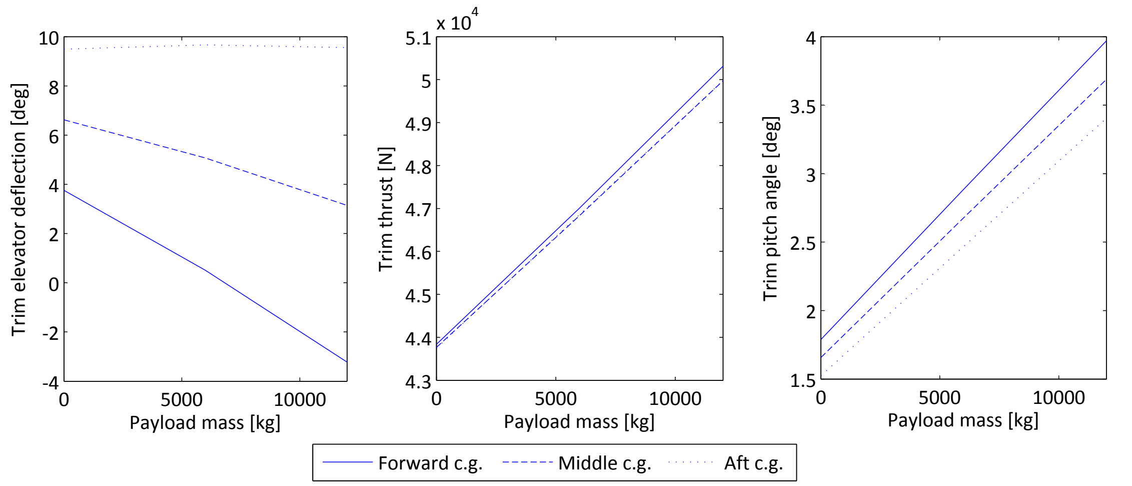

Figure 7-9: Steady, horizontal flight trim variables for varying mass and c.g. location.

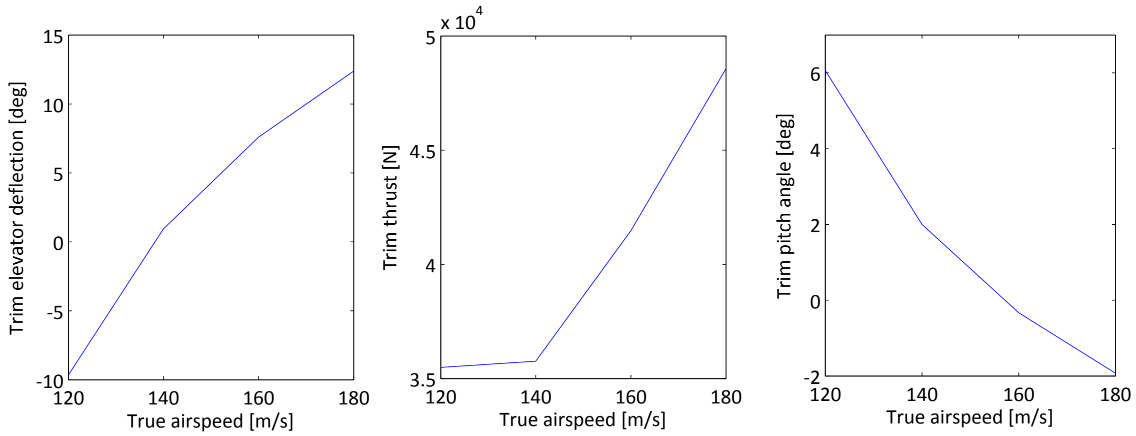

Figure 7-10: Steady, horizontal flight trim variables for different airspeeds.

Figure 7-11 shows the effect that the flight path angle has on the trim variables, for steady, climbing flight with an airspeed of 150 m/s and an initial altitude of 11 km. Again, these results are as expected. For the flight path angle to increase, the lift must increase, requiring a larger pitch angle. The increase in lift also causes an increase in induced drag, which must be counteracted by a larger thrust. More thrust is also required, in order to maintain the aircraft true airspeed, now that aircraft weight has a force component that opposes the direction of flight. Lastly, the elevator deflection angle is highly important for the desired flight path angle. For descending flight, the negative aircraft pitch angle and the associated lower lift, require a negative elevator deflection. This causes a decrease of the upward horizontal tail force, thus restoring moment balance. For climbing flight, the opposite occurs.

7-4 Summary

In this chapter, the AFM model has been verified, which increases the credibility of the results obtained with the model. First, a qualitative analysis was performed to show that

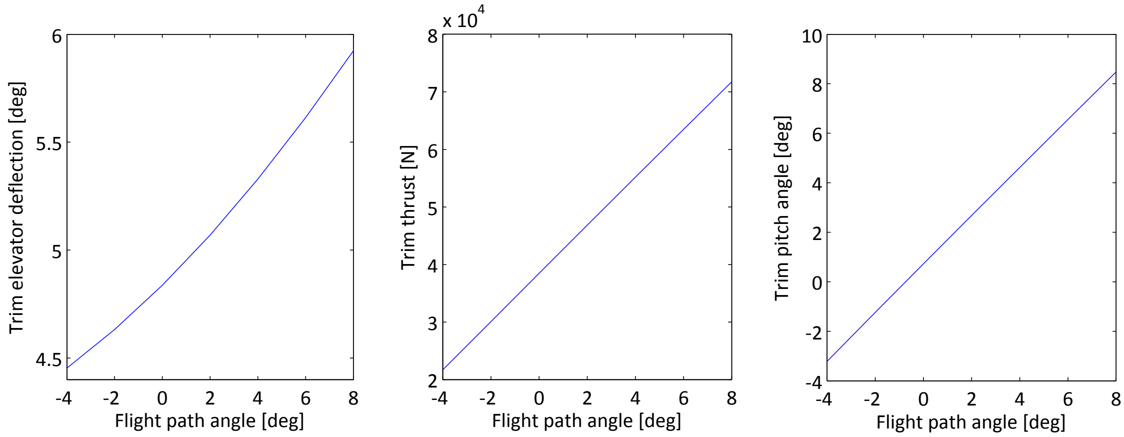

Figure 7-11: Steady, horizontal flight trim variables for different flight path angles.

the model is able to determine a realistic trim condition and that it correctly responds to control input. Thereafter, the flight mechanics layer of the model was verified by performing a stability analysis on the rigid aircraft and comparing the results with literature. With the exception of C_{X_q}, all stability and control derivatives corresponded to values found in literature. Lastly, the aircraft was trimmed for various values of payload mass, aircraft center of gravity, airspeed and flight path angle. The results corresponded to the expectations and trends found in literature.

To summarize, the complete AFM model behaves as expected, as was presented in this chapter and in chapter 4. This positively concludes the verification of the model.

Chapter 8

Flight Mechanics Analysis

In this chapter, interesting analyses with the Aeroelastic Flight Mechanics (AFM) model are discussed. First, the effect of aeroelasticity on flight mechanics is investigated in section 8-1. Subsequently, load prediction and the influence of aeroelasticity thereon is analyzed for various flight conditions, in section 8-2. Lastly, in section 8-3, the current model is compared to the previously created Lumped-Parameter Method (LPM) model.

8-1 Effect of Aeroelasticity on Flight Mechanics

The effect of aeroelasticity on flight mechanics is investigated by comparing the rigid and flexible A320-like aircraft (described in appendices A and B). For steady, horizontal flight at a flight speed of 150 m/s and an altitude of 11 km, the trimmed situation is investigated, as well as the stability characteristics. In addition, the linearized model is compared to the full nonlinear model.

8-1-1 Trim and Stability

Table 8-1 shows information regarding the trim control variables and the flight mechanics modes. Values are shown for aircraft with rigid wings, flexible wings and very flexible wings. The latter are still the wings of the A320-like aircraft, but the natural frequencies of the wing deformation modes were decreased by a factor 5, for illustrative purposes. The modes that are abbreviated are the Short-Period (SP), Dutch Roll (DR) and Roll Subsidence (RS) modes. Note that for aperiodic modes, the damping ratio is given as either -1 for an unstable mode or 1 for a stable mode. For instance, the table indicates that this particular aircraft has an unstable spiral mode.

As can be seen in the table, the difference between the rigid and the flexible trim control variables is certainly not negligible. For the very flexible case, the difference is very large. On the contrary, the flight mechanics modes are hardly influenced by the inclusion of aeroelasticity. The period and damping ratio of the modes for the rigid and flexible case differ by less

Table 8-1: Trim control and flight mechanics modes for rigid, flexible and very flexible aircraft.

	Rigid	**Flexible**	**Diff. [%]**	**Very flexible**	**Diff. [%]**
Elevator defl. [°]	4.659	4.837	3.82	9.203	97.5
Thrust [kN]	38.46	38.47	0.02	38.80	0.88
Pitch attitude [°]	0.771	0.723	-6.25	-0.523	-167.8
Phugoid period [s]	66.03	66.03	0.01	65.73	-0.45
Phugoid damping ratio [-]	0.095	0.101	0.05	0.101	0.56
SP period [s]	3.090	3.090	-0.00	3.251	5.21
SP damping ratio [-]	0.311	0.309	-0.02	0.313	0.50
DR period [s]	14.10	14.12	0.07	14.33	1.63
DR damping ratio [-]	0.448	0.445	-0.55	0.383	-14.5
RS period [s]	6.039	6.027	-0.20	5.747	-4.83
RS damping ratio [-]	1	1	-	1	-
Spiral period [s]	30.33	30.38	0.14	31.32	3.24
Spiral damping ratio [-]	-1	-1	-	-1	-

than one percent. This can be explained by the fact that the trimmed flight condition is the same for both cases (i.e. steady, horizontal flight). Although different control input is required to attain this trimmed condition, it is apparent that the aircraft responds to perturbations in roughly the same way, whether it has rigid or flexible wings. In order to illustrate that aeroelasticity can have a profound effect on the flight mechanics modes, the very flexible case was included in the analysis. For this case, there is a substantial influence on the modes. Relatively large differences were found for all modes, except the phugoid.

In addition to the flight mechanics modes, it is also interesting to investigate the stability and control derivatives. These derivatives are strongly related to the flight mechanics modes, which were just discussed. Tables 8-2 and 8-3 show the symmetric and asymmetric stability and control derivatives for the rigid and the flexible case. Again these derivatives were determined around steady, horizontal flight. By looking at the effect of aeroelasticity on e.g. C_{n_p}, the relation between derivatives and flight mechanics modes becomes clear. This derivative is important for roll-yaw coupling and therefore has a large influence on the Dutch Roll mode. Indeed, the effect of aeroelasticity on C_{n_p} is relatively large, just as the influence of aeroelasticity was largest for the Dutch roll mode (see table 8-1).

In general, tables 8-2 and 8-3 show that some derivatives are affected by aeroelasticity to the order of 1%. For most derivatives, however, the effect of aeroelasticity is negligible, which corresponds to the effect on flight mechanics modes. This confirms that wing flexibility has little effect on the stability characteristics of the A320-like aircraft.

8-1-2 Time Domain Analysis and Linearization

Linearization was used in the stability analysis of the previous section. The flight mechanics modes and the stability derivatives were determined based on the linear effect that perturbations have on the aircraft state. In this section, the linearized models are further investigated and compared to the nonlinear model.

Table 8-2: Symmetric stability and control derivatives for the rigid and flexible aircraft.

	Rigid [-]			Flexible [-]			Diff. [%]		
	$C_{X\_}$	$C_{Z\_}$	$C_{m\_}$	$C_{X\_}$	$C_{Z\_}$	$C_{m\_}$	$C_{X\_}$	$C_{Z\_}$	$C_{m\_}$
u	-0.293	-1.873	0.174	-0.295	-1.873	0.174	0.56	-0.02	-0.03
α	0.794	-7.474	-3.529	0.788	-7.474	-3.529	-0.86	0.01	0.00
q	1.878	-5.407	-25.15	1.872	-5.407	-25.15	-0.31	0.01	-0.02
δ_e	0.093	-0.424	-1.558	0.091	-0.424	-1.557	-2.35	-0.01	-0.05

Table 8-3: Asymmetric stability and control derivatives for the rigid and flexible aircraft.

	Rigid [-]			Flexible [-]			Diff. [%]		
	$C_{Y\_}$	$C_{l\_}$	$C_{n\_}$	$C_{Y\_}$	$C_{l\_}$	$C_{n\_}$	$C_{Y\_}$	$C_{l\_}$	$C_{n\_}$
β	-1.412	-0.169	0.654	-1.412	-0.167	0.654	0.00	0.00	0.00
p	-0.396	-0.370	0.031	-0.396	-0.370	0.031	0.01	-0.02	1.32
r	0.702	0.178	-0.296	0.702	0.179	-0.296	0.02	0.13	0.02
δ_a	-0.022	-0.036	-0.002	-0.022	-0.036	-0.002	0.04	-0.00	-1.54
δ_r	-0.448	-0.057	0.242	-0.448	-0.057	0.242	0.00	0.00	0.00

First consider figure 8-1, which shows the longitudinal response of the aircraft due to a step elevator input of 10 degrees after two seconds. The left figure shows the pitch angle θ during 100 seconds and the right figure shows the angular velocity around the Y_b-axis, q, during 18 seconds. Three flexible and one (nonlinear) rigid model are presented. The flexible models are the complete nonlinear model, the reduced-order linear model and the full-order linear model. Note that both linear models are based on a state-space approximation of the aircraft response, and that, in addition, the reduced-order model neglects all asymmetric aircraft motion.

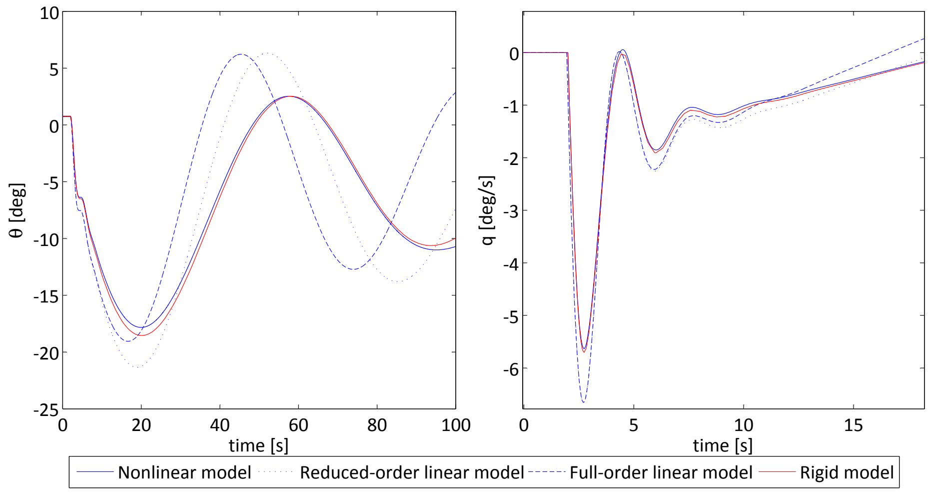

Figure 8-1: Symmetric response of various models due to a 10° elevator step input at t=2 s.

As can be seen in the figure, there is a substantial difference between the linear and the nonlinear models. Just after the elevator input, the linear models predict the aircraft response relatively accurately. They only fail at predicting the peaks of the oscillations. These peaks are lower for the nonlinear models. When time passes, the linear models become less accurate. The linear estimation of the phugoid clearly shows an error in both the amplitude and the period. This also means that there is a slight error in the flight mode data presented in table 8-1, which was determined using linear analysis. For instance, linear analysis predicted a phugoid period of 66.03 s and a short-period period of 3.09 s. Inspection of the nonlinear model, however, indicates the phugoid period is 75.08 s and the short-period period is 3.28 s.

Furthermore, the figure shows that the nonlinear flexible and rigid model show almost identical behavior, which corresponds to the conclusion that was drawn from table 8-1. At this point, the very flexible case is investigated, just like in the table. Remember that for that case, the natural frequencies associated with wing deformation were artificially reduced by a factor 5. Figure 8-2 shows the response to the 10° elevator step input at t = 2 s, for the rigid, the flexible and the very flexible case. The rigid and flexible case show similar behavior, but the very flexible case shows substantial differences, similar to what was found in section 8-1-1. It can be observed that between 8 and 10 seconds, q oscillates at a frequency that is slightly higher than the short-period frequency. This is very interesting, since the frequency corresponds to that of the first wing deformation mode. In other words, the frequency separation between flight mechanics and structural vibration has become very small, and wing deformation substantially affects flight mechanics.

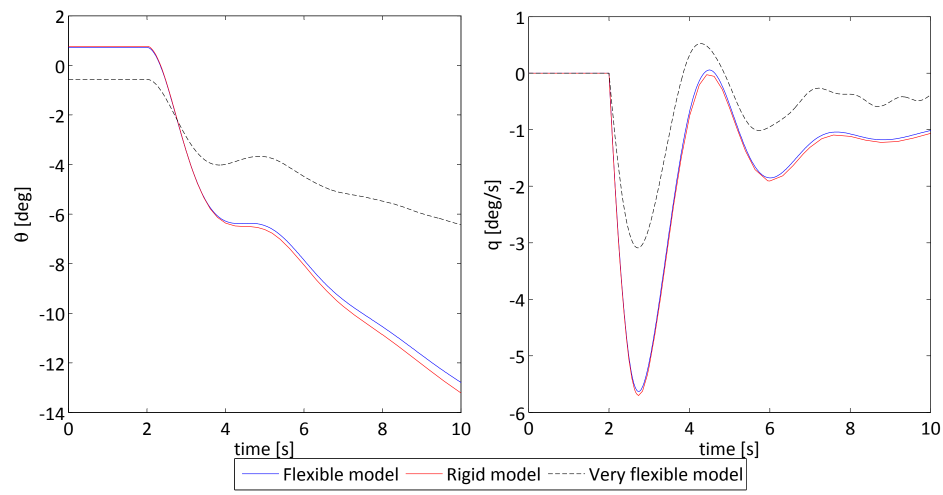

Figure 8-2: Symmetric response of models with varying flexibility due to a 10° elevator step input at t=2 s.

Similar conclusions can be drawn from figure 8-3, which shows the asymmetric aircraft response due to a rudder impulse input with a length of 0.2 seconds and an amplitude of 10 degrees. These figures clearly show the Dutch roll, in which the angular velocity about the X_b-axis (p) and about the Z_b-axis (r) oscillate. The linear model describes the aircraft behavior accurately just after the control input, but as time passes the linear model becomes inaccurate. The linear model again overestimates the amplitude of the oscillation. In addition, the linear model predicts that the aircraft will slowly enter a rightward spiral. This can be deduced from the increase of the mean value of p, causing the aircraft to roll right, and the slight increase of the mean value of r, causing the aircraft to yaw right. This spiral instability was also shown in table 8-1. The nonlinear model, however, does not show this unstable spiral behavior. Again, there is a difference in the aircraft modes predicted using linear analysis and the actual behavior of the aircraft.

Investigation of figures 8-3 and 8-4 shows that the rigid and flexible nonlinear models show nearly identical behavior. Just as with the symmetric input and response, the very flexible response substantially deviates from the rigid and flexible responses. Angular velocity p shows oscillations with a relatively high frequency, corresponding to asymmetric wing vibration. This mainly affects p because of the relatively low aircraft roll inertia (compared to yaw and pitch inertia) and because asymmetric wing deformation primarily causes asymmetric lift, leading to a rolling moment.

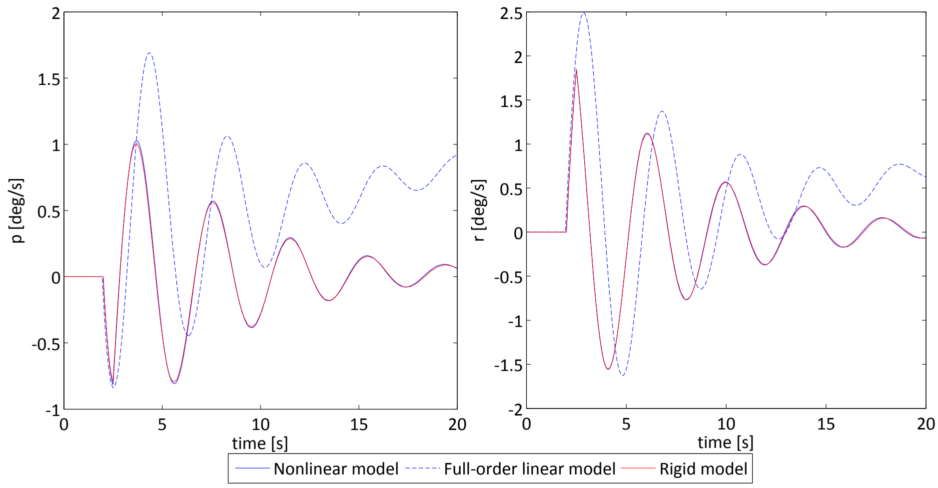

Figure 8-3: Asymmetric response of various models due to a $10°$ rudder impulse input at t=2 s.

It was found that linear models can cause inaccuracy. However, these models have one key advantage, which is the extremely short computational time. Table 8-4 shows the computational time that is required for simulating the 100-second aircraft response after an elevator step input and the 20-second aircraft response after a rudder impulse input. These simulations were performed on a 64-bit operating system with 1.85 GB usable RAM. It is clear that the computational time of the linear models is orders of magnitude smaller than for the nonlinear models. Note that even with the nonlinear model, the computational time approximately equals the simulated time. Real-time simulation therefore becomes a possibility, as well as piloted simulation with a flight simulator such as FlightGear [104].

As long as deviations from the initial situations are small, the linear model can give extremely fast predictions of the aircraft behavior. For larger deviations, caused by e.g. more control input or a longer simulation, such a linear model will become inaccurate, and a computationally more expensive nonlinear model should be used.

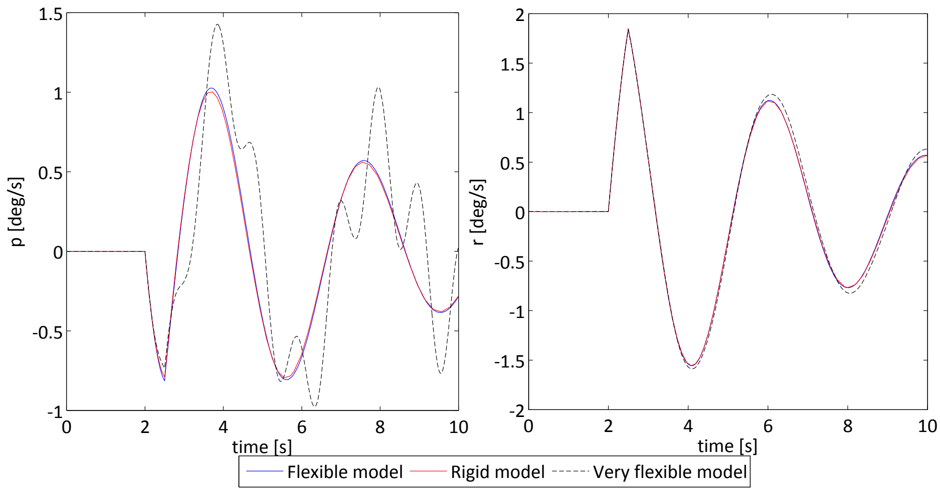

Figure 8-4: Asymmetric response of models with varying flexibility due to a $10°$ rudder impulse input at t=2 s.

Table 8-4: Computational time using different models.

Model	100 second elevator input	20 second rudder input
Nonlinear flexible	104.6 s	26.40 s
Full-order linear flexible	0.008 s	0.009 s
Reduced-order linear flexible	0.008 s	-
Nonlinear rigid	57.00 s	17.24 s

8-2 Effect of Aeroelasticity on Load Prediction

Besides prediction of the aircraft flight mechanics behavior, an important functionality of the AFM model is prediction of the wing root loads. The predicted values may for instance be used by a load alleviation algorithm.

In this section, five different flight conditions are analyzed. They are summarized in table 8-5, in which also the rigid and flexible trim control variables to attain the flight condition are present. The first four flight conditions are completely described by the airspeed V and the flight path angle γ. The last is a pull-up from level flight with an upwards acceleration of 1.5 g. The level flight condition will be used for disturbance analyses. The responses to a maximum elevator, aileron and rudder deflection of respectively 17°, 25° and 12° are simulated. Furthermore, the response following a "1-cos" gust, with a length of 0.5743 s (the period of the first wing mode) and a maximum (upward) gust velocity of 10.11 m/s, is determined. These flight conditions and disturbances were inspired by the CS-23 and CS-25 regulations [65, 66].

For each of these flight conditions, the Wing Root Bending Moment (WRBM) is investigated. Table 8-6 shows the WRBM in case of a rigid wing and a flexible wing, and the percentage difference between the two. For non-steady flight conditions (the bottom four), the maximum WRBM is shown in the table. Note that a positive WRBM corresponds to upward deflection

Table 8-5: Several trim flight conditions and the associated trim control parameters.

	Maneuver		Rigid trim			Flexible trim		
Maneuver	V [m/s]	γ [°]	δ_e [°]	T [kN]	θ [°]	δ_e [°]	T [kN]	θ [°]
Level	150	0	4.659	38.5	0.772	4.837	38.5	0.723
Climb	150	2	4.890	46.8	2.726	5.069	46.8	2.677
Descent	150	-2	4.455	30.1	-1.193	4.631	30.1	-1.241
High-speed	180	0	11.93	48.5	-1.817	12.38	48.6	-1.928
1.5g pull-up	150	0	-7.510	40.7	5.543	-7.443	40.8	5.474

Table 8-6: Peak rigid and flexible wing root bending moments (WRBM) for various maneuvers.

Maneuver	WRBM Rigid [kNm]	WRBM Flexible [kNm]	Difference [%]
Climb	596.4	596.5	0.013
Descent	603.0	603.2	0.018
High-speed	618.4	627.4	1.443
1.5g pull-up	851.0	839.4	-1.365
Max elevator	600.1	600.2	0.014
Max aileron	669.1	669.2	0.137
Max rudder	600.4	600.5	0.009
Gust	744.8	719.1	-3.455

of the wing. For some maneuvers or disturbances, the inclusion of flexibility has a very small effect on the peak WRBM. For others, there is a non-negligible on the peak WRBM. In the high-speed and the pull-up case, the lift forces acting on the wing and therefore the wing deformation are relatively large, causing a change in the wing loading. In case of the gust, the effective angle of attack increases. This again leads to an increase in lift and wing deformation, and therefore to an increased WRBM.

Table 8-6 only showed the peak WRBM for the non-steady flight conditions. The time histories of the WRBMs are interesting as well. They are shown in figure 8-5. The maximum WRBM associated with elevator deflection is not affected by flexibility (as was concluded from table 8-6). However, the time history reveals that there are non-negligible differences between the rigid and the flexible model. These differences are caused by the changes in the effective angle of attack due to the flight mechanics motion that follows after the elevator input. The changes in effective angle of attack cause the wing to deform and the wing loading to change.

Rudder deflection has a negligible influence on the wing loads. The largest differences occur after the aileron deflection and the gust disturbance, where the wing clearly shows vibration. The aileron deflection causes wing vibration, since it creates forces directly on the wing, as opposed to the rudder or elevator. The gust causes wing vibration, because the gust length equaled the period of the first wing deformation mode, which is therefore triggered. This wing vibration is overlaid on the changes in WRBM due to flight mechanics, which were also present after e.g. the elevator deflection.

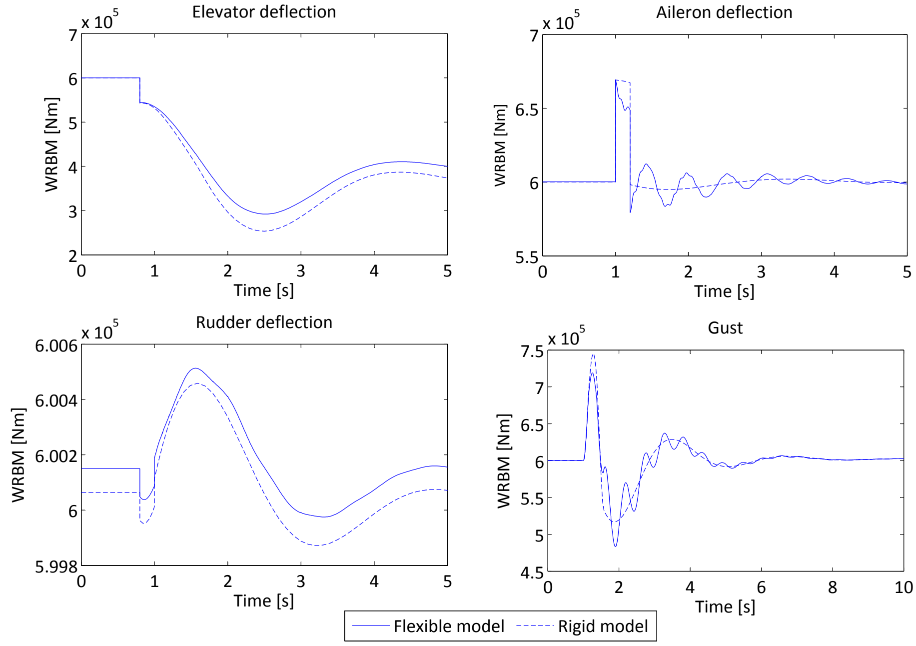

Figure 8-5: Wing root bending moment (WRBM) after control and gust input.

8-3 Comparison of Lumped-Parameter Method

In this section, the AFM, based on the modal approach, will be compared to an AFM model, based on the LPM approach (discussed in section 2-1-3). Improving on this LPM-based model was one of the main goals of the current research (see chapter 1). The LPM was created by Mark Voskuijl and created again for the current research, so that it completely corresponds to the modal model. The theory of the LPM model and the connection between the LPM model and the modal model was extensively discussed in section 4-4. For the analysis in this section, an AFM model has been created that includes the aeroelastic wing model described in section 4-4, instead of the modal model used in the rest of this thesis. In other words, the only difference between the two models is the aeroelastic wing model that is employed.

In order to make comparison between the LPM and the modal model possible, wing deformation data should be available for both types of models. Unfortunately, no real aircraft was found, for which this was the case. Therefore, an artificial wing will be used for the comparison. The aircraft that is modeled is still the A320-like aircraft. The A320-like wing is used in the following analysis, although with some differences. It is assumed that the elastic axis of the wing has no sweep, no dihedral and no twist. Furthermore, it is assumed that the elastic axis and the center of gravity of the wing are located at the midchord line. Lastly, the deformation data is determined by assuming that the flexible wing is a solid aluminium, rectangular beam with a length of 17.1 m (the semispan), a width of 1.6 m (the tip chord) and a height of 1 m. All other parameters are the same as for the A320-like wing. Note that this wing is purely virtual, since it combines the deformation properties of the rectangular beam with the aerodynamic and inertial properties of the actual A320-like wing.

Three different models are compared to each other. First, an LPM model with six generalized beam elements per wing is employed. Each generalized beam element consists of two wing sections, and two generalized coordinates (twist and bend). Therefore, there are 12 sections and 12 generalized coordinates per wing. Second, a modal model is used with the same number of sections (12) and generalized coordinates (12), i.e. included mode shapes, per wing. The complexity of this model is exactly equal to the complexity of the LPM model, since the mode shapes were determined from the LPM model (see section 4-4-1). Third, a modal model is used with the same number of generalized coordinates (12), but a higher number of sections (20) per wing. Because of the increased number of sections, both the aerodynamic and the structural calculations are expected to be more accurate. Since the number of generalized coordinates is not increased, this accuracy improvement is expected to come at little additional computational cost. Note that the modes for the third model should be more accurate than those of the second model, because of the increased number of sections. Therefore, an LPM model with 50 generalized beam elements was used for modal analysis. This LPM model was not used for further analysis. Also note that for both modal models, the modes have been determined from the LPM model, instead of with a more accurate Finite Element Analysis (FEA) approach. This inaccuracy was introduced deliberately, for the modal and LPM models to show similar behavior.

These three models are now subjected to a time-domain analysis following an upward gust of 11.15 m/s, with a length of 1 s. The results are shown in figure 8-6, which shows the tip plunge, the tip twist and the WRBM of the right wing (positive for upward deflection). The differences between the responses predicted by the three models are small. This is expected, since the input for the three models represented exactly the same wing. The small difference between the LPM and the modal models can be explained by the fact that the transient wing deformation of the three models could not be matched (see section 4-4-2). Also, the small difference may be caused by the small-angle approximation, which was used to determine the plunge displacement from the bending deflection (see section 4-4-1).

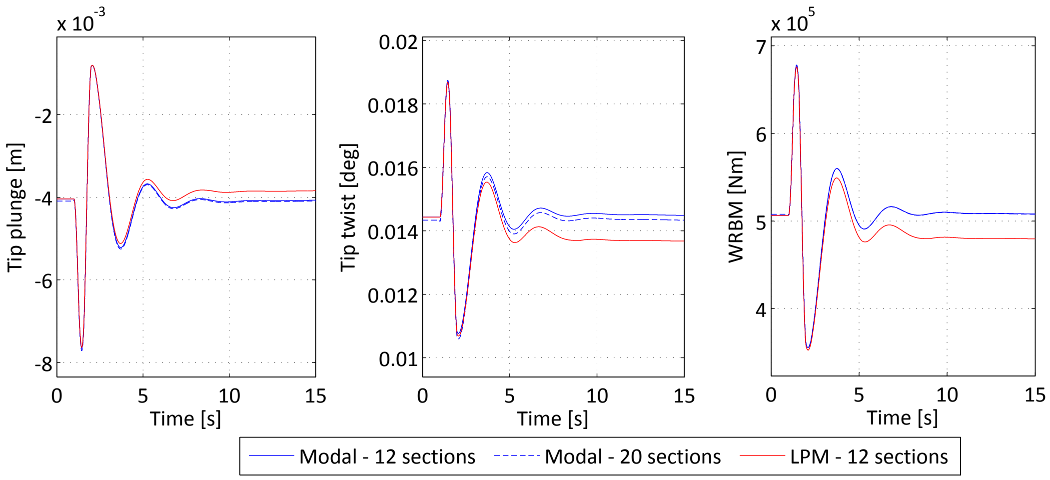

Figure 8-6: Wing response after a 1 s gust for different structural models.

At this point, it is interesting to compare the computational time and the accuracy of the three models for the 15 s gust response shown in figure 8-6. The three models were simulated on a 64-bit operating system with 1.85 GB usable RAM. The computational time of the 12-section modal model was the lowest at 359 s. Furthermore, the computational time of the 20-section modal model was 402 s and the computational time of the LPM model was 1820 s. The computations took a relatively long time, because of the high natural frequencies associated with the stiff solid aluminium beam, which required a small time step. The computational effort required for the modal model with 12 sections is approximately five times lower than that of the LPM model. This is a substantial improvement, but is smaller than the factor 18 effort reduction that was found in section 4-4-2 for the aeroelastic wing models. This is the case, because the flight mechanics layer is the same for both models, and a significant part of the computational effort is required for time integration of the nonlinear flight mechanics equation of motion. The computational effort of the modal model with 20 sections is roughly 12% higher than for the modal model with 12 sections. This small increase in computational effort results in a more accurate aerodynamic and structural wing model.

The accuracy of the three models is also of interest. Because of the absence of validation data, no definitive conclusion can be drawn on this matter. However, the accuracy of the wing deformation models can be investigated qualitatively. For the gust response analysis of the previous paragraph, figure 8-7 shows the final shape of the modal model with 20 sections and the LPM model with 12 sections. The plunge displacement of both models is similar, but the twist deflection is not. The twist deflection estimated by the LPM model is clearly inaccurate, since a smooth twist distribution is expected for the wing. The modal model with 20 sections shows a smooth twist distribution, which is closer to reality. The improved accuracy is explained by the more accurate modal analysis that was performed (with 50 instead of 6 generalized beam elements). The more accurate modal analysis does not require additional computational effort during the time domain simulation, only in a pre-processing step. This is a great advantage of the modal model over the LPM model, since improving structural accuracy only affects the pre-processing step. For actual, complex wings, the modes can be determined using FEA. This increases structural accuracy greatly, without affecting the computational effort during the simulation.

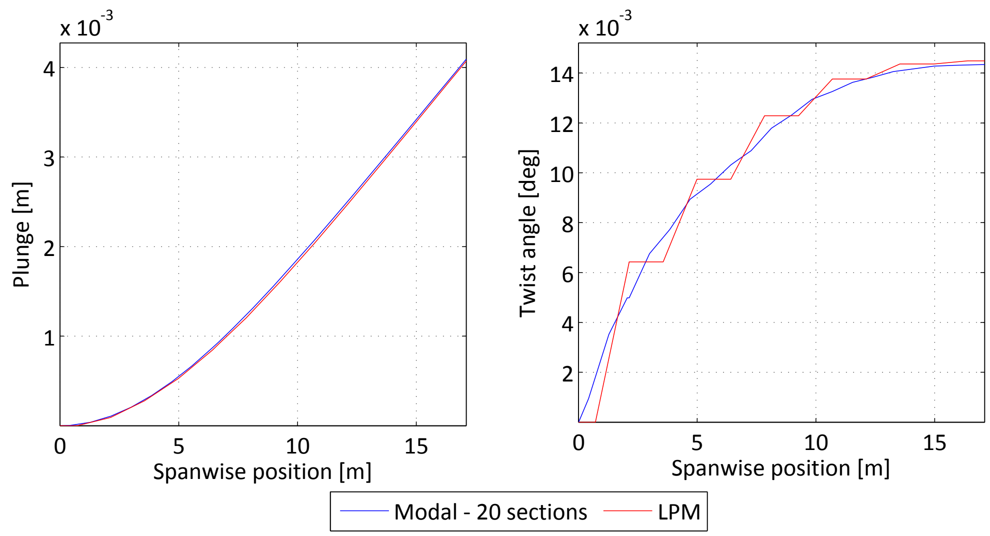

Figure 8-7: Final wing shape of the LPM model and the modal model with 20 sections.

8-4 Summary

This chapter presented several interesting analysis using the AFM model. First, it was shown that aeroelasticity has a substantial effect on the trim control variables required for steady, horizontal flight. On the contrary, the effect of aeroelasticity on the flight mechanics modes and stability derivatives was almost negligible for the A320-like aircraft. When wings become more flexible, however, they are affected.

Also, linearized models were investigated. They delivered accurate results of the aircraft response just after a control input. When time passed, however, the simulations with the linear models became inaccurate. For short periods of time, or small control input, the linear models might still be the better option, because of the associated computational time, which is many orders of magnitude smaller than of nonlinear models.

The peak loads predicted with a rigid wing model and a flexible wing model are identical for some maneuvers. However, for maneuvers or disturbances that create much lift, and thus wing deformation, the peak loads are different. Examples are high-speed flight, a pull-up or an upward gust. Moreover, wing loads are particularly affected by disturbances that have a direct effect on the wing, i.e. aileron deflection and an upward gust.

For a modal model and an LPM model of the same complexity, the computational effort of the latter is five times higher than that of the former. In addition, the structural accuracy of the modal model may be improved at only a small additional computational cost. This is the case, because the mode shapes, which constitute the structural accuracy, are determined in a pre-processing step.

Chapter 9

Conclusions

The main goal of the current research was the creation of a model, capable of simulating the dynamic aeroservoelastic response of a single wing, and the flight mechanics of aircraft with flexible wings. The various disciplines associated with Aeroelastic Flight Mechanics (AFM) are shown in table 9-1. This table also shows the approaches used to model each of these disciplines, as well as the associated assumptions (in italics). Both the aeroelastic wing model and the AFM model were extensively verified, giving credibility to the results of the model. Validation proved to be difficult and was not performed, because of the absence of complete validation data.

The research questions were stated in chapter 1 and are as follows.

a. Can a lumped-parameter model for load prediction of subsonic, flexible aircraft be improved in terms of accuracy and computational cost by using structural modal superposition and quasi-steady aerodynamics in a multibody system environment?

b. What is the effect of elasticity of lifting surfaces on aircraft flight mechanics?

The first question can be answered positively. A modal model and a Lumped-Parameter Method (LPM) model of the same complexity and accuracy were created. It was found that the modal aeroelastic wing model was 18 times faster than the LPM wing model. For the AFM models, simulation of the aircraft response after a gust required roughly 5 times more effort for the LPM than for the modal model. Although the specific numbers may vary, it can be concluded that the computational effort has been decreased multiple times by replacing the LPM model with a modal model.

The above comparison of computational effort was performed for models with similar complexity and accuracy. It was found that the accuracy of the modal model can be increased at a small additional computational cost. This is possible since the structural information is determined via a modal analysis in a pre-processing step. During the simulation, only the mode amplitudes need to be calculated, and the accuracy or complexity of the modes has no influence on the computational effort. This is not possible for the LPM model, in which increasing accuracy comes at a relatively steep additional computational cost. From this it can be deduced that the accuracy of the modal model is higher than that of the LPM model,

Table 9-1: The approaches taken for the various disciplines.

Discipline	Approach
Structures	Modal approach in a linear time-invariant state-space system *Free-free in vacuo mode shapes* *Neglect high frequency modes* *Small deformation* *No concentrated nonlinearities* *Rayleigh damping*
Aerodynamics	Look-up tables using the quasi-steady α_{eff} *Subsonic flight* *Low frequency motion* *Strip theory* *Corrected aerodynamic coefficients near wing tip*
Control surfaces	Only consider aerodynamic contribution *Neglect dynamics, inertia and actuation of control surface* *Idealized control force at trailing edge*
Load prediction	Summation of forces (with Multibody System Dynamics (MSD))
Fluid-structure interaction	Conventional serial staggered partitioned approach
Flight Dynamics	Multibody System Dynamics *Neglected changes in inertia and mass distribution due to deformation* *Structural deformation superposed on flight dynamics*
Trimming	Combined implicit and explicit Jacobian approach
Linearization	Jacobian linearization

as long as accurate modal analysis is performed (e.g. using finite-element analysis). Only this qualitative conclusion can be drawn, since the absence of validation data prevents formulation of a quantitative conclusion.

The second research question, regarding the effect of aeroelasticity on flight mechanics, has also been answered in the current research. An A320-like aircraft has been analyzed to assess this matter. The trim control variables are substantially affected by the inclusion of wing flexibility. On the contrary, the effect of aeroelasticity on the flight mechanics modes and stability derivatives was almost negligible. This is the case, because these parameters are determined around the same flight situation (steady, horizontal flight) for both the rigid and flexible case. It was found that as flexibility increases, the flight mechanics modes and stability derivatives were influenced by the inclusion of flexibility. For increased flexibility, the high-frequency flight mechanics modes (the short-period) and the low-frequency wing deformation modes are close to one another, thus causing the influence of flexibility on flight mechanics.

Furthermore, it was found that aeroelasticity has a non-negligible effect on the (peak) wing loads after maneuvers or disturbances. Especially for maneuvers or disturbances that increase lift, and therefore wing deformation, the peak loads are affected. Examples are high-speed flight, a pull-up or an upward gust. Moreover, wing loads are particularly affected by disturbances that have a direct effect on the wing, e.g. aileron deflection or an upward gust.

Concludingly, several flight mechanics aspects are affected by the inclusion of wing flexibility. This is even the case for the relatively rigid A320-like aircraft, for which flexibility is usually neglected. For more flexible designs, most flight mechanics aspects are influenced substantially by aeroelasticity. Indeed, aeroelasticity should be included in flight mechanics models in order to obtain accurate results, even in the preliminary design phase.

Many analyses were performed to reach the conclusions stated above. Because of the qualitative nature of the conclusions, and because of accordance with literature, it is probable that the conclusions apply to any conventional, low aspect-ratio aircraft in the subsonic flight regime. Although it is probable, it is not certain, since only one aircraft (and variants based on it) was investigated in a limited number of flight conditions. Moreover, the absence of validation data prevents definitive conclusions to be drawn. In any case, the conclusions presented in the current research cannot be extended to aircraft that require nonlinear structural analysis, such as boxed-wing or high aspect-ratio aircraft, nor to aircraft that require nonlinear aerodynamic analysis, typically necessary in the transonic flight regime.

Chapter 10

Recommendations

Much work has been performed for the current research. The research is not finished, however, and several recommendations can be given regarding the next steps that can be taken. The recommendations fall into three categories: improvement of the model, extension of the model and expansion of the basis for the conclusions, i.e. with validation. These are now discussed.

Improvement of the model

The aeroelastic flight mechanics model can still be improved in order to increase the accuracy of the predictions. Three improvements are suggested in the following, in no particular order.

Firstly, the aerodynamic model can be improved. Currently, a quasi-steady model is employed, which works well for low-frequency aircraft motion. Higher frequency motion, such as rapid maneuvers or flutter, cannot be accurately modeled by a quasi-steady model (see section 2-2-2). In these cases, unsteady models are required. For medium-fidelity aeroelastic models, a doublet-lattice method with strip theory, or a linearized 3D unsteady vortex-lattice method are particularly suited [89].

Secondly, a flexible fuselage can be included. Once the fuselage mode shapes are known, fuselage flexibility can be included using the same approach as for the flexible wings. Inclusion of fuselage flexibility primarily influences the angle of attack of the empennage, because of fuselage bending [16].

Thirdly, the control surfaces can be modeled more accurately. In the current model, only the aerodynamic contributions of the control surfaces are taken into account. In reality, the dynamics and inertia of the control surfaces also affect the flight mechanics. These can be included by introducing flapping modes in the model (see section 2-4). Actuation of the control surface can also be included, by introducing actuator dynamics blocks in SimMechanics. In this manner, the effect of pilot input is accurately modeled, as opposed to ignoring pilot input and directly modeling the control surface deflection angle (done in the current model).

Extension of the model

The scope of the research was defined in section 1-2-2. For future research, it is interesting to develop the model beyond this scope. Four extensions are suggested below, in no particular order.

Firstly, a flight control algorithm can be created for the flexible aircraft. An automatic flight control system can be developed, but also an analytical human pilot model [16]. The latter could also be used for a detailed analysis of the effect of aeroelasticity on piloting tasks.

Secondly, an active load alleviation algorithm can be developed. Load prediction was the goal of the current model, and forms the first step in load alleviation. With load alleviation, passenger comfort can be increased, structural fatigue can be reduced and (peak) loads on the wing structure can be decreased.

Thirdly, the model can be included in a design optimization algorithm, such as the Design and Engineering Engine mentioned in section 1-2-2. This leads to more accurate designs and possibly to lighter designs, when a load alleviation algorithm is present, that reduces wing (peak) loads in design flight conditions.

Fourthly, the current model was created for conventional aircraft. An extension to the model can be made, such that it can also be used for non-conventional aircraft. Hybrid-wing-body aircraft can be included with relative ease, once fuselage flexibility is included in the model and fuselage and wing mode shapes are known. Joined-wing aircraft are much harder to model, because of the structural nonlinearity associated with the statically indeterminate structure [105].

Expansion of the basis for the conclusions

The conclusions in chapter 9 were based on analyses with an A320-like model and a derived rectangular beam model. These models have been extensively verified, but have not been validated, because complete validation data was scarce. Three investigations are proposed to expand the basis, and thereby the credibility, of the conclusions.

Firstly, the aeroelastic flight mechanics model can be validated using MSC NASTRAN, once the correct license (FlightLoads) is available at the TU Delft. With the FlightLoads license, NASTRAN is capable of high-fidelity aeroelastic flight mechanics analysis [106].

Secondly, the University of Michigan is currently creating an aircraft flight test model, for aeroelastic validation purposes [101]. Information regarding these flight tests will be published and is expected to become available in the near future. The current model may be validated using this information.

Thirdly, more case studies can be performed, in order to check whether the conclusions of chapter 9 uphold for a whole range of aircraft. The required input data for the different aircraft may be determined using the Design and Engineering Engine (DEE) of the TU Delft. This program is currently under construction and it is expected that it will soon be CPACS-compatible. CPACS, or Common Parametric Aircraft Configuration Scheme, is a standardized aircraft data model and allows easy exchange of information between tools [107]. Once both the DEE and the current model are CPACS-compatible, they can be easily connected and many case studies can be performed.

Appendix A

Aerodynamic Data Tables

This appendix contains the aerodynamic data of the A320-like wing, control surfaces and tail surfaces. This information was obtained from a DATCOM model [72]. It has been assumed that the airfoil of the horizontal and vertical tail surfaces is the NACA0009 airfoil. Since this airfoil is symmetric, it creates no aerodynamic moment. Note that the control surface coefficients are not dimensionless (see section 3-3-1), and that they are dependent on both the deflection angle and the clean wing angle of attack (α).

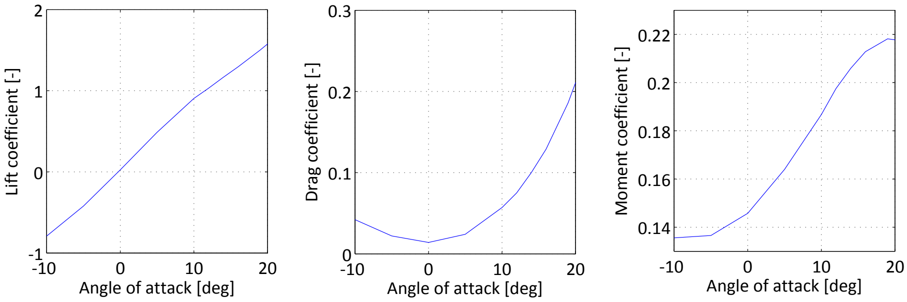

Figure A-1: Lift, drag and moment coefficients for the A320-like wing.

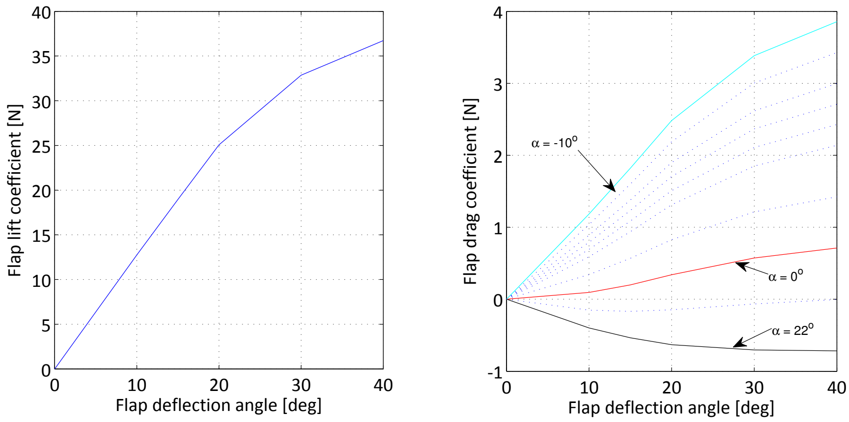

Figure A-2: Lift and drag force coefficients for the flap.

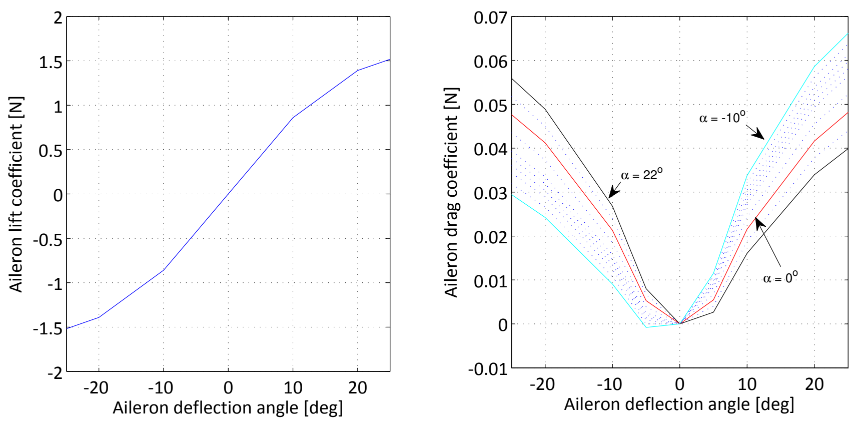

Figure A-3: Lift and drag force coefficients for the aileron.

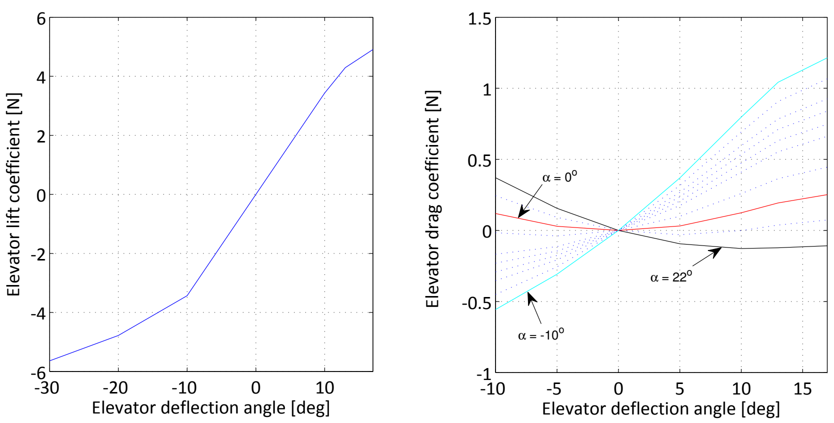

Figure A-4: Lift and drag force coefficients for the elevator.

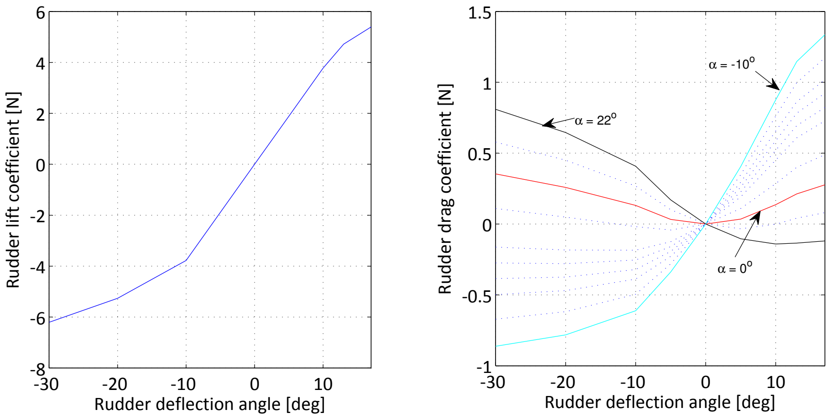

Figure A-5: Lift and drag force coefficients for the rudder.

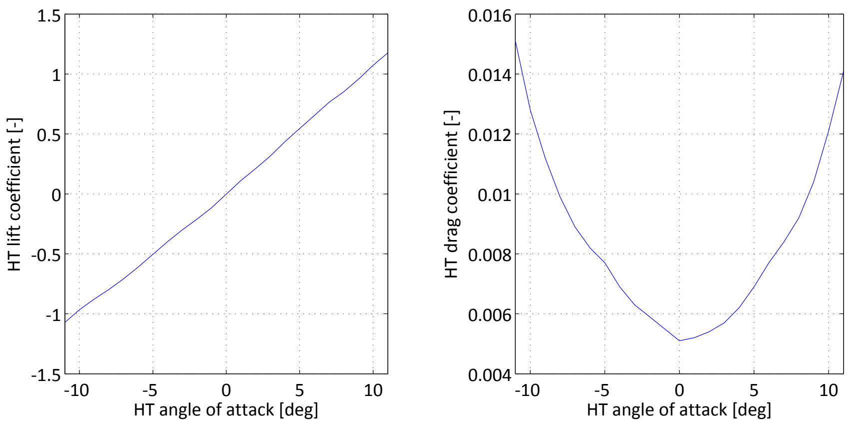

Figure A-6: Lift and drag coefficients for the horizontal tail (HT).

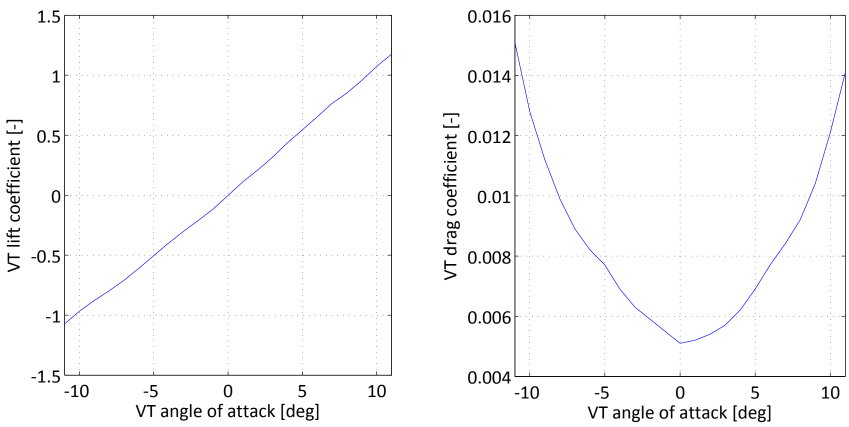

Figure A-7: Lift and drag coefficients for the vertical tail (VT).

Appendix B

Structural Data

This appendix contains structural data. The mode shapes of the A320-like wing, geometric data about the A320-like wing and mode shapes of the rectangular beam (from section 4-4) are presented.

B-1 Mode Shapes of the A320-like Wing

Tables B-1, B-2 and B-3 show the mass-normalized mode shapes of the A320-like wing, defined at 18 spanwise sections [71]. In these tables, η is the dimensionless semispan, h is the downward displacement, g is the forward displacement and ξ is the pitch-up twist deflection. These mode shapes were determined using a finite element analysis in MSC NASTRAN.

B-2 Geometric Information of the A320-like Wing

The geometric information of the A320-like wing is presented in this section [72, 71]. Table B-4 shows the general wing parameters and table B-5 shows the mass and inertia of 8 wing sections. Note that the location of the elastic axis (e.a.), of the aerodynamic center (a.c.), of the center of gravity (c.g.) and of the application point (a.p.) is as the distance from the leading edge, as a fraction the local chord.

B-3 Mode Shapes of the Rectangular Beam

Tables B-7 and B-8 show the mass-normalized mode shapes of the rectangular beam, which was the subject of section 4-4. In these tables, η is the dimensionless semispan, h is the downward displacement, g is the forward displacement and ξ is the pitch-up twist deflection. These mode shapes were determined using the approach presented in section 4-4-1.

Table B-1: Mass-normalized mode shapes of the A320-like wing.

	Mode 1 - 1.741 Hz			Mode 2 - 4.299 Hz			Mode 3 - 5.015 Hz		
η	h [m]	g [m]	ξ [deg]	h [m]	g [m]	ξ [deg]	h [m]	g [m]	ξ [deg]
0.000	0.00e0	0.00e0	0.00e0	0.00e0	0.00e0	0.00e0	0.00e0	0.00e0	0.00e0
0.059	-1.37e-4	-1.34e-7	-2.27e-3	-4.69e-6	-1.16e-4	-6.25e-4	-6.41e-4	3.60e-6	-1.49e-3
0.118	-4.41e-4	-4.65e-7	-5.79e-3	-1.96e-5	-3.93e-4	-1.61e-3	-1.85e-3	1.03e-5	-2.22e-3
0.177	-9.23e-4	-1.06e-6	-9.68e-3	-4.19e-5	-8.54e-4	-2.77e-3	-3.43e-3	1.91e-5	9.85e-4
0.235	-1.61e-3	-1.99e-6	-1.40e-2	-8.35e-5	-1.51e-3	-3.74e-3	-5.27e-3	2.78e-5	7.51e-3
0.294	-2.52e-3	-3.45e-6	-1.88e-2	-1.38e-4	-2.38e-3	-3.62e-3	-7.24e-3	3.15e-5	1.51e-2
0.353	-3.66e-3	-4.45e-6	-2.41e-2	-1.65e-4	-3.44e-3	-3.51e-3	-8.98e-3	4.75e-5	1.91e-2
0.412	-5.04e-3	-5.53e-6	-2.99e-2	-1.81e-4	-4.73e-3	-3.40e-3	-1.03e-2	6.85e-5	2.55e-2
0.471	-6.68e-3	-6.64e-6	-3.60e-2	-1.85e-4	-6.26e-3	-3.18e-3	-1.11e-2	9.55e-5	3.68e-2
0.529	-8.58e-3	-7.77e-6	-4.26e-2	-1.72e-4	-8.02e-3	-2.87e-3	-1.12e-2	1.29e-4	5.36e-2
0.588	-1.08e-2	-8.94e-6	-4.93e-2	-1.40e-4	-1.00e-2	-2.47e-3	-1.02e-2	1.69e-4	7.68e-2
0.647	-1.32e-2	-1.01e-5	-5.63e-2	-8.38e-5	-1.23e-2	-1.98e-3	-7.93e-3	2.15e-4	1.07e-1
0.706	-1.60e-2	-1.13e-5	-6.36e-2	-2.24e-6	-1.48e-2	-1.42e-3	-4.18e-3	2.68e-4	1.42e-1
0.765	-1.89e-2	-1.26e-5	-6.99e-2	1.06e-4	-1.75e-2	-7.91e-4	1.18e-3	3.27e-4	1.82e-1
0.824	-2.22e-2	-1.38e-5	-7.62e-2	2.41e-4	-2.05e-2	-1.47e-4	8.14e-3	3.92e-4	2.25e-1
0.882	-2.56e-2	-1.51e-5	-8.19e-2	3.98e-4	-2.36e-2	4.47e-4	1.65e-2	4.60e-4	2.65e-1
0.941	-2.91e-2	-1.64e-5	-8.54e-2	5.71e-4	-2.68e-2	9.00e-4	2.59e-2	5.32e-4	2.96e-1
1.000	-3.26e-2	-1.77e-5	-8.77e-2	7.49e-4	-3.00e-2	1.13e-3	3.57e-2	6.05e-4	3.12e-1

Table B-2: Mass-normalized mode shapes 4-6 of the A320-like wing.

	Mode 4 - 7.830 Hz			Mode 5 - 11.123 Hz			Mode 6 - 12.445 Hz		
η	h [m]	g [m]	ξ [deg]	h [m]	g [m]	ξ [deg]	h [m]	g [m]	ξ [deg]
0.000	0.00e0	0.00e0	0.00e0	0.00e0	0.00e0	0.00e0	0.00e0	0.00e0	0.00e0
0.059	-4.33e-4	4.32e-5	3.24e-2	1.15e-3	1.90e-4	3.84e-2	5.19e-4	-5.11e-4	1.35e-2
0.118	-8.90e-4	1.15e-4	8.59e-2	3.43e-3	5.34e-4	9.57e-2	1.50e-3	-1.46e-3	3.34e-2
0.177	-1.29e-3	2.06e-4	1.52e-1	5.70e-3	1.00e-3	1.48e-1	2.37e-3	-2.80e-3	5.01e-2
0.235	-1.33e-3	3.00e-4	2.27e-1	7.68e-3	1.56e-3	1.94e-1	2.71e-3	-4.43e-3	7.16e-2
0.294	-1.02e-3	3.68e-4	2.93e-1	8.90e-3	2.15e-3	2.22e-1	2.50e-3	-6.28e-3	1.15e-1
0.353	2.51e-4	3.68e-4	3.32e-1	8.66e-3	2.50e-3	2.38e-1	2.58e-3	-7.73e-3	1.52e-1
0.412	2.31e-3	3.42e-4	3.63e-1	6.90e-3	2.75e-3	2.49e-1	2.34e-3	-8.93e-3	1.87e-1
0.471	4.60e-3	2.76e-4	3.90e-1	3.53e-3	2.83e-3	2.60e-1	1.60e-3	-9.65e-3	2.26e-1
0.529	6.79e-3	1.68e-4	4.11e-1	-1.16e-3	2.69e-3	2.76e-1	4.11e-4	-9.69e-3	2.70e-1
0.588	8.46e-3	1.22e-5	4.24e-1	-6.46e-3	2.27e-3	3.08e-1	-1.09e-3	-8.82e-3	3.23e-1
0.647	9.09e-3	-1.94e-4	4.27e-1	-1.13e-2	1.52e-3	3.63e-1	-2.61e-3	-6.84e-3	3.86e-1
0.706	8.17e-3	-4.53e-4	4.17e-1	-1.41e-2	4.20e-4	4.51e-1	-3.75e-3	-3.59e-3	4.60e-1
0.765	5.25e-3	-7.64e-4	3.93e-1	-1.35e-2	-1.07e-3	5.73e-1	-4.02e-3	1.06e-3	5.46e-1
0.824	7.58e-5	-1.12e-3	3.59e-1	-8.31e-3	-2.92e-3	7.33e-1	-3.04e-3	7.10e-3	6.42e-1
0.882	-7.28e-3	-1.52e-3	3.20e-1	1.98e-3	-5.10e-3	9.05e-1	-6.23e-4	1.44e-2	7.39e-1
0.941	-1.63e-2	-1.95e-3	2.86e-1	1.63e-2	-7.50e-3	1.06e+0	2.95e-3	2.25e-2	8.25e-1
1.000	-2.59e-2	-2.38e-3	2.66e-1	3.24e-2	-9.98e-3	1.15e+0	6.98e-3	3.09e-2	8.71e-1

Table B-3: Mass-normalized mode shapes 7-9 of the A320-like wing.

	Mode 7 - 14.997 Hz			Mode 8 - 17.936 Hz			Mode 9 - 22.135 Hz		
η	h [m]	g [m]	ξ [deg]	h [m]	g [m]	ξ [deg]	h [m]	g [m]	ξ [deg]
0.000	0.00e0	0.00e0	0.00e0	0.00e0	0.00e0	0.00e0	0.00e0	0.00e0	0.00e0
0.059	1.76e-5	7.63e-5	-2.53e-2	2.75e-3	1.06e-4	4.38e-2	1.66e-3	-3.28e-4	-2.05e-3
0.118	-1.71e-4	2.36e-4	-6.53e-2	7.28e-3	2.56e-4	1.02e-1	4.00e-3	-8.29e-4	-9.91e-3
0.177	-4.82e-4	4.76e-4	-1.08e-1	9.83e-3	3.88e-4	1.17e-1	4.58e-3	-1.46e-3	-5.08e-2
0.235	-1.22e-3	7.94e-4	-1.42e-1	9.29e-3	4.20e-4	1.04e-1	1.75e-3	-2.24e-3	-7.62e-2
0.294	-2.11e-3	1.20e-3	-1.34e-1	5.53e-3	1.84e-4	9.05e-2	-3.61e-3	-3.36e-3	3.24e-2
0.353	-3.69e-3	1.74e-3	-5.18e-2	2.77e-4	5.37e-5	4.45e-2	-4.10e-3	-2.00e-3	9.45e-2
0.412	-5.38e-3	2.27e-3	7.79e-2	-5.34e-3	-9.43e-5	-6.99e-3	-1.84e-3	1.29e-5	1.39e-1
0.471	-6.01e-3	2.72e-3	2.50e-1	-9.80e-3	-2.38e-4	-4.53e-2	1.71e-3	2.68e-3	1.76e-1
0.529	-5.18e-3	3.01e-3	4.69e-1	-1.12e-2	-3.61e-4	-6.59e-2	5.24e-3	5.62e-3	1.80e-1
0.588	-2.76e-3	3.04e-3	7.28e-1	-8.22e-3	-4.46e-4	-7.39e-2	6.79e-3	8.29e-3	1.39e-1
0.647	7.16e-4	2.73e-3	1.02e+0	-1.10e-3	-4.69e-4	-8.88e-2	5.05e-3	1.00e-2	4.49e-2
0.706	4.19e-3	1.97e-3	1.32e+0	8.17e-3	-4.11e-4	-1.44e-1	1.20e-4	1.01e-2	-8.65e-2
0.765	6.13e-3	7.19e-4	1.62e+0	1.57e-2	-2.54e-4	-2.80e-1	-5.85e-3	7.78e-3	-2.18e-1
0.824	4.88e-3	-1.06e-3	1.87e+0	1.69e-2	1.14e-5	-5.26e-1	-9.11e-3	2.66e-3	-3.02e-1
0.882	-6.28e-4	-3.31e-3	2.08e+0	8.16e-3	3.79e-4	-8.71e-1	-5.96e-3	-5.31e-3	-3.04e-1
0.941	-1.01e-2	-5.91e-3	2.22e+0	-1.02e-2	8.21e-4	-1.23e+0	4.52e-3	-1.55e-2	-2.37e-1
1.000	-2.18e-2	-8.64e-3	2.29e+0	-3.32e-2	1.30e-3	-1.46e+0	1.92e-2	-2.66e-2	-1.63e-1

Table B-4: Geometrical parameters of the wing.

Parameter	Value	Parameter	Value
Semispan [m]	17.1	Setting angle [deg]	6
Root chord [m]	7.0	Wing twist [deg]	2
Taper [-]	0.229	Location of e.a. [chords]	0.33
LE Sweep [deg]	26	Location of a.c. [chords]	0.25
Dihedral [deg]	5.1	Location of c.g. [chords]	0.43

Table B-5: Mass and inertia of sections of the A320-like wing.

Section	Mass [kg]	Roll inertia [kgm^2]	Pitch inertia [kgm^2]	Yaw inertia [kgm^2]
1	2.927e3	1.295e3	5.052e3	5.985e3
2	2.443e3	1.055e3	3.491e3	4.296e3
3	2.010e3	0.848e3	2.322e3	3.004e3
4	1.670e3	0.665e3	1.463e3	2.023e3
5	1.259e3	0.510e3	0.865e3	1.313e3
6	0.936e3	0.373e3	0.463e3	0.803e3
7	0.669e3	0.263e3	0.219e3	0.466e3
8	0.442e3	0.172e3	0.084e3	0.250e3

Table B-6: Parameters regarding objects on the wing.

Parameter	Engine	Landing gear	Flap	Aileron
Spanwise location [-]	0.392	0.120	0.453	0.877
Location of a.p. [chords]	-0.44	0.53	1.00	1.00
Location of e.a. [chords]	0.33	0.33	0.33	0.33
Mass [kg]	2359	1425	-	-

Table B-7: Mass-normalized mode shapes 4-6 of the rectangular beam.

	Mode 1 - 136.5 Hz			Mode 2 - 155.9 Hz			Mode 3 - 342.6 Hz		
η	h [m]	g [m]	ξ [rad]	h [m]	g [m]	ξ [rad]	h [m]	g [m]	ξ [rad]
0.042	0	0	-1.07e-7	-8.25e-8	0	0	0	0	2.31e-7
0.125	0	0	-1.07e-2	-8.25e-3	0	0	0	0	2.31e-2
0.208	0	0	-1.07e-2	-2.48e-2	0	0	0	0	2.31e-2
0.292	0	0	-1.94e-2	-4.80e-2	0	0	0	0	1.88e-2
0.375	0	0	-1.94e-2	-7.79e-2	0	0	0	0	1.88e-2
0.458	0	0	-2.53e-2	-1.12e-1	0	0	0	0	-2.33e-3
0.542	0	0	-2.53e-2	-1.51e-1	0	0	0	0	-2.33e-3
0.625	0	0	-2.87e-2	-1.93e-1	0	0	0	0	-2.19e-2
0.708	0	0	-2.87e-2	-2.37e-1	0	0	0	0	-2.19e-2
0.792	0	0	-3.02e-2	-2.83e-1	0	0	0	0	-3.26e-2
0.875	0	0	-3.02e-2	-3.30e-1	0	0	0	0	-3.26e-2
0.958	0	0	-3.06e-2	-3.77e-1	0	0	0	0	-3.52e-2
1.000	0	0	-3.06e-2	-4.00e-1	0	0	0	0	-3.52e-2

Table B-8: Mass-normalized mode shapes 4-6 of the rectangular beam.

	Mode 4 - 391.2 Hz			Mode 5 - 522.9 Hz			Mode 6 - 597.2 Hz		
η	h [m]	g [m]	ξ [rad]	h [m]	g [m]	ξ [rad]	h [m]	g [m]	ξ [rad]
0.042	1.79e-7	0	0	0	0	-2.30e-7	-1.78e-7	0	0
0.125	1.79e-2	0	0	0	0	-2.30e-2	-1.78e-7	0	0
0.208	5.36e-2	0	0	0	0	-2.30e-2	-5.33e-2	0	0
0.292	8.60e-2	0	0	0	0	1.78e-2	-5.74e-2	0	0
0.375	1.15e-1	0	0	0	0	1.78e-2	-3.00e-2	0	0
0.458	1.28e-1	0	0	0	0	2.17e-2	5.21e-4	0	0
0.542	1.24e-1	0	0	0	0	2.17e-2	3.41e-2	0	0
0.625	1.05e-1	0	0	0	0	-6.13e-3	4.61e-2	0	0
0.708	7.14e-2	0	0	0	0	-6.13e-3	3.66e-2	0	0
0.792	2.93e-2	0	0	0	0	-2.81e-2	1.02e-2	0	0
0.875	-2.10e-2	0	0	0	0	-2.81e-2	-3.32e-2	0	0
0.958	-7.33e-2	0	0	0	0	-3.40e-2	-8.12e-2	0	0
1.000	-1.00e-1	0	0	0	0	-3.40e-2	-1.07e-1	0	0

Appendix C

Stability and Control Derivatives

This appendix will contain information regarding the stability and control derivatives that were discussed in section 7-2.

C-1 Non-dimensionalization Factors

Table C-1 shows the non-dimensionalization factors that were used in order to determine the dimensionless stability and control derivatives [85].

C-2 Detailed Results of Stability Analysis

This section contains the detailed results (i.e. numerical values) of the analysis presented in section 7-2. Firstly, table C-2 shows the symmetric and asymmetric stability and control derivatives for the rigid A320-like aircraft. Secondly, table C-3 shows the effect of a unit change (m/s, N or rad) of a state or control variable on the Wing Root Bending Moment (WRBM) of the left and right wing. Note that for both wings, a positive WRBM corresponds to upward deflection.

Table C-1: Non-dimensionalization factors for the stability and control derivatives.

	Symmetric			Asymmetric		
	$C_{X\_}$	$C_{Z\_}$	$C_{m\_}$	$C_{Y\_}$	$C_{l\_}$	$C_{n\_}$
u	$\frac{1}{2}\rho VS$	$\frac{1}{2}\rho VS$	$\frac{1}{2}\rho VS\bar{c}$	$\frac{1}{2}\rho VS$	$\frac{1}{2}\rho VS\bar{c}$	$\frac{1}{2}\rho VS\bar{c}$
α	$\frac{1}{2}\rho VS$	$\frac{1}{2}\rho VS$	$\frac{1}{2}\rho VS\bar{c}$	$\frac{1}{2}\rho VS$	$\frac{1}{2}\rho VS\bar{c}$	$\frac{1}{2}\rho VS\bar{c}$
q	$\frac{1}{2}\rho VS\bar{c}$	$\frac{1}{2}\rho VS\bar{c}$	$\frac{1}{2}\rho VS\bar{c}^2$	$\frac{1}{2}\rho VS\bar{c}$	$\frac{1}{2}\rho VS\bar{c}^2$	$\frac{1}{2}\rho VS\bar{c}^2$
δ_e	$\frac{1}{2}\rho VS$	$\frac{1}{2}\rho VS$	$\frac{1}{2}\rho VS\bar{c}$	$\frac{1}{2}\rho VS$	$\frac{1}{2}\rho VS\bar{c}$	$\frac{1}{2}\rho VS\bar{c}$
β	$\frac{1}{2}\rho VS$	$\frac{1}{2}\rho VS$	$\frac{1}{2}\rho VSb$	$\frac{1}{2}\rho VS$	$\frac{1}{2}\rho VSb$	$\frac{1}{2}\rho VSb$
p	$\frac{1}{2}\rho VSb$	$\frac{1}{2}\rho VSb$	$\frac{1}{2}\rho VSb^2$	$\frac{1}{2}\rho VSb$	$\frac{1}{2}\rho VSb^2$	$\frac{1}{2}\rho VSb^2$
r	$\frac{1}{2}\rho VSb$	$\frac{1}{2}\rho VSb$	$\frac{1}{2}\rho VSb^2$	$\frac{1}{2}\rho VSb$	$\frac{1}{2}\rho VSb^2$	$\frac{1}{2}\rho VSb^2$
δ_a	$\frac{1}{2}\rho VS$	$\frac{1}{2}\rho VS$	$\frac{1}{2}\rho VSb$	$\frac{1}{2}\rho VS$	$\frac{1}{2}\rho VSb$	$\frac{1}{2}\rho VSb$
δ_r	$\frac{1}{2}\rho VS$	$\frac{1}{2}\rho VS$	$\frac{1}{2}\rho VSb$	$\frac{1}{2}\rho VS$	$\frac{1}{2}\rho VSb$	$\frac{1}{2}\rho VSb$

Table C-2: Symmetric and asymmetric stability and control derivatives for the rigid aircraft.

	Symmetric			Asymmetric		
	$C_{X\_}$	$C_{Z\_}$	$C_{m\_}$	$C_{Y\_}$	$C_{l\_}$	$C_{n\_}$
u	-0.293	-1.873	0.174	0.001	0.001	-0.004
α	0.794	-7.474	-3.529	-0.000	-0.000	0.000
q	1.878	-5.407	-25.15	-0.001	-0.001	0.004
δ_e	0.093	-0.424	-1.558	0	0	0
β	0.001	-0.000	-0.000	-1.412	-0.169	0.654
p	0.000	-0.000	-0.000	-0.396	-0.370	0.031
r	-0.001	0.000	0.000	0.702	0.178	-0.296
δ_a	0.000	0.000	0.000	-0.022	-0.036	-0.002
δ_r	-0.000	0.000	0.000	-0.448	-0.057	0.242

Table C-3: Effect of parameter disturbances on the wing root bending moments [kNm].

	Left wing WRBM effect [kNm]	Right wing WRBM effect [kNm]
u	8.134	8.150
w	19.68	19.68
q	-117.0	-117.1
δ_e	-337.7	-337.7
v	11.08	-11.08
p	42.70	-42.70
r	-165.7	165.6
δ_a	-10.95	10.95
δ_r	562.7	-562.8

Appendix D

Model User Guide

This appendix contains a user guide for the Aeroelastic Flight Mechanics (AFM) model. The steps that should be taken for the various analysis are discussed, as well as data handling in the model. Note that ample comments are available in the code itself and that an interactive help menu is included in the model initialization file. Before any analysis can be performed, the user must type "initialize" in the command window.

Time Domain Simulation

For a time domain simulation, the following steps should be taken. It is assumed that the user has not trimmed the aircraft yet. If trim has already been performed, steps 1-3 can be skipped.

1. Specify aircraft parameters and control input in aircraft_description.m
2. Specify trim parameters (e.g. flight condition) in aircraft_trim.m
3. Trim the aircraft by typing "aircraft_trim"
4. Load trimmed situation by typing "trimmed_input(trim,stoptime,true)", where stoptime is a numerical value
5. If required, (re)create the SimMechanics model by typing "aircraft_generator"
6. Perform simulation by typing "time_domain_simulation"
7. If required, create results by typing "plot_simulation_results(input_par,simulation)"
8. Results: all information is in the simulation struct. Plotted results are in the Results folder

Aircraft Trim

Aircraft trim may be performed to determine the control input and aircraft attitude, that are required for a certain flight condition. The following steps should be taken to perform trim.

1. Specify aircraft parameters in aircraft_description.m
2. Specify trim parameters (e.g. flight condition) in aircraft_trim.m
3. Trim the aircraft by typing "aircraft_trim"
4. Results: all information is in the trim struct. Type "trim.result" to view the result. This information is also saved to the Results folder.

Stability Analysis

Stability analysis may be performed, to determine the stability and control derivatives around a trimmed point. zthe following steps should be taken.

1. Specify aircraft parameters in aircraft_description.m
2. Specify trim parameters (e.g. flight condition) in aircraft_trim.m and derivatives.m
3. Perform the trim and the stability analysis by typing "derivatives"
4. Results: all derivatives are in the deriv struct and extended information in the DNC struct. This information is also saved to the Results folder.

Linearization and Mode Determination

The nonlinear flight mechanics model may be linearized. The result is a state-space system that can rapidly assess flight mechanics behavior. The linearized model is also used to determine information about the flight mechanics modes.

1. Specify aircraft parameters in aircraft_description.m
2. Specify trim parameters (e.g. flight condition) in aircraft_trim.m and model_linearization.m
3. Perform the trim and the linearization by typing "model_linearization"
4. Results: the linearized models, as well as the flight mechanics modes are in the linearization struct. This information is also saved to the Results folder.

Frequency Sweep Analysis

A frequency sweep analysis may be performed to determine the transfer functions and create the associated bode plots between pilot input and flight mechanics states. The following steps should be taken.

1. Make sure that the aircraft parameters and control input are correctly specified in aircraft_description.m
2. Make sure that the trim parameters are correctly specified in aircraft_trim.m
3. Make sure that the frequency sweep analysis input is correctly specified in freq_sweep_analysis.m
4. Perform the analysis by typing "freq_sweep_analysis"
5. Results: all information is in the freq_sweep struct. Plotted results are in the Results folder

Data Handling and Folder Structure

Data can only be effectively stored in the following MATLAB structures:

- input_par: last-used input parameters. Note that "Data/input_par.mat" is used in simulations
- simulation: results of a time-domain simulation
- trim: results of a trim analysis
- deriv: results of a stability analysis
- linearization: results of linearization
- freq_sweep: results of a frequency sweep analysis
- analysis: structure used for defining input on a higher level, e.g. to run multiple trim analyses
- DNC: general structure that is never cleared and can be used to store any variable

Furthermore, the model consists of the following folders:

- Top level: contains the script "initialize" for model initialization and the simulink model "Aircraft.mdl"
- Analyses: contains the scripts for all the analysis, that a user will typically do
- Data: contains the modal data (in folder "Mode data"), as well as aerodynamic data ("aero.mat"). Furthermore, the input parameters are stored in this folder, as well as images for the SimMechanics model.

- Results: all results are stored in this folder. This folder may not exist, if no results have ever been produced.
- Utilities: contains MATLAB functions and regular scripts, that do not perform an analysis. Most of these functions are typically called by other MATLAB scripts, not by the user.

Bibliography

[1] M. Bianchin, G. Quaranta, and P. Mantegazza, "State space reduced order models for static aeroelasticity and flight mechanics of flexible aircraft," in *Proceedings of the XVII Congresso Nazionale AIDAA*, (Rome, Italy), AIDAA, 2003.

[2] D. Inman, *Engineering Vibrations.* Upper Saddle River, USA: Prentice-Hall, 2nd ed., 2001.

[3] L. Cavagna, P. Masarati, and G. Quaranta, "Coupled Multibody/Computational Fluid Dynamics Simulation of Maneuvering Flexible Aircraft," *Journal of Aircraft*, vol. 48, no. 1, pp. 92–106, 2011.

[4] H. Mai, J. Neumann, and H. Hennings, "Gust Response: A Validation Experiment and Preliminary Numerical Simulations," in *Proceedings of the International Forum on Aeroelasticity and Structural Dynamics*, (Paris, France), 2011.

[5] O. Wright, "Flying-machine," 1906.

[6] A. Collar, "The Expanding Domain of Aeroelasticity," *Journal of the Royal Aeronautical Society*, 1946.

[7] E. H. Dowell, R. Clark, and D. Cox, *A Modern Course in Aeroelasticity.* Dordrecht, The Netherlands: Kluwer Academic Publishers, 4th ed., 2004.

[8] P. P. Friedmann, "Renaissance of Aeroelasticity and Its Future," *Journal of Aircraft*, vol. 36, no. 1, pp. 105–121, 1999.

[9] S. Ricci and A. Scotti, "Wind Tunnel Testing of an Active Controlled Wing under Gust Excitation," in *Proceedings of the 49th AIAA/ASME/ASCE/AHS/ASC Structures, Structural Dynamics, and Materials Conference*, (Schaumburg, USA), American Institute of Aeronautics and Astronautics, 2008.

[10] E. Livne, "Future of Airplane Aeroelasticity," *Journal of Aircraft*, vol. 40, no. 6, pp. 1066–1092, 2003.

[11] R. Yurkovich, D. Liu, and P. Chen, “The State-of-the-Art of Unsteady Aerodynamics for High Performance Aircraft,” in *Proceedings of the 39th AIAA Aerospace Sciences Meeting & Exhibit*, (Reno, USA), 2001.

[12] E. Dowell, J. Edwards, and T. Strganac, “Nonlinear Aeroelasticity,” *Journal of Aircraft*, vol. 40, no. 5, pp. 857–874, 2003.

[13] L. Meirovitch and I. Tuzcu, “Integrated Approach to the Dynamics and Control of Maneuvering Flexible Aircraft,” tech. rep., NASA, 2003.

[14] B. Etkin and L. Reid, *Dynamics of Flight: Stability and Control.* New York, USA: Prentice-Hall, 1996.

[15] D. McLean, *Automatic Flight Control Systems.* New York, USA: Wiley, 1990.

[16] J. Pedro and C. Bigg, “Development of a Flexible Embedded Aircraft/Control System Simulation Facility,” in *Proceedings of the AIAA Modeling and Simulation Technologies Conference and Exhibit*, (San Fransisco, USA), American Institute of Aeronautics and Astronautics, 2005.

[17] M. Waszak and D. Schmidt, “Flight Dynamics of Aeroelastic Vehicles,” *Journal of Aircraft*, vol. 25, no. 6, pp. 563–571, 1988.

[18] C. Reschke, “Flight Loads Analysis with Inertially Coupled Equations of Motion,” in *AIAA Atmospheric Flight Mechanics Conference and Exhibit*, (San Fransisco, USA), 2005.

[19] A. Schütte, G. Einarsson, and A. Raichle, “Numerical Simulation of Maneuvering Aircraft by Aerodynamic, Flight Mechanics and Structural Mechanics Coupling,” *Journal of Aircraft*, vol. 46, no. 1, pp. 53–64, 2009.

[20] R. Snyder, J. Hur, D. Strong, and P. Beran, “Aeroelastic Analysis of a High-Altitude Long-Endurance Joined-Wing Aircraft,” in *Proceedings of the 46 th AIAA/ASME/ASCE/AHS/ASC Structures, Structural Dynamics and Materials Conference*, (Austin, USA), American Institute of Aeronautics and Astronautics, 2005.

[21] D. E. Raveh, “Computational-fluid-dynamics-based aeroelastic analysis and structural design optimization,” *Computer Methods in Applied Mechanics and Engineering*, vol. 194, no. 30, pp. 3453–3471, 2005.

[22] W. R. Krüger and M. Spieck, “Aeroelastic Effects in Multibody Dynamics,” *Vehicle System Dynamics*, vol. 41, no. 5, pp. 383–399, 2004.

[23] M. Spieck, W. Krüger, and J. Arnold, “Multibody Simulation of the Free-Flying Elastic Aircraft,” in *Proceedings of the 1st AIAA Multidisciplinary Design Optimization Specialist Conference*, (Austin, USA), American Institute of Aeronautics and Astronautics, 2005.

[24] Z. Zhao and G. Ren, “Multibody dynamic approach of flight dynamics and nonlinear aeroelasticity of flexible aircraft,” *AIAA journal*, vol. 49, no. 1, pp. 41–54, 2011.

[25] L. Cavagna, S. Ricci, and L. Travaglini, "NeoCASS: An Integrated Tool for Structural Sizing, Aeroelastic Analysis and MDO at Conceptual Design Level," *Progress in Aerospace Sciences*, vol. 47, no. 8, pp. 621–635, 2011.

[26] V. Chudnovsky, A. Mukherjee, J. Wendlandt, and D. Kennedy, "Modeling Flexible Bodies in SimMechanics and Simulink," *MATLAB Digest*, May 2006.

[27] O. Wallrapp, "Flexible Bodies in Multibody System Codes," *Vehicle System Dynamics*, vol. 30, no. 3-4, pp. 237–256, 1998.

[28] M. Karpel, B. Moulin, and M. H. Love, "Modal-Based Structural Optimization with Static Aeroelastic and Stress Constraints," *Journal of Aircraft*, vol. 34, no. 3, pp. 433–440, 1997.

[29] M. Mohammadi-Amin, B. Ghadiri, M. M. Abdalla, H. Haddadpour, and R. De Breuker, "Continuous-time state-space unsteady aerodynamic modeling based on boundary element method," *Engineering Analysis with Boundary Elements*, vol. 36, no. 5, pp. 789–798, 2012.

[30] G. La Rocca, *Knowledge Based Engineering Techniques to Support Aircraft Design and Optimization*. Dissertation, Delft University of Technology, 2011.

[31] M. Karpel and Z. Sheena, "Structural Optimization for Aeroelastic Control Effectiveness," *Journal of Aircraft*, vol. 26, no. 5, pp. 493–495, 1989.

[32] J. Banerjee, "Explicit analytical expressions for frequency equation and mode shapes of composite beams," *International Journal of Solids and Structures*, vol. 38, pp. 2415–2426, Apr. 2001.

[33] D. E. Raveh and M. Karpel, "Structural Optimization of Flight Vehicles with Computational-Fluid-Dynamics-Based Maneuver Loads," *Journal of Aircraft*, vol. 36, no. 6, pp. 1007–1015, 1999.

[34] I. Chowdhury and S. Dasgupta, "Computation of Rayleigh Damping Coefficients for Large Systems," *The Electronic Journal of Geotechnical Engineering*, vol. 8.0, no. C, 2003.

[35] G. P. Guruswamy, D. E. MacMurdy, and R. K. Kapania, "Static Aeroelastic Analysis of Wings using Euler/Navier-Stokes Equations Coupled with Improved Wing-Box Finite Element Structures," in *AIAA/ASME/ASCE/AHS/ASC Structures, Structural Dynamics, and Materials Conference*, (Hilton Head, USA), NASA, 1994.

[36] E. Livne and T. Weisshaar, "Aeroelasticity of Nonconventional Airplane Configurations-Past and Future," *Journal of Aircraft*, vol. 40, no. 6, pp. 1047–1065, 2003.

[37] M. Goland and Y. Luke, "The Flutter of a Uniform Wing with Tip Weights," *Journal of Applied Mechanics*, vol. 15, no. 1, pp. 13–20, 1948.

[38] H. Haddadpour and R. D. Firouz-Abadi, "Evaluation of quasi-steady aerodynamic modeling for flutter prediction of aircraft wings in incompressible flow," *Thin-Walled Structures*, vol. 44, no. 9, pp. 931–936, 2006.

[39] J. S. Bae, S. M. Yang, and I. Lee, "Linear and Nonlinear Aeroelastic Analysis of Fighter-Type Wing with Control Surface," *Journal of Aircraft*, vol. 39, no. 4, pp. 697–708, 2002.

[40] M. Patil and D. Hodges, "On the importance of aerodynamic and structural geometrical nonlinearities in aeroelastic behavior of high-aspect-ratio wings," *Journal of Fluids and Structures*, vol. 19, no. 7, pp. 905–915, 2004.

[41] H. A. Baluch, *Aeroelastic Loads Modeling for Composite Aircraft Design Support.* Dissertation, Delft University of Technology, 2009.

[42] N. Abramson, "Reflections on Fifty SDM Conferences," in *Proceedings of the 50th AIAA/ASME/ASCE/AHS/ASC Structures, Structural Dynamics, and Materials Conference*, (Reston, Virigina), American Institute of Aeronautics and Astronautics, 2009.

[43] M. Patil, D. Hodges, and C. S. Cesnik, "Nonlinear Aeroelastic Analysis of Complete Aircraft in Subsonic flow," *Journal of Aircraft*, vol. 37, no. 5, pp. 753–760, 2000.

[44] B. Moulin and M. Karpel, "Gust Loads Alleviation Using Special Control Surfaces," *Journal of Aircraft*, vol. 44, no. 1, pp. 17–25, 2007.

[45] M. Karpel and B. Moulin, "Aeroservoelastic Gust Response Analysis for the Design of Transport Aircrafts," in *45th AIAA/ASME/ASCE/AHS/ASC Structures, Structural Dynamics & Materials Conference*, (Palm Springs, USA), American Institute of Aeronautics and Astronautics, 2004.

[46] A. Datta and W. Johnson, "An Assessment of the State-of-the-art in Multidisciplinary Aeromechanical Analyses," tech. rep., NASA AMES Research Center, 2008.

[47] J. Anderson, *Fundamentals of Aerodynamics.* New York, USA: McGraw-Hill, 2nd ed., 2001.

[48] D. M. Schuster, D. D. Liu, and L. J. Huttsell, "Computational Aeroelasticity: Success, Progress, Challenge," *Journal of Aircraft*, vol. 40, no. 5, pp. 843–856, 2003.

[49] J. Heeg, P. Chwalowski, J. P. Florance, C. D. Wieseman, D. M. Schuster, and B. Perry III, "Overview of the Aeroelastic Prediction Workshop," in *Proceedings of the 51st AIAA Aerospace Sciences Meeting*, (Grapevine, USA), American Institute of Aeronautics and Astronautics, 2013.

[50] L. Demasi and E. Livne, "Dynamic Aeroelasticity of Structurally Nonlinear Configurations using Linear Modally Reduced Aerodynamic Generalized Forces," *AIAA Journal*, vol. 47, no. 1, pp. 70–90, 2009.

[51] B. W. Van Oudheusden, "On the Quasi-Steady Analysis of One-Degree-of-Freedom Galloping with Combined Translational and Rotational Effects," *Nonlinear Dynamics*, vol. 8, no. 4, pp. 435–451, 1995.

[52] D. H. Hodges and A. G. Pierce, *Introduction to Structural Dynamics and Aeroelasticity.* Cambridge, UK: Cambridge University Press, 2nd ed., 2011.

[53] M. Van Dyke, *An Album of Fluid Motion.* Stanford, USA: Parabolic Press Inc., 12th ed., 1982.

[54] M. C. Van Schoor and A. H. Von Flotow, "Aeroelastic Characteristics of a Highly Flexible Aircraft," *Journal of Aircraft*, vol. 27, no. 10, pp. 901–908, 1990.

[55] S. L. Brunton and C. W. Rowley, "Empirical state-space representations for Theodorsen's lift model," *Journal of Fluids and Structures*, vol. 38, pp. 174–186, 2013.

[56] R. Bisplinghoff, H. Ashley, and R. Halfman, *Aeroelasticity.* New York, USA: Dover Publications, 1955.

[57] R. Palacios, J. Murua, and R. Cook, "Structural and Aerodynamic Models in Nonlinear Flight Dynamics of Very Flexible Aircraft," *AIAA journal*, vol. 48, no. 11, pp. 2648–2659, 2010.

[58] C. Farhat and M. Lesoinne, "Higher-Order Staggered and Subiteration Free Algorithms for Coupled Dynamic Aeroelasticity Problems," in *Proceedings of the 36th Aerospace Sciences Meeting and Exhibit*, (Reno, USA), American Institute of Aeronautics and Astronautics, 1998.

[59] C. Michler, S. Hulshoff, E. van Brummelen, and R. de Borst, "A monolithic approach to fluid-structure interaction," *Computers & Fluids*, vol. 33, no. 5-6, pp. 839–848, 2004.

[60] J. G. Leishman and K. Q. Nguyen, "State-Space Representation of Unsteady Airfoil Behavior," *AIAA journal*, vol. 28, no. 5, pp. 836–844, 1990.

[61] P. Marzocca, L. Librescu, and D. H. Kim, "Development of an indicial function approach for the two-dimensional incompressible/compressible aerodynamic load modelling," *Journal of Aerospace Engineering*, vol. 221, no. 3, pp. 453–463, 2007.

[62] R. Milne, *Dynamics of the Deformable Aeroplane.* London, UK: HM Stationery Office, 1964.

[63] T. Theodorsen, "General Theory of Aerodynamic Instability and the Mechanism of Flutter," tech. rep., National Advisory Committee for Aeronautics, 1935.

[64] S. Kuzmina, F. Ishmuratov, M. Zichenkov, and V. Chedrik, "Analytical-Experimental Study on Using Different Control Surfaces to Alleviate Dynamic Loads," in *47th AIAA/ASME/ASCE/AHS/ASC Structures, Structural Dynamics, and Materials Conference*, no. May, (Reston, Virigina), American Institute of Aeronautics and Astronautics, 2006.

[65] European Aviation Safety Agency, "CS23: Certification Specifications for Normal, Utility, Aerobatic, and Commuter Category Aeroplanes," Tech. Rep. July, 2012.

[66] European Aviation Safety Agency, "CS25: Certification Specifications and Acceptable Means of Compliance for Large Aeroplanes," 2013.

[67] K. Gupta, "Development of a Finite Element Aeroelastic Analysis Capability," *Journal of Aircraft*, vol. 33, no. 5, pp. 995–1002, 1996.

[68] E. C. Yates, "AGARD Standard Aeroelastic Configurations for Dynamic Response 1: Wing 445.6," in *The 61st Meeting of the Structures and Materials Panel*, (Oberammergau, Germany), 1988.

[69] A. Elham, G. La Rocca, and M. J. L. van Tooren, "Development and Implementation of an Advanced, Design-Sensitive Method for Wing Weight Estimation," *Aerospace Science and Technology*, vol. 29, no. 1, pp. 100–113, 2013.

[70] Y. Luo, "An Efficient 3D Timoshenko Beam Element with Consistent Shape Functions," *Advances in Theoretical and Applied Mechanics*, vol. 1, no. 3, pp. 95 – 106, 2008.

[71] R. De Breuker, "A320-like NASTRAN model," Nov. 2013.

[72] P. Wu, "A320 DATCOM model," 2014.

[73] R. Bennett and J. Edwards, "An overview of recent developments in computational aeroelasticity," *AIAA paper*, 1998.

[74] T. Megson, *Aircraft Structures for Engineering Students.* Burlington, USA: Butterworth-Heinemann, 4th ed., 2007.

[75] R. Hibbeler, *Mechanics of Materials.* Singapore: Prentice-Hall, 6th ed., 2005.

[76] E. Hearn, "Torsion of Non-Circular and Thin-Walled Sections," in *Mechanics of Materials 2: The Mechanics of Elastic and Plastic Deformation of Solids and Structural Materials*, ch. 5, pp. 141–165, Oxford, UK: Butterworth-Heinemann, 3rd ed., 1997.

[77] S. Timoshenko, *Strength of Materials.* New York, USA: Van Nostrand, 1930.

[78] D. Inman, "Solutions to Chapter 4," in *Engineering Vibrations*, vol. 1, ch. 4, pp. 375–388, 3rd ed., 2009.

[79] O. Agrawal and A. Shabana, "Application of Deformable-Body Mean Axis to Flexible Multibody System Dynamics," *Computer Methods in Applied Mechanics and Engineering*, vol. 56, no. 2, pp. 217–245, 1986.

[80] A. A. Shabana, "Flexible Multibody Dynamics: Review of Past and Recent Developments," *Multibody System Dynamics*, vol. 1, no. 2, pp. 189–222, 1997.

[81] A. Shabana, *Dynamics of Multibody Systems.* New York, USA: Cambridge University Press, 3rd ed., 2005.

[82] R. Palacios, "Re-examined structural design procedures for very flexible aircraft," in *International Forum of Aeroelasticity and Structural Dynamics*, (Stockholm, Sweden), pp. 1–19, 2007.

[83] L. S. Vinh, J. W. Edwards, D. A. Seidel, and J. T. Batina, "Transonic stability and control of aircraft using CFD methods," in *AIAA Atmospheric Flight Mechanics Conference*, (Minneapolis, USA), pp. 394–404, American Institute of Aeronautics and Astronautics, 1988.

[84] M. Dreier, "Trimming," in *Introduction to Helicopter and Tiltrotor Flight Simulation*, pp. 367–391, Arlington, USA: American Institute of Aeronautics and Astronautics, 2007.

[85] J. Mulder, W. van Staveren, and J. van der Vaart, *Flight Dynamics.* Delft, The Netherlands: Delft University of Technology, 2013.

[86] V. Mistler, A. Benallegue, and N. M'Sirdi, "Exact linearization and noninteracting control of a 4 rotors helicopter via dynamic feedback," in *Proceedings 10th IEEE International Workshop on Robot and Human Interactive Communication*, (Paris, France), pp. 586–593, IEEE, 2001.

[87] J. Hauser, S. Sastry, and P. Kokotovid, "Nonlinear Control Via Approximate Input-Output Linearization: The Ball and Beam Example," *IEEE Transactions on Automatic Control*, vol. 37, no. 3, pp. 392–398, 1992.

[88] K. Aström and R. Murray, "Input / Output Behavior," in *Analysis and Design of Feedback Systems*, pp. 87–108, California Institute of Technology, 2004.

[89] H. Hesse, J. Murua, and R. Palacios, "Consistent Structural Linearization in Flexible Aircraft Dynamics with Large Rigid-Body Motion," in *Proceedings of the 53rd AIAA/ASME/ASCE/AHS/ASC Structures, Structural Dynamics & Materials Conference*, no. April, (Honolulu, USA), American Institute of Aeronautics and Astronautics, 2012.

[90] D. P. Raymer, *Aircraft Design: A Conceptual Approach.* Reston, USA: American Institute of Aeronautics and Astronautics, 5 ed., 2012.

[91] R. Finck and D. Hoak, "Mass and Inertia," in *USAF Stability and Control DATCOM Volume 4*, ch. 8, 1978.

[92] J. Roskam, *Airplane Design Part VI.* Kansas, USA: Roskam Aviation and Engineering Corporation, 1987.

[93] MathWorks, "Choosing a Solver." [Online]. Available: http://www.mathworks.nl/help/simulink/ug/choosing-a-solver.html [Accessed: 20 May 2014], 2014.

[94] MathWorks, "SimMechanics and Simulink Limitations." [Online]. Available: http://www.mathworks.nl/help/physmod/sm/mech/ug/limitations.html [Accessed: 20 May 2014], 2014.

[95] H. Shintani, "Modified Rosenbrock Methods for Stiff Systems," *Hiroshima Mathematical Journal*, vol. 12, no. 3, pp. 543–558, 1982.

[96] MathWorks, "Simulink Documentation Center: Linearizing Models." [Online]. Available: http://www.mathworks.nl/help/simulink/ug/linearizing-models.html [Accessed: 15 Oct. 2013], 2013.

[97] D. H. Baldelli, P. C. Chen, and J. Panza, "Unified Aeroelastic and Flight Dynamic Formulation via Rational Function Approximations," *Journal of Aircraft*, vol. 43, no. 3, pp. 763–772, 2006.

[98] R. Pratt, *Flight Control Systems: Practical Issues in Design and Implementation.* Herts, United Kingdom: Institution of Electrical Engineers, 1st ed., 2000.

[99] Z. Sotoudeh, D. H. Hodges, and C. S. Chang, "Validation Studies for Aeroelastic Trim and Stability of Highly Flexible Aircraft," *Journal of Aircraft*, vol. 47, pp. 1240–1247, July 2010.

[100] A. D. Gaspari, S. Ricci, L. Riccobene, and A. Scotti, “Active Aeroelastic Control over a Multi-Surface Wing : Modelling and Wind Tunnel Testing,” in *Proceedings of the 48th AIAA/ASME/ASCE/AHS/ASC Structures, Structural Dynamics & Materials Conference*, no. April, (Honululu, USA), American Institute of Aeronautics and Astronautics, 2007.

[101] P. Senatore, B. Davis, and E. Prentice, “X-HALE: A Very Flexible UAV for Nonlinear Aeroelastic Tests.” [Online]. http://gust.engin.umich.edu/research/xhale_design.html [Date accessed: 21 May 2014], 2014.

[102] Anonymous, “Verzameling van Grootheden Betreffende Stabiliteit en Besturing van Moderne Vliegtuigen,” tech. rep., Nationaal Lucht- en Ruimtevaartlaboratorium, Amsterdam, 1960.

[103] M. Patil and D. Hodges, “Flight Dynamics of Highly Flexible Flying Wings,” *Journal of Aircraft*, vol. 43, no. 6, pp. 1790–1799, 2006.

[104] FlightGear, “FlightGear Flight Simulator.” [Online]. Available: http://www.flightgear.org/ [Accessed: 12 June 2014], 2014.

[105] C. E. S. Cesnik and W. Su, “Nonlinear Aeroelastic Modeling and Analysis of Fully Flexible Aircraft,” in *Proceedings of the 46th AIAA/ASME/ASCE/AHS/ASC Structures, Structural Dynamics & Materials Conference*, (Austin, USA), American Institute of Aeronautics and Astronautics, 2005.

[106] G. Sikes, “MSC/Flight Loads and Dynamics.” [Online]. http://web.mscsoftware.com/support/library/conf/amuc98/p01198.pdf [Date accessed: 11 June 2014], 1998.

[107] B. Nagel and D. Böhnke, “Communication in Aircraft Design: Can we establish a Common Language?,” in *28th International Congress of the Aeronautical Sciences*, (Brisbane, Australia), 2012.